UNIVERSITÉ DU LUXEMBOURG

PhD-FSTM-2023-126
The Faculty of Science, Technology and Medicine

DISSERTATION

Defence held on 30/10/2023 in Esch-sur-Alzette

to obtain the degree of

DOCTEUR DE L'UNIVERSITÉ DU LUXEMBOURG

EN SCIENCES DE L' INGÉNIEUR

by

Chrysovalantou KALAITZIDOU
Born on 5, March 1991 in Stuttgart, (Germany)

UNVEILING THE HIDDEN LANGUAGE OF EXTRACELLULAR MATRIX DEFORMATIONS:
A TALE OF CELLULAR WHISPERS AND UNSTABLE FIBERS

Dissertation defence committee

Dr. Andreas Zilian, dissertation supervisor
Professor, Université du Luxembourg

Dr. Phoebus Rosakis, dissertation co-supervisor
Professor, University of Crete, Greece

Dr. Alexander Skupin, Chairman
Professor, Université du Luxembourg

Dr Ioannis Iliopoulos, external examiner
Professor, University of Crete, Greece

Dr Stéphane Bordas, Vice Chairman
Professor, Université du Luxembourg

PhD DISSERTATION

Unveiling the Hidden Language of Extracellular Matrix Deformations

A tale of cellular whispers and unstable fibers

by

Chrysovalantou Kalaitzidou

Department of Engineering
UNIVERSITÉ DU LUXEMBOURG

November 2023

This work was financially supported by Fonds National de la Recherche (FNR), Luxembourg through AFR PhD programme (AFR2020/14582656).

Dedication

Στη μητέρα μου Δέσποινα και τον πατέρα μου Γιάννη, στους ακλόνητους αυτούς πυλώνες της αγάπης και της καθοδήγησης, των οποίων η απεριόριστη στήριξη με έχει διαμορφώσει σε αυτό που είμαι σήμερα.

To my parents Despoina and Ioannis, the unwavering pillars of love and guidance, whose boundless support has shaped me into who I am today.

Prelude

Picture your body as a big puzzle crafted from tiny pieces known as cells. Think of these cells as the essential building blocks that create who you are. Now, envision these cells dwelling in a cozy, bustling neighborhood. This community is called the Extracellular Matrix, or ECM for short. The ECM is like the open space between the cells, but it's not just emptiness – it's brimming with a variety of useful materials. It's a complex network formed from tiny fibers that encircle your cells, acting like a sturdy framework to support them. Imagine it as a vast interconnected web that holds everything in place. However, this web is not merely a quiet background. It is a dynamic environment that cells interact with; this interaction is really crucial for many of your body's activities, such as healing, growth, and overall well-being. At the same time, cells communicate with each other by using this intricate fiber web. This communication helps cells understand what they should do and when as well as how to collaborate effectively.

Scientists have always been curious about how individual cells in our bodies interact with each other; and indeed, cells interact through various ways. For example, cells can push or pull on each other, a bit like a team collaborating to shift objects or reshape their environment. When cells push and pull, they create patterns which look like bands that interconnect them. These bands are in essense lines where ECM fibers are packed together and align with each other, forming paths that join the cells and help them in processes like movement, invasion, and growth. When cells communicate by pushing and pulling, they are sending signals about how things are going in our body. By understanding these signals and the modifications they do, scientists can get clues about our health. If something is not working right, these signals might change, and we can catch problems earlier.

Figuring out how all of this works means understanding how the ECM and its constituent fibers behave. In the past, scientists examined how these tiny fibers function and discovered some interesting things about them; these fibers have a special structure that affects how they behave when they're being pulled or squeezed. But, as much as we have learnt for these fibers, we still do not fully understand how cells can modify them in a way that serves their purpose. So, in this study, we try to fill this gap. We created mathematical and computational models to investigate how these fibers respond when cells pull on them and, in addition, how they interact with each other. We imagine that these fibers harden when pulled but become floppy when pushed. Our computer simulations reveal that, when things get squeezed, the floppy fibers lead interesting changes in the ECM .

Our findings are essential because they can help us understand better how our tissues form and change. Our research gives new ways to explore how cells change the fiber web around them and how this affects their interaction. We are actually diving into a world of insights that can make us healthier, improve medical treatments, and even inspire new inventions.

Abstract

One of the key questions in cellular biology revolves around comprehending the intricate interplay between an individual cell and its neighboring counterparts within a tissue. Beyond the cell's innate genetic blueprint, external influences, such as those exerted by its microenvironment, drive most of its functions. The main component of this microenvironment is the Extracellular Matrix (ECM), a convoluted network of fibrous proteins which interact directly with cells. The ECM serves as a scaffold that facilitates intercellular signal exchange, including biomechanical forces. Cells actively respond to mechanical action and induce deformation patterns which take the form of bands that interconnect neighbouring cells. These bands include tracts of elevated matrix densification and fiber alignment and orchestrate vital cellular processes like migration, invasion and proliferation, while there is strong evidence of their contribution to intercellular communication. Unraveling the mechanisms underpinning these phenomena equates to deciphering the mechanical properties of ECM and by that, the mechanical traits of its constituent fibers.

Prior research into the mechanics of fibers has uncovered unusual mechanical phenomena driven in part by their inherent hierarchical structure. These phenomena encompass unique behaviors such as unstable responses of fibers when subjected to compressive loads. This instability is characterized by transitions from heightened fiber stiffness (in which the fiber becomes harder) to the loss of fiber stiffness (causing the fiber to become less stiff and buckle).

In light of these findings, we have developed models that encompass the distinct intrinsic characteristics of fiber structure and mechanics, and investigate deformations of the Extracellular Matrix (ECM) induced by cells. We have analyzed and modelled the mechanical properties of the ECM from a macroscopic perspective. Our fundamental assumption is that individual fibers can withstand tension but buckle and collapse when subjected to compression.

We compare two families of fiber mechanics models: Family 1, characterized by stable responses of individual fibers under compression, and Family 2, exhibiting unstable responses of individual fibers under compression. Our simulations expose diverse compression instabilities inherent to each Family. These instabilities lead to the formation of densely packed ECM regions, featuring strongly aligned fibers. These regions emanate either from individual contractile cells or join neighboring cells, mirroring observations from experiments. We show that both fiber alignment and ECM densification are prevented in the absence of elevated compression.

Our models demonstrate that material instabilities wield a dominant role in the mechanical behavior of the fibrous ECM. Despite substantial disparities in the responses of the two model families, our research underscores the pivotal role played by compression instabilities in the behavior of fibrous biological tissues. This has implications to a number of cellular and tissue processes, particularly in understanding cancer invasion and metastasis. Our findings introduce novel perspectives for investigating how fibers respond to deformations induced by cells and the ensuing implications for biomechanical interactions between cells.

Acknowledgements

Writing this thesis and conducting the research it documents, has been a long, meandering, and solitary journey. However, along this path, just as on all the roads that led me to it, I encountered numerous individuals who provided assistance, motivation, or nudged me in the correct course. Additionally, there were those who journeyed beside me, offering support, encouragement, and uplifting spirits. Here, I would like to take a moment and extend my heartfelt gratitude to all of these people. This thesis stands as a testament not only to my own efforts, but also to the indelible mark each of them has left on this chapter of my life.

I wish to express my deepest gratitude to my esteemed supervisors, Prof. Dr. Andreas Zilian and Prof. Dr. Phoebus Rosakis, for their consistent guidance, invaluable insights, and support throughout the entirety of my doctoral journey. Their mentorship has not only honed my research skills but has also contributed significantly to my personal and professional growth. Andreas placed his trust in me from the outset of this journey, without second considerations. Thus, I would like to first thank you Andreas; I am fortunate to have had the opportunity to work under your supervision and to benefit from your profound commitment to academic ethics. The genesis of this journey is attributed to Prof. Dr. Phoebus Rosakis. Therefore, I extend my heartfelt gratitude to you, Phoebus, for not only sharing this endeavor with me but also for affording me the autonomy to cultivate my research, as well as my professional and academic pursuits, in any manner that I saw it fit. I am grateful for your firm support which has been a cornerstone of my academic journey.

Additionally, I would like to extend my deepest appreciation to another great pillar of this work, Dr. Georgios Grekas, for his invaluable contributions to this research. I am indebted to Georgios for his endless patience, constructive feedback, and his willingness to engage in thoughtful discussions, which have significantly enriched the quality of my research. He has been an exceptional colleague and his insights have played a significant role in shaping the direction and quality of this work. Thank you Giorgos, I am truly fortunate to have had the privilege of working alongside you. You have been a source of inspiration and a true friend throughout this journey.

I am profoundly grateful to Luxembourg National Research Fund (FNR) for the generous funding I was awarded with and supported my doctoral research. This exceptional individual grant has been instrumental in enabling me to pursue my academic aspirations.

One of the main reasons these PhD years have been life changing for me is my involvement in Greek Women in STEM, which has become my second family. Through this volunteer organization, I have had the opportunity to grow as a scientist and as a person. Our collaborative endeavors in science communication and women empowerment have significantly influenced my enthusiasm and outlook on research. It is a profound honor to work alongside extraordinary women scientists, who inspire me in countless ways. To my dear superheroes, this loving, uplifting and resilient group of wonder women, thank you for your invaluable lessons and for

being a source of boundless support and creativity. I have learnt so much from each and every one of you.

The bedrock of my fortitude during these years came from the emotional sustenance provided by my friends, both longstanding and newfound, whether they were close by or miles away. Thank you to the extended family created in Luxembourg, Dimitrios Kyriakis, my dog Eddie, Kyriaki Barmpa and Giannis Karagiannis, for being there to address both the minor and major concerns, to celebrate, to argue, to explore, to dream. Gratitude goes out to those special individuals we crossed paths with, each contributing to my self-discovery and shaping my perspective as both a scientist and, above all, as a person. Lina Ntokou, Kelly Kousi, Tatiana Styliari, Danai Korre, Giannoula Mitrou, Vangelis Theodorakis, Georgia Kanli, Georgios Varisteas, Anastasia Seni, Vangelis Ikonomidis, Myrto Patraskaki, Anastasia Papangelou, Vasiliki Moschou, Alexandra Vatikioti, Maria-Grazia Vatikioti, Vu M. Chau, Michal Habera, Diego Kozlowski, Ilya Potapov and Srikanth Ravichandran. A heartfelt appreciation goes to my PhD-sister, Adelene Lai. In the most trying moments of this journey, you would offer me a safe place to breathe and a shoulder to lean on, providing a sanctuary to regather my strength. I extend my gratitude to the family of mentors for engaging in enriching discussions on scientific practice and providing invaluable guidance. Without them, my entire academic journey would have been markedly different, Tamara Aid-Pavlidis, Pavlos Pavlidis, Zacharias Papadovasilakis, Ioannis Iliopoulos, Emmanouela Kapsetaki, Tereza Manousaki, Panayiota Poirazi and Spyros Chavlis. I wish to extend a heartfelt acknowledgment to my exceptional friend Katerina Bopota, who didn't let me fall apart especially during the last painful stretch of this road. You were there, I mean —literally— everywhere; to laugh, to hold, to make me feel at home. I want to dedicate a sincere acknowledgment to my dearest friend Chrysa Kazantzidou who stood by me during the highs and lows, offering solace in times of frustration and celebrating every achievement, big or small. You have been wandering with me through the peaks of triumph and the valleys of self-doubt, offering sage advice, a listening ear, and unlimited empathy. I am deeply grateful for the countless ways you have enriched my journey, all these years. Last but not least, thank you to Iordan Iordanov, for being the first person that believed in my potential as a researcher. Your warmth, kindness, and bottomless support have been a guiding light. I firmly believe that I owe much of my presence here to you, your unconditional guidance and your invaluable friendship.

Finally, I would like to dedicate a special acknowledgment to my family, the tapestry of my academic journey, the threads that formed the unbreakable foundation, woven with love, sacrifice, and boundless encouragement. To the best friend I could ever hope for, Ioanna Athanasiadou, for every time I crumbled, you would hold my pieces carefully in your hands until I could put them back together. Thank you for always being the steady anchor in a sea of challenges. To my siblings, Zoe Kalaitzidou, Dimitra Kalaitzidou and Vasilis Kalaitzidis, you are the steadfast pillars, standing tall in the face of my absence and the demands of scholarly pursuit. Your unwavering pride in my accomplishments has been the wind beneath my wings. To my parents, Despoina Kalaitzidou and Ioannis Kalaitzidis, whose hearts beat in rhythm with my aspirations, you have been the compass guiding me through the uncharted territories of life. Your belief in me has been a beacon, lighting the path to knowledge and to life in general. In this tale, each chapter is dedicated to you, for you have penned the prologue of my milestones with ink made of love and understanding. This thesis is as much yours as it is mine. Σας ευχαριστώ για όλα. Είστε η δύναμή μου, πάντα.

Happiness can be found even in the darkest of times, if one only remembers to turn on the light.

— Albus Percival Wulfric Brian Dumbledore

Declaration of originality

I hereby confirm that the PhD thesis entitled *Unveiling the Hidden Language of Extracellular Matrix Deformations: A tale of cellular whispers and unstable fibers* has been written independently and without any other sources than cited or acknowledged. Furthermore, this doctoral thesis has been examined by the following committee members:

Prof. Dr. Andreas Zilian, supervisor .....
Department of Engineering, University of Luxembourg, Luxembourg

Prof. Dr. Phoebus Rosakis, co-supervisor .....
Department of Mathematics and Applied Mathematics, University of Crete, Greece

Prof. Dr. Alexander Skupin, chair .....
Luxembourg Centre for Systems Biomedicine, University of Luxembourg, Luxembourg

Prof. Dr. Stéphane Bordas, vice-chair .....
Department of Engineering, University of Luxembourg, Luxembourg

Prof. Dr. Ioannis Iliopoulos, external examiner .....
Medical School, University of Crete, Greece

Luxembourg, November 2023
Chrysovalantou Kalaitzidou

Table of Contents

CHAPTER 1

Introduction

Οὐθὲν γάρ μάτην ἡ φύσις ποιεῖ

Ἀριστοτέλης, *Πολιτικά I*

The study of biomechanics and its concepts are traced back to Aristotle (384-322 B.C.) and his classic *On the Parts of Animals*. Biomechanics is mechanics applied to biology. Specifically, it involves the exploration of the arrangement, function, and movement of living systems, spanning various scales from complete organisms to organs, cells, and even the smallest parts within cells. The motivation behind studying biomechanics is to understand how living things move and function and stems from realizing the fact that biology can no longer be understood without it. The field seeks to understand the normal, or sometimes the abnormal, functions of living things, their organs, and tissues under the presence of stimuli, and propose methods of artificial intervention. A very intriguing revelation that interconnects the fields of mechanics and biology is Robert Hooke (1635-1703). The English polymath gave us not only the so-called *Hooke's law* in mechanics but also coined the term *cell** in his book *Micrographia* (1665), during his observations that led to the development of the classical cell theory.

The cell is the fundamental building block of life. Cellular fate processes constitute a fundamental system of complex cascades of intracellular signalling pathways and interactions between cells and their microenvironment. Variations in the cellular microenvironment due to biochemical, mechanical and topographical signals regulate fundamental cell functions such as state, movement, shape and adhesion. Cells are continually faced with the complex task of sensing these variations and processing the signals internally through signal transduction and gene regulatory networks. However, each cell is not only controlled by its microenvironment but

* from Latin *cellula*, meaning "small room"

at the same time induces changes and modifications to it. This creates a dynamic relationship between cells and their surrounding environment, with the Extracellular Matrix (ECM) being a key element in this interaction. This interplay is of great interest as it modulates cell motility and migration in normal and pathological conditions, tissue morphology and cell-cell communication. But most importantly it entails the presence of forces and thus, mechanotransduction processes.

In this chapter, we introduce the Extracellular Matrix (ECM) and its characteristics that orchestrate specific mechanotransduction processes. We report important outcomes of these processes and present experimental cases that highlight their contribution specifically to intercellular communication which triggered the research herein. The chapter closes with the significance of studying this particular aspect of cell-ECM interaction.

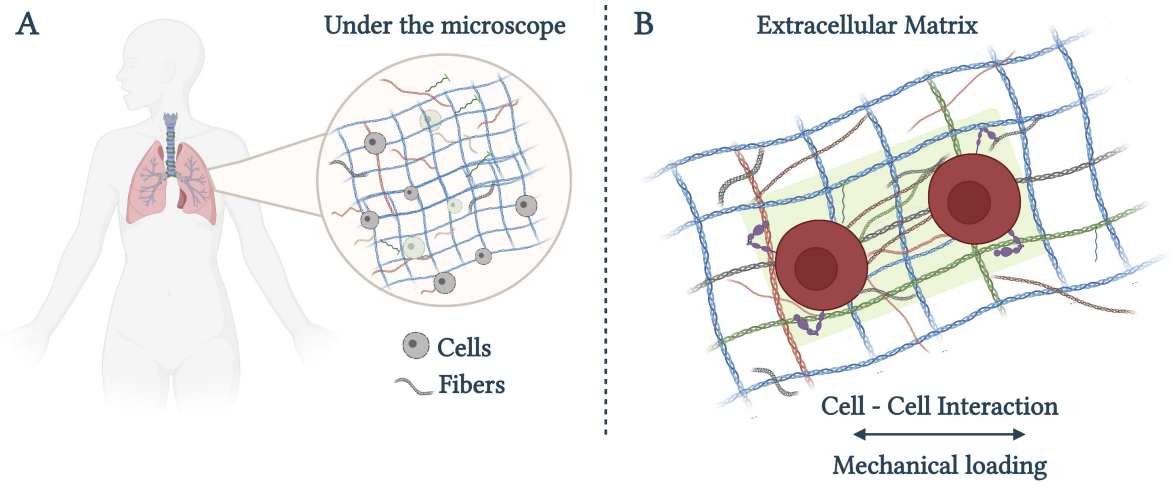

FIGURE 1.1. **Under the microscope: a glimpse inside our tissues.** Schematic depiction of the dynamic cellular microenvironment and its major component, the fibrous Extracellular Matrix (ECM).
Created with BioRender.com

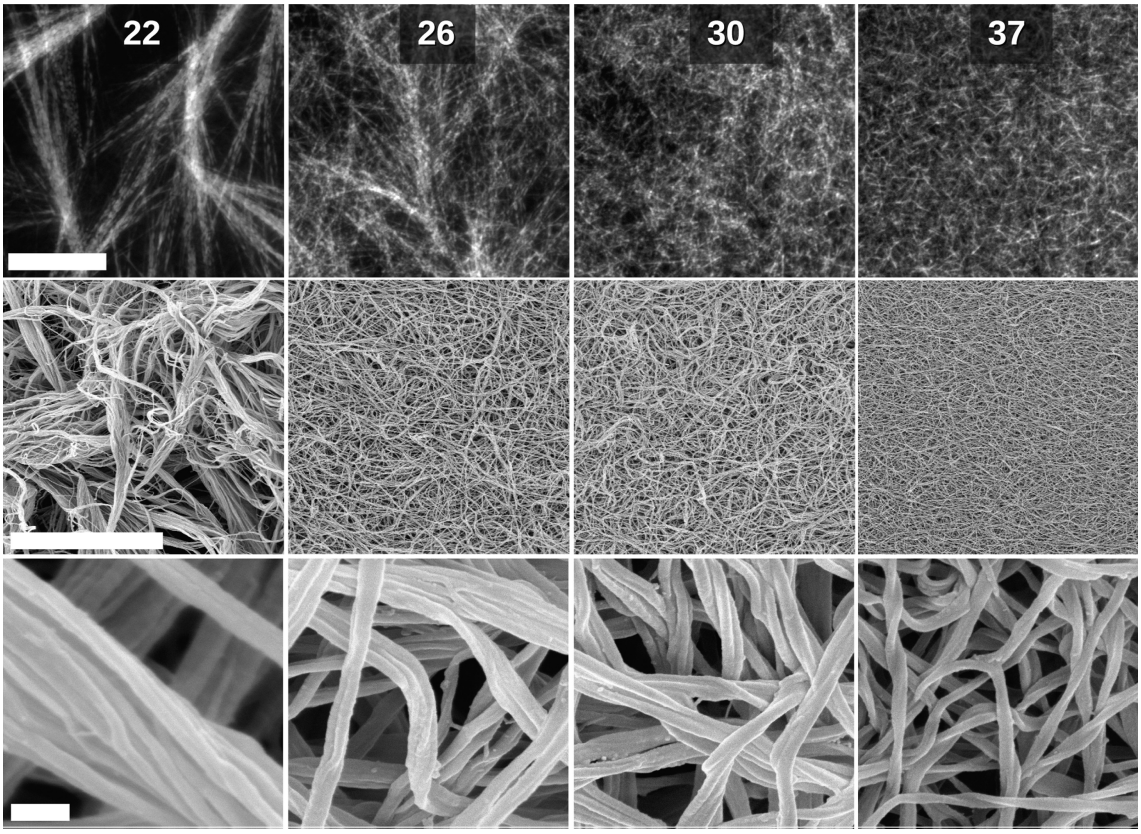

FIGURE 1.2. **The microstructure of a collagen network.** Temperature dependence of the microstructure of collagen networks at different temperatures indicated above each column (units of $°C$). *Upper row:* Confocal reflection images depicting an open network of collagen fibril bundles at $22°C$. Note that the network becomes more homogeneous and progressively denser as temperature increases. *Middle and lower row:* Scanning electron microscopy images at two different magnifications. The scale bars represent 20 mm (upper and middle rows) and 200 nm (lower row).
Reproduced from [36].

1.1 The Extracellular Matrix, a critical regulator of developmental dynamics

The Extracellular Matrix, an enigmatic tapestry woven into the very fabric of life, is a realm unseen yet profoundly felt. It is the silent architect, sculpting the stage upon which the drama of cells unfolds. Like a poet's ink, it composes the verses of tissue, a symphony of fibers, sugars, and proteins, where cells take their cues and dance their destinies. Within this intricate ballet, a narrative of adhesion, growth, and transformation plays out, whispered by the matrix's tactile whispers. A canvas for life's vibrant hues, it is a sanctuary of support and a realm of revelation, where biology's secrets are elegantly penned.

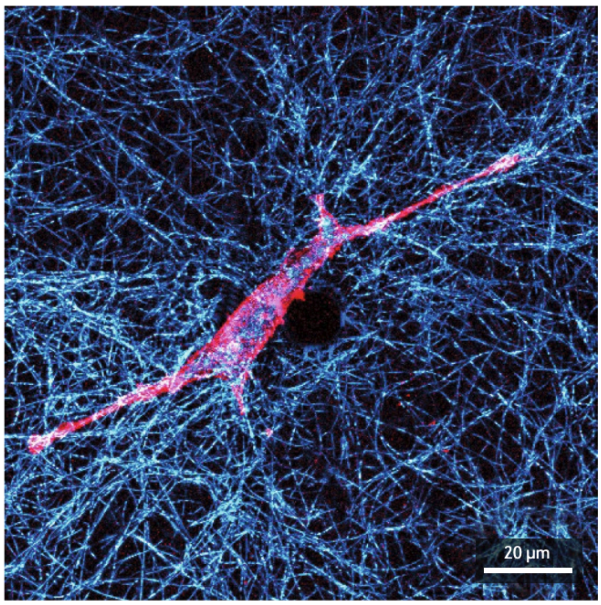

FIGURE 1.3. **The Extracellular Matrix.** An example of a collagen matrix (blue fibers) and a cell (in red). Reproduced from [10].

From a scientist's perspective, cells and tissues hold great intrigue due to their unique blend of impressive mechanical resilience alongside the ability to expand, alter form, and respond to surroundings. This special mix of strength and flexibility is vital for sustaining life. In fact, cells and tissues endure substantial mechanical forces, underscoring the significance of their mechanical robustness for survival and ability to adjust. For instance, lung epithelial cells experience significant tensile stresses with each breath we take [10]. As we move, our muscles, tendons, and skin stretch, while cartilage gets compressed. Cells and tissues manage these mechanical demands effectively, thanks to filamentous protein networks that serve as a highly effective form of structural support.

The extracellular matrix (ECM) (Fig. 1.2 - 1.3) is an intricate random network of fibrous proteins, such as collagen and elastin, organized in a tissue-specific manner and composed of an array of macromolecules with distinct physical and biochemical properties. While playing a fundamental role as the physical foundation for cellular components, the ECM also triggers vital chemical and mechanical signals necessary for tissue development and homeostasis. It

is also involved in repairing damaged tissue; abnormal changes in the matrix may lead to the development of certain diseases. In cancer, for instance, changes in the ECM physiology affect how cancer cells grow and spread [71]. At its core, the ECM is made up of water, fibrous proteins, and polysaccharides. Nevertheless, each type of tissue possesses an ECM that holds a distinct topology and structure. This uniqueness is established as the tissue develops, involving an interactive exchange of both mechanical and chemical signals among different cellular elements (like epithelial, fibroblast, and endothelial components) and the evolving protein environment. This bi-directional crosstalk between living cells and the ECM modulates various cellular functions such as proliferation, gene expression, differentiation and motility. Essential aspect of this crosstalk refers to the mechanical state of the matrix. Cells have the ability to perceive and react to the physical properties of the matrix by producing forces. Simultaneously, they detect any changes happening in their surroundings. This capacity of cells to recognize and respond to mechanical action in their environment is termed as *mechanosensing*.

Mechanosensing is a fundamental biological process that plays a crucial role in various physiological and developmental processes. At the cellular level, mechanosensing involves specialized proteins and structures that are capable of converting mechanical stimuli into biochemical signals. These mechanosensitive proteins are typically located on the cell membrane or within the cytoskeleton. They can sense a wide range of mechanical forces, including tension, compression, shear stress, and fluid flow. Key components of mechanosensing are integrins (Fig. 1.4), transmembrane proteins that connect the ECM to cell's cytoskeleton. When mechanical forces are applied to the ECM, integrins undergo conformational changes, transmitting the force to the cytoskeleton and initiating a signaling cascade within the cell through mechanotransduction, a process through which cells convert mechanical forces into biochemical signals and cellular responses [41]. Mechanotransduction is a complex and dynamic process that involves a network of mechanosensitive proteins, signaling molecules, and downstream effectors. This process enables cells to actively detect and respond to physical cues from their surroundings [53]. This helps with the morphogenesis, development, and adjustment of tissues to cope with shifts in mechanical conditions. The signaling pathways activated by mechanotransduction ultimately lead to specific cellular responses. The way cells react can differ based on the specific cell type and situation. However, typically, these responses involve adjustments in cell shape, movement, growth, specialization, release of signal substances, or modifications in the ECM. Most importantly, these responses influence how cells interact with each other. Cells are not isolated entities but exist in a dynamic environment where they interact with neighboring cells. These interactions involve biochemical exchange, physical contacts as well as mechanical forces, which can influence cellular behavior and communication. Cells can both transmit and receive mechanical cues, allowing them to coordinate their responses with neighboring cells. Mechanical forces generated by one cell can be transmitted through the extracellular matrix to neighboring

cells, altering their behavior. Similarly, cells can sense mechanical cues from their surroundings and respond by adapting their own mechanical properties and signaling activities.

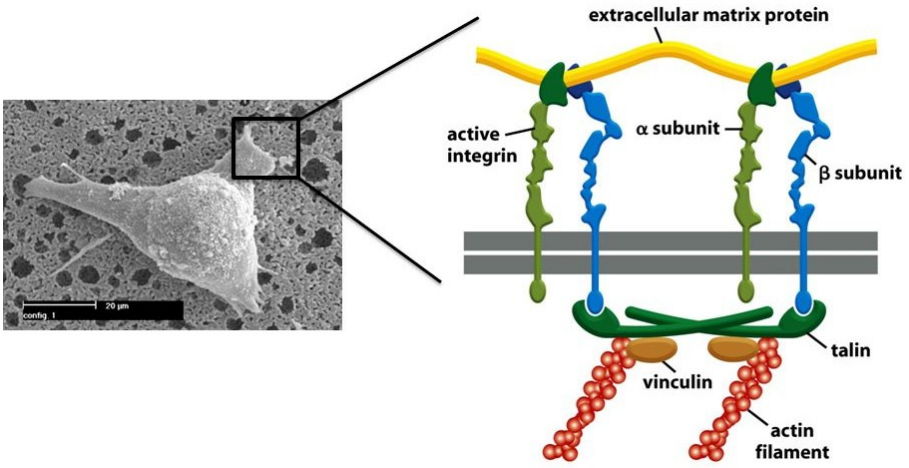

FIGURE 1.4. **Integrins anchor the cells to the matrix.** A scheme of cell surface integrin binding to ECM fiber protein.
Source: Owen Mason, Lecture *The ECM, Cell Adhesion, and Integrins.*

The physical signals present in the Extracellular Matrix (ECM) have a central role in coordinating how cells act and how tissues change over time. Thus, the ECM is not a passive structural scaffold, but rather a dynamic interface that actively communicates with cells through mechanical signals. These cues encompass a spectrum of mechanical forces, including tension and compression, that deform the matrix in interesting ways and bring about unique patterns with significant implications.

1.2 Tales from Biology

The Extracellular Matrix (ECM) is a landscape where tales of fundamental cellular functions such as adhesion, migration, and growth are written. The mechanical cues in the ECM are like verses etched into life's parchment, their eloquence shaping tissues, sculpting destinies, and writing tales of health and malady. A certain tale arises from a profound dialogue that unfolds between neighboring cells, a communication far beyond spoken words. In this unspoken language, tissues form, wounds heal, and whispers of diseases arise. The cell-cell mechanical communication within the Extracellular Matrix is a ballet of forces, a choreography of touch that shapes life's narrative, transforming biology into an orchestra where each note is felt, not just heard.

The mechanical dialogue between cells and the ECM is dearly important as it regulates a number of cellular processes [15, 56]. Ranging from cell motility and migration in physiological [45, 58] and pathological [59, 61, 64, 79] conditions, stem cell differentiation [17, 22], as well as cell and tissue morphology [31, 70, 74, 83], the force-generated crosstalk between cells and matrix underlies important aspects of cell and tissue dynamics. Important feature of this crosstalk is the intrinsic actomyosin machinery which enables cells to contract. By contracting, cells pull at the fibers on which they are attached. As cells contract their microenvironment, it triggers a series of actions that lead to notable alterations in structure that can stretch over distances equivalent to tens of cell diameters [29, 31, 52, 81]. These phenomena lay the groundwork for far-reaching cell-cell mechanical communication, a process that mechanically bridges distant cells, orchestrating intricate processes like capillary sprouting [42] and synchronized beating [50]. This cell-induced tension in the matrix results in the formation of some very special structures that entail fiber rearrangements. The importance of the appearance of such structures lies in experimental observations since as early as the previous century, which revealed a strong relation of these structures with cell orientation, motility and coordination with other cells.

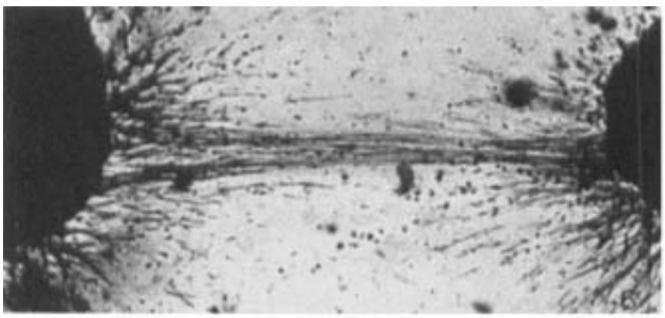

FIGURE 1.5. **Two ganglia connected by a tract of cells and fibers.** Early observations of a dense pattern consisting of roughly parallel lines that connect two contracting clusters. Weiss called this pattern *bridge*. Cells from both ends were observed to enter the bridge and travel towards the opposite center. Reproduced from Paul Weiss, 1934.

Back in 1934, Paul Weiss in his work *In vitro experiments on the factors determining the course of the outgrowing nerve fiber* examined the leading role of mechanical structures in orienting the growth of nerves. He started with the assumption that nerve fibers in tissue culture should be subjected, if possible, to all of the following conditions: chemical, electrical and mechanical, which were then believed to guide the nerve growth of neuroblasts. However, due to his past experience with different cell types, he believed that the mechanical factor would be the most important one; his previous results demonstrated that "cell patterns in vitro arise on the basis of corresponding structural patterns in the medium in which the cells move and grow". Remarkably, his experiments with neuroblasts exposed additional important aspects. When neuroblasts were cultured alone, the nerve fibers grew in various directions without any noticeably preferred orientation. However, where neuroblasts were mixed with proliferating glial cells, their nerve fibers tended to follow paths where significant tension was generated. The contrast between the reactions of pure nerve cultures and mixed nerve cultures provided an important clue. It was observed that the necessary tension to create guiding structures in the environment only occurs when some form of *contraction* is present, induced when the rapidly growing glial cells in the mixed cultures kept dehydrating their surrounding medium by absorbing enough water from the surrounding extracellular matrix, leading it to contract or shrink.

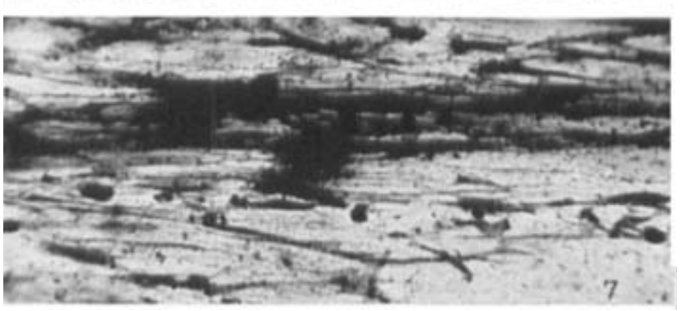

FIGURE 1.6. **Definite orientation of cells and nerve fibers along the organized *bridge*.** Higher magnification of Fig. 1.5 depicting cells and nerve fibers moving along parallel lines over the *bridge* that interconnects the two centers. Reproduced from Paul Weiss, 1934.

Strikingly, apart from this orientation effect guided by tensional pull, Weiss' experiments with neuroblasts exposed an additional prominent aspect: **the formation of connecting tracts between two contracting cell clusters.** When he wondered what must be the system of tensions arising from two centers of contraction and carried on with the experiments, he exposed a unique structural reorganization of the medium: a dense arrangement of nearly parallel lines that link the two contracting centers. He called this characteristic pattern *bridge*, as it not only seemed to connect the two clusters but served as a highway that cells from both ends use, move along it and finally reach the opposite center. His observations, though, did not stop there. Apart from the definite, sharp orientation of the cells and fibers along the organized 'bridge' one is struck also by the

fact that cells and their nerve fibers grew much farther in that particular direction than in any other. This specific finding indicated that growth consistently improves in the 'organized' parts of the medium. Weiss further explained that this growth enhancement along the organized areas is mostly because the cells in those regions have a smoother access to the nutritious and growth-promoting fluids present in the medium. This smoother access is a result of the unique mechanical characteristics of the 'organized' zones themselves. This particular study not only revealed these unique observations but most importantly showed that, both the directive and growth-promoting effects, which create straight links of cells and fibers connecting two growth centers, can be adequately understood by considering the mechanical restructuring of the medium, including the formation of the 'bridge', excluding any other chemotactic events. But why? Well, the explanation lies in the necessary presence of contractile activity. 'Bridges' connecting two cell cultures arose only when both cultures kept dehydrating their surrounding medium and, in turn, this dehydration shrinkage would result in tensile tractions. In experiments with cultures containing only neuroblasts, no contractility and thus no tension were induced and, consequently, no 'bridge' formed; there was not any trace of mutual influence between the two cell centers with regard to orientation and growth rate of the outgrowing nerve fibers. On the contrary, nerve fibers of neuroblasts exhibited a rather haphazard distribution, with no inclination to deviate from their random courses and orient toward the neighboring culture. Noticeably, the resulting irregular pattern of the nerve fibers was not different from what it would be expected if the two centers had been cultivated each in a separate medium. As a result, the nerve fibers in these conditions didn't show any tendency to align with the opposing culture. This strongly suggested that their orientation was indeed influenced by the presence of underlying oriented structures, provoked by the cells' own contracting activity in the related cultures, which was prompted by the dehydration of the metabolic medium. Weiss attributed the contractility and its important effects to the presence of glial cells and particularly their proliferation that induced dehydration of the substrate.

Decades after this classic work of Weiss, Stopak and Harris in 1982 and their seminal work in [74] demonstrated that Weiss' proposed dehydration theory is inadequate to explain the distortion of collagen gels around clusters of cells. Through experiments involving hygroscopic salts and rapidly growing but weakly contractile transformed fibroblasts, they established that these distortions in collagen structure are not caused by dehydration or other chemical changes resulting from cell metabolism. Instead, these distortions stem directly from the effects of cell contractility. In fact, their findings revealed that the distinctive distortion caused by glial cells, as compared to neuroblasts, is attributed to the greater contractile strength of the former, rather than their rate of growth as Weiss had suggested. Specifically, their observations highlighted that it was the connection between glial cells and the surface they adhere to, coupled with the contractile forces generated during their movement, that led to the deformation of

the substrate. Notably, these specific experiments unveiled two distinct forms of substrate deformation associated with glial cells (Fig. 1.7):

- *compression wrinkles* appeared directly underneath individual cells, running perpendicular to the cells' long axes, and to their direction of locomotion
- *tension wrinkles* extended radially outward from the edges of the cells, and formed parallel to the cells' long axes.

Furthermore, they conducted experiments using explants containing fibroblasts. When two explants were cultured together in the same dish, the collagen fibers reoriented themselves to align parallel with the line connecting the two cell clusters. This area of alignment formed a discontinuous tract that extended linearly through the matrix, approximately one-third the diameter of each explant.

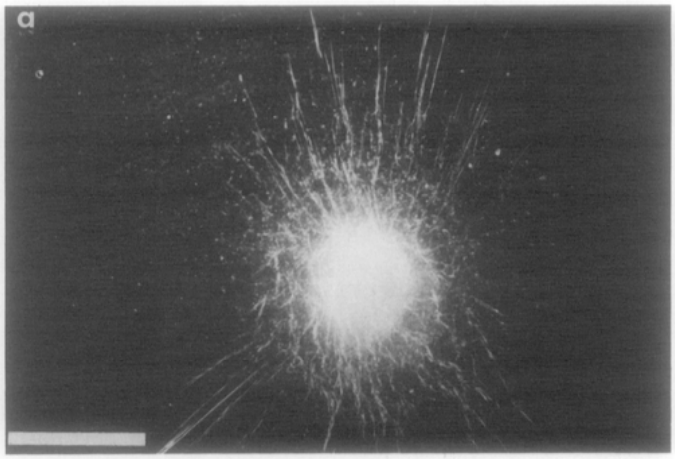

FIGURE 1.7. **Wrinkles emanate from a single ganglion.** Matrix distortion around a single ganglion (bright body in the center). We observe the wavy lines which surround the ganglion, termed as *wrinkles*. The wrinkles emanating radially and extend a few millimeters outward from the ganglion are tension wrinkles, whereas compression wrinkles take on a more intricate arrangement that surrounds the ganglion circumferentially. Scale bar equals 1 mm. Reproduced from [74].

Importantly, this realignment of collagen between the explants led to the alignment of fibroblasts and prompted their movement towards the adjacent explant. While this new alignment pattern formed between the explants, the original radial alignment in the form of wrinkles remained unaffected on the opposite sides of the explants (Fig. 1.8). On these sides, extra pathways of well-aligned collagen developed, extending over significant distances toward the edge of the substrate. These supplementary collagen tracts exhibited a similar appearance, density, and width to the ones that emerge between the explants. Finally, when additional explants were dispersed within a collagen gel, they formed a pattern comprising a series of axial traction fields and collagen alignment linking pairs of nearest neighbors.

This study overall highlighted two important aspects of extracellular matrix cell-induced deformations. To begin with, the ability to contract is crucial for the striking spatial arrangements

of increased density and fiber alignment. Secondly, in the regions between explants, the centripetal force orchestrates the alignment of collagen fibers into linear pathways. However, in the immediate vicinity of the explants, this traction effect results in the compression of collagen fibers, forming a compact, capsule-like circumferential enclosure.

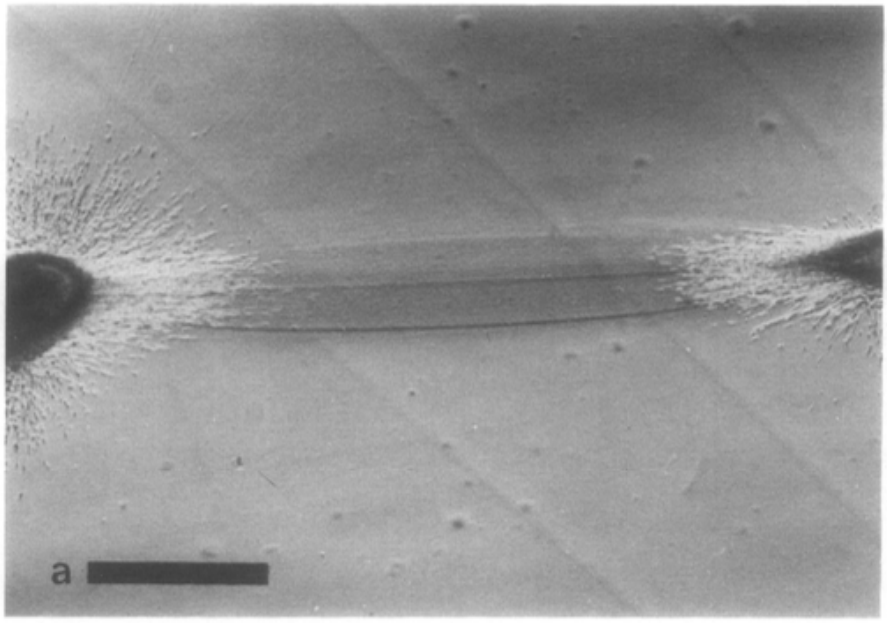

FIGURE 1.8. **Axial fiber alignment between explants.** When two explants were cultured together, collagen fibers underwent realignment, arranging themselves parallel to the axis that connected the explants. This aligned region was observable as a discontinuous dense segment cutting straight across the matrix. The width of this aligned area was roughly one-third the diameter of an individual explant. Scale bar equals 1mm.
Reproduced from [74].

The essential findings described above were backed up by more recent studies. In particular, Provenzano et al. in [61] showed that when collagen fibers align perpendicular to the boundary of tumor-explants, it encourages local invasion of both human and mouse mammary epithelial cells (Fig. 1.10). They explain that cells achieve this by using their contractility to rearrange the extracellular matrix (ECM), aligning the collagen framework. This alignment offers a pathway that guides cell movement, as cells make use of these organized pathways like roadways. Additional cancer studies have demonstrated the preference of tumor cells to invade along densified regions of ECM [19, 61, 84]. In another pivotal study, Notbohm et al. in [52] conducted experiments with contractile fibroblasts and revealed that densified bands of aligned fibers were spotted to join individual cells as well (Fig. 1.9). They reported measurements of three-dimensional matrix displacements induced by cells and documented the following observations:

i. Displacements decrease at a considerably slower rate with increasing distance from the cell compared to what linear elasticity would predict.

ii. Densification of the matrix and pronounced fiber alignment occur specifically within bands that connect individual cells. These densified bands were termed *tethers*.

iii. Cells react to localized tension by extending protrusions towards each other, a response guided by the densely aligned fibers present within these tethers.

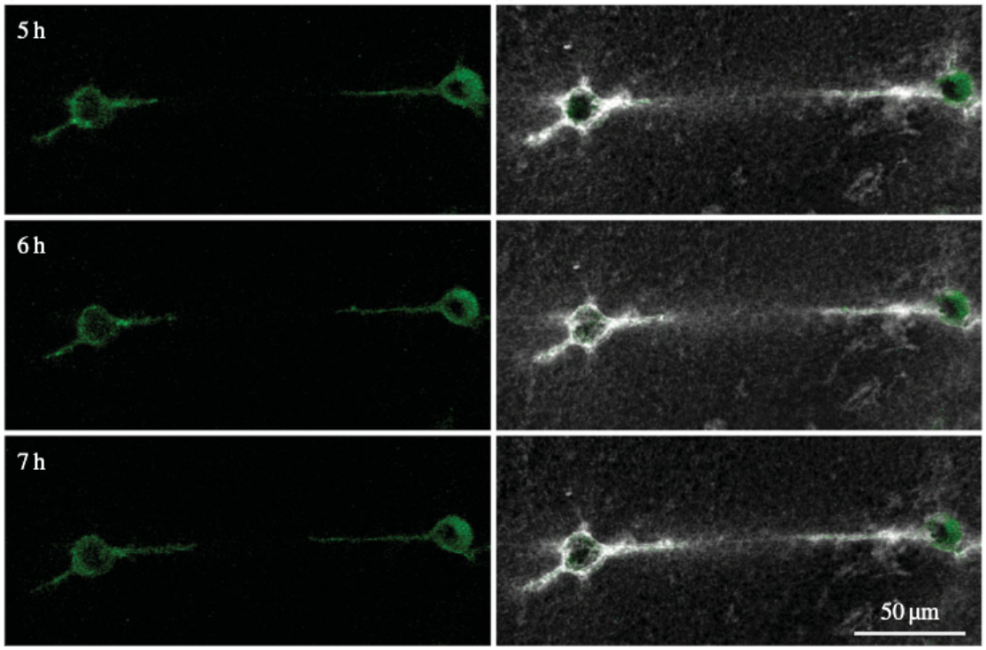

FIGURE 1.9. **Cells extend protrusions towards each other along densified matrix regions.** Pairs of cells 5,6 and 7 hours after they have been seeded in a fibrin matrix. The cells induce tensile forces to the matrix which result in *tethers* that connect the two cells. White regions indicate high density of fibers. The cells grow protrusions along the tethers.
Reproduced from [52].

Whether they are called “bands”, “tethers”, “wrinkles”, or “bridges”, these striking structural patterns exhibit intensified fiber alignment and substantial material densification due to cell contractility and mechanosensing processes. While the exact mechanism leading to their development remains unestablished, the provided evidence strongly suggests their involvement in mechanical intercellular communication, as well as cell motility and invasion, and underscores the importance of understanding the mechanism behind their formation. To achieve this, it becomes imperative to elucidate ECM behavior when subjected to cell-induced forces by unveiling its mechanical properties that facilitate such deformations.

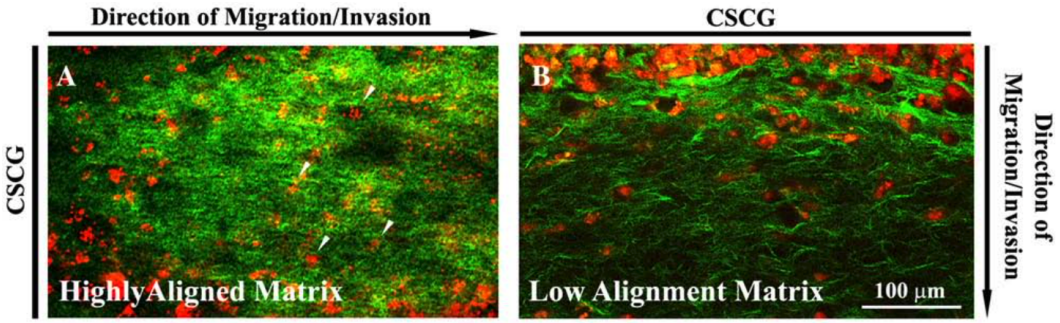

FIGURE 1.10. **Carcinoma cells invade into aligned collagen matrix.** Carcinoma cells primarily exhibited invasive behavior within aligned regions of the matrix. This observation implies that the radial alignment of collagen fibers offers directional guidance through distinct alignment of the collagen matrix. The extent of migration into these aligned regions significantly surpassed the migration seen in cells invading regions with low alignment.
Reproduced from [61].

1.3 A symphony of mechanical traits within the Extracellular Matrix

Within the ECM, mechanical cues, like ancient scrolls of wisdom, convey tales of tension, compression, and gentle caresses. These cues are not mere vibrations lost in the void; they are the architects of cellular destiny, guiding dances of adhesion, migrations of purpose, and metamorphoses of growth. Imperative it becomes to delve into the subtle undertones, the intricate symphony detailing the mechanical properties of the ECM. A necessary precursor to this endeavor resides in unfurling the tapestry of its structural essence, a canvas inherently shaped and reshaped through the caress of traction fields woven by the orchestrating cells. This indispensable groundwork shall discern the profound artistry of cells, shaping their surroundings with purposeful intent; a prelude necessary to fathom the orchestration of ECM deformations.

It is crucial to investigate and comprehend the subtext that describes the mechanical traits of the ECM and supports the promotion of a desired cell function. Essential prerequisite to this is to explore ECM structural characteristics and how they are being deformed as a result of traction fields that cells create. These factors taken together will aid our understanding in how cells alter the environment around them to drive a particular function, which in some cases leads to the emergence of a disease.

Across diverse tissues, the mechanical properties of the ECM exhibit variability and assume a pivotal role in tissue development, homeostasis, and disease processes. In general, the ECM's key mechanical traits encompass the following:

- **Remodelling:** The ECM exhibits the ability to remodel. As we have extensively disscussed

in (1.2), cells can actively modify the composition and organization of the ECM in response to mechanical cues and other stimuli. This remodeling capability allows tissues to adapt to changing mechanical environments and is crucial during processes such as wound healing, tissue regeneration, and tissue remodeling in response to disease or injury.

- **Elasticity and Stiffness:** ECM stiffness describes how resistant it is to deformation under applied forces. The ECM can exhibit a wide range of stiffness, from soft and compliant (e.g., brain tissue) to stiff and rigid (e.g., bone tissue) [30]. This stiffness is determined by the composition, organization, and crosslinking of ECM components. The ECM's elasticity describes its ability to return to its original shape after deformation, and it is influenced by factors such as the density of crosslinks and the presence of elastic fibers like elastin. ECM stiffness and elasticity play a critical role in cell adhesion, migration, differentiation, and tissue integrity and homeostasis.

- **Nonlinearity:** The ECM displays nonlinear mechanical behavior [34, 80], meaning its response to forces is not strictly proportional. The fibrous matrix displays a nonlinear elastic response that is manifested by *strain stiffening in tension* [32, 57, 75, 78, 80] and *compression softening due to buckling* [8, 40, 49, 52]. These effects stem from the mechanical behavior of the individual fibers that constitute the matrix. Fibrous proteins exhibit a unique nonlinear behavior which is attributed their natural structure. We will discuss later more details on this.

- **Anisotropy:** Many tissues display anisotropic behavior [24, 54], meaning that their mechanical characteristics change based on the direction in which forces are applied. For example, tendons have higher stiffness along the direction of collagen fibers, enabling them to resist tensile forces efficiently. Anisotropy arises from the organization and alignment of ECM fibers within tissues.

- **Heterogeneity:** The ECM is remarkably diverse in terms of its composition, structure, and mechanical properties [47]. Different regions of a tissue or even adjacent ECM components can exhibit variations in stiffness and other mechanical characteristics. This heterogeneity affects how mechanical forces spread within tissues, which can strongly impact how cells behave and how tissues function.

The intricate mechanical behavior of the Extracellular Matrix (ECM) is ascribed to an interplay of factors, encompassing the physiology, organization, and interactions of its diverse components. Thus, in order to unveil the profound mechanics of the ECM under loading, we need to investigate its composition and the structural characteristics of the individual fibers.

The physical composition of the ECM is not only tissue-specific, but is also noticeably heterogeneous. The ECM is made up primarily of two types of large molecules: proteoglycans (PGs) and fibrous proteins. The primary fibrous proteins in the ECM include collagens, elastins

and fibronectins [20]. Proteoglycans, in the form of a hydrated gel, occupy most of the extracellular space within the tissue. The role of fibrous proteins is primarily structural. They provide strength and resistance to stresses and they contribute overall in maintaining tissue homeostasis.

Collagen

Collagens (Fig. 1.2), which constitute the core structural component of the ECM, provide strength under tension, givern cell adhesion, aid in chemotaxis and movement, and guide tissue growth [67]. Collagen fibers are made up of collagen molecules that assemble into a hierarchical structure. Collagen fibers contribute to the mechanical strength and stability of tissues. Their structural arrangement allows them to resist tensile forces, providing tissues with resistance against stretching and deformation. Collagen fibers undergo continuous remodeling throughout life to maintain tissue homeostasis and repair damage. Specialized cells called fibroblasts are responsible for synthesizing and remodeling collagen fibers. During tissue repair processes, new collagen is deposited to replace damaged or degraded fibers, helping to restore tissue structure and function. Collagen associates with elastin, another crucial fiber within the ECM.

Elastin

Elastin fibers are a type of fibrous protein found in the extracellular matrix (ECM) of various tissues. They are primarily responsible for providing elasticity, resilience, and recoil properties to tissues that require flexibility and stretching capabilities. Elastin fibers are most abundant in tissues such as the skin, lungs, blood vessels, and elastic cartilage. Elastin fibers provide tissues with the ability to stretch and deform under mechanical forces and then return to their original shape. This elasticity is crucial for maintaining tissue integrity, allowing tissues to expand and contract, and ensuring proper functioning of organs like the lungs and blood vessels. Elastin fibers store mechanical energy during deformation and release it during recoil, contributing to the efficient functioning of elastic tissues.

Fibronectin

Fibronectin (FN) is pivotal in adjusting cell attachment and function. Moreover, it directly contributes to the organization of the interstitial ECM. Cellular forces can stretch FN multiple times its original length, as observed in [72]. This stretching unveils concealed integrin-binding sites within FN, which leads to a wide range of alterations in cell behavior. These changes highlight FN's role as an extracellular mechanoregulator.

Fibrin

Fibrin, yet another fibrous protein, is crucial for maintaining homeostasis and plays a significant role in processes like blood clotting, wound healing, and various other biological functions and medical conditions [35]. Within a blood clot, a network of fibrin forms the sturdy backbone,

offering mechanical support and durability. This fibrin network acts like a structure that captures blood cells, platelets, and other elements, forming a clot. It serves as a scaffold for repairing and regenerating tissue, enabling cells to move into the wounded area and encourage healing.

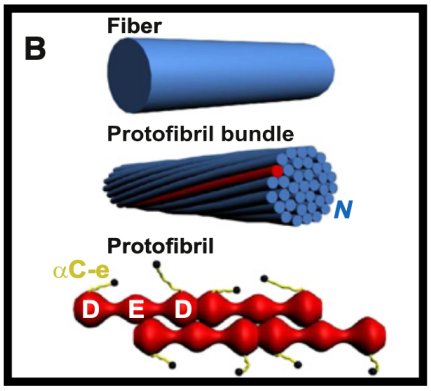

FIGURE 1.11. **Fiber hierarchical structure.** Illustration of fibrin fibers and their hierarchical architecture: at the top, fibers are collections of protofibrils (shown in the middle); these protofibrils, in turn, are made up of two partially aligned strands of fibrin monomers, as depicted at the bottom.
Reproduced from [57].

Fibrous proteins exhibit a hierarchical structure that aligns with their specialized roles in providing mechanical support, elasticity, and structure to various biological tissues. This hierarchy encompasses different levels of organization, each contributing to the protein's overall function. Specifically, the extracellular polymers form complex filaments with an exceptionally structured molecular arrangement, driven by particular interactions among the component proteins. For instance, fibrin fibers are made up of collections of protofibrils (Fig. 1.11, middle). These protofibrils, in turn, consist of two strands of fibrin monomers arranged in a staggered manner (depicted at the bottom of Fig. 1.11). These monomers are composed of three pairs of polypeptide chains named Aa, Bb, and g. These chains are folded into a central E-region and two outer D-regions. This intricate arrangement gives fibrin fibers a multifaceted and hierarchical structure. Similarly, collagen's hierarchical organization spans multiple levels. This intricate organization grants collagen its unique ability to endure tension, making it a principal contributor to tissue strength. In bone, it provides rigidity; in skin, it maintains elasticity; in tendons, it confers tensile strength. The hierarchical structure of fibers becomes of paramount importance when subjected to loading, as it directly influences their mechanical response, durability, and ability to withstand forces. The arrangement of different structural levels, from the molecular to the macroscopic, allows fibers to absorb and dissipate energy, preventing sudden fractures or deformations. This is particularly crucial in materials like bones and tendons, which experience varying and dynamic loads. In essence, the hierarchical structure of fibers under loading conditions ensures that biological tissues can effectively handle physiological stresses. This organized architecture prevents structural failure, maintains tissue function, and enables the seamless adaptation of tissues to changing mechanical demands.

1.3.1 When fibers bear the weight

When fibers bear the weight of the world, they become tales of strength and resilience, embodying the secrets of fortitude woven into their very essence. Amidst the trials of tension and the dance of compression, fibers are the protagonists in a story of endurance. They harmonize with the demands of the world, each strain etching its chapter into their very being. With every load they bear, they reveal the artistry of their hierarchical design, distributing the burdens of existence with an elegance that belies their simplicity.

The way natural fibrous matrices respond to mechanical forces is directly linked to how their individual fibers react mechanically. Thus, in order to explore ECM deformations, we need to address how a single fiber behaves when subjected to external forces. As discussed above, one of key mechanical traits of the ECM refers to nonlinearity: in general, the fibrous matrix exhibits nonlinear elastic responses, which are evident through the effects of compression softening and tension stiffening. We saw that rather than homogeneous rods, ECM fibers have a bundle-like morphology (Fig. 1.2) characterized by a complex hierarchical structure (Fig. 1.11) [10, 57]. This assembly gives rise to unexpected mechanical effects when fibers are subejcted to external forces. In particular, subjected to large strains, fibers can be extremely extensible without breaking [10] and they stiffen with increasing tension [32, 78]. When tension increases, the stiffness or resistance to deformation also increases. Initially, when the material is under low levels of tension, the fibers may have a loose or random arrangement. When tension is exerted, the fibers start to elongate and align themselves in the direction of the applied force. This alignment and stretching increase the effective stiffness of the fibers, resulting in a higher overall stiffness of the matrix. Matrices stiffen as they are being increasingly deformed, in order to prevent deformations that could threaten the structural integrity of a

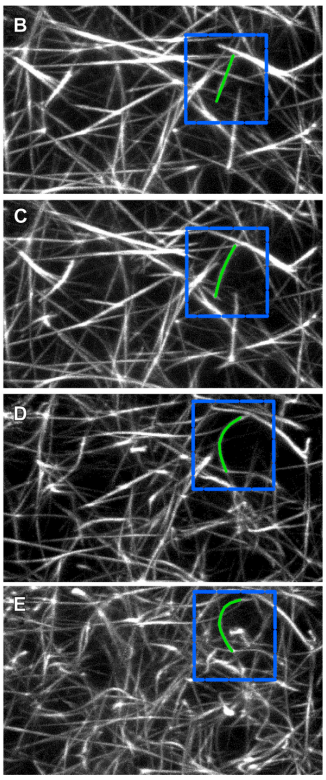

FIGURE 1.12. **Fibers buckle under compression.** Alterations in the structure of a fibrin network as it undergoes various levels of compression. We witness a single fiber (blue boxes) undergoing a gradual series of buckling. With an escalation in the level of compression, the fiber takes on an increasingly distinct curve, and the network becomes tightly packed. Reproduced from [40].

tissue. The characteristic where stiffness grows as deformation increases is referred to as *strain stiffening* and is a vital mechanical trait of fibrous matrices.

Previous studies [7, 11, 13, 34, 39] verified that fibrous matrices exhibit lower stiffness in compression than in tension. And indeed, the cases where fibers are subjected to compressive forces are particularly interesting. Fibers under compression buckle, losing stiffness and eventually collapsing [9, 43, 52, 66]. In Fig. 1.12 (Fig. 5 in [40]) we see an example of fiber buckling. The blue boxes emphasize a single fiber that gradually buckles under varying compressive strains within a fibrin network. As the degree of compression within the network intensifies, the individual fiber displays a growing curvature, ultimately culminating in its complete collapse (buckling). The reduction in stiffness when the matrix is subjected to compressive forces is known as *compression softening*. However, when it comes to compression, things are not trivial.

Fibers become unstable under compressive loading

Lakes et al., in [43] studied compressive behavior in the larger scale of open cell foams. Their experiments revealed multiple regimes of force-stretch* response marked by a nonlinear softening *instability* in compression. The cause of the instability was identified as buckling of fibers or polyhedral fiber elements [43]. The same theory, i.e. fiber buckling, was used in [40] and their experiments with fibrin networks to describe the behavior we see in Fig. 1.12. Through these experiments, two distinct transitions between softening and hardening were unveiled as the networks underwent compressive loads. Specifically, softening emerged at lower and intermediate levels of compression, whereas hardening became prominent with greater degrees of compression. These experiments highlighted that the softening of the fibrin network resulted from the buckling and bending of individual fibers when subjected to compression (Fig. 1.12). In both cases, the material instabilities were identified as a special nonlinearity in individual fibers under compression. The fundamental ingredient of this nonlinearity is a non-monotonic microscopic force-stretch response marked by a softening-stiffening (hardening) transitional response to compression. This means that a fiber under compression shows resistance to a compressive force (becoming stiffer) before it collapses (buckling).

More recently, Tarantino and Danas performed uniaxial compression experiments on beams with hierarchical structure [76] that resembles the hierarchical structure of fibers. These experiments revealed a post buckling response that is much more unstable than that of homogeneous (non hierarchical) beams. This response remarkably involves a transition from hardening to softening with increasing compression.

Overall, these studies highlight that the mechanics of single fibers under compression is far more complicated. Fibers exhibit unstable behavior under compression, as this hardening regime, where they resist the compressive loading, that proceeds their collapse (softening) leads to unexpected effects.

* *stretch*: measure of extension, the ratio between the final and the initial length of a material line

1.4 Crafting the fiber symphony: a journey through virtual realms

Fibers bow and sway, revealing the secrets of their vulnerability and resilience. Meanwhile, tension paints a portrait of adaptability, where the matrix learns to waltz gracefully between rigidity and compliance. This ballet of mechanics, guided by the cells' gentle embrace, weaves the narrative of tissue's strength, responsiveness, and its delicate equilibrium between creation and adaptation. Emerging like starlight, computational models assume the mantle of essential companions in exploring the intricate dance of ECM deformations, gifted with the power to choreograph complex mechanical phenomena.

How fiber mechanics entangles with cell-induced deformations? In other words, considering what we know so far about the behavior of individual fibers under loading, how can we investigate cell-induced deformations and predict certain patterns that have been observed and analyzed experimentally?

Computational models arise to this aid as essential tools for investigating ECM deformations due to their ability to simulate complex mechanical behaviors, bridge knowledge gaps, and offer insights that are challenging to obtain through experiments alone. Several key reasons underscore the importance of using computational models in studying ECM deformations:

- **Complexity:** The ECM is a intricate arrangement of fibrous proteins and cells. Computational models can capture this intricate structure and simulate the interactions between its components, providing a holistic view of the mechanical behavior.

- **Predictive Insights:** Computational models allow researchers to predict how the ECM will respond to different loading conditions, aiding in understanding how tissues react to mechanical forces and guiding potential interventions or treatments.

- **Inaccessible Scales:** Some aspects of ECM behavior occur at microscopic or molecular scales, making direct experimental observation difficult. Computational models can simulate these scales, providing insights into behaviors that are challenging to measure experimentally.

- **Time Efficiency:** Simulating ECM deformations computationally can be much faster than conducting physical experiments, enabling researchers to explore a wide range of scenarios in a shorter time frame.

- **Understanding Mechanisms:** Computational and mathematical models allow researchers to isolate specific mechanisms contributing to ECM deformations, aiding in deciphering complex mechanical responses. Furthermore, they facilitate the exploration of

how different parameters, such as material properties or loading conditions, affect ECM behavior. This helps identify critical factors influencing deformations.

In essence, computational models serve as virtual laboratories, enabling researchers to explore and understand the mechanics of the ECM across different scales, loading conditions, and scenarios. They complement experimental techniques, enhance our understanding of tissue behavior, and offer valuable insights for biomedical research, tissue engineering, and clinical applications.

When it comes to computations, mathematical models that describe the constitutive mechanical behavior of a fiber are being used. A constitutive relation for a fiber is a mathematical description that defines the mechanical response of the fiber under different loading conditions. In essence, it outlines how the fiber's deformation and stress are related to the applied forces. This relation provides a quantitative understanding of how fibers behave under various mechanical scenarios. The importance of a constitutive relation for fibers lies in its ability to capture the intricate mechanical behavior of these essential structural elements. Fibers are not simple linear materials; they exhibit complex nonlinear responses, including phenomena like strain stiffening, fiber reorientation, and buckling.

In summary, a constitutive relation for fibers is a mathematical framework that allows us to understand, model, and predict the complex mechanical behavior of these critical components of the extracellular matrix. It bridges the gap between experimental observations and theoretical understanding, facilitating advances in fields ranging from biology and medicine to biomechanics and tissue engineering.

1.5 Summary

In preceding sections, we unveiled instances of the intricate mechanical conversation between cells and the ECM. In particular, we illuminated the role of the intrinsic actomyosin machinery, enabling cellular contractions that, in turn, exert tractions upon the fibrous ECM. This dynamic interplay manifests as spatial patterns of localized deformation [26, 52, 71, 74, 77]. While the exact mechanism for the formation of these patterns remains elusive, compelling evidence supports their pivotal role in intercellular mechanical communication, cell motility and invasion. These patterns are characterized by fiber alignment and profound material densification, localized within *tethers* linking neighboring cell assemblies such as tumors [31, 71] or individual cells [52, 77]. These tethers stand as bands of heightened density, up to three to fivefold denser than the surrounding matrix.
At the core of investigating these phenomena lies the mechanical symphony of natural fibrous matrices, orchestrated by the behavior of their intrinsic fibers. Consequently, the exploration of ECM deformations rests upon understanding the individual fiber's response to external forces. With this in mind, we delved into the nonlinear elasticity of fibers, a characteristic unveiled by prior investigations [34, 80]. This quality sheds light on why cell-induced deformations reverberate far beyond the confines of cell boundaries [52, 69] facilitating profound intercellular exchanges. Later on, we discussed that this nonlinearity is manifested by strain stiffening in tension [32, 57, 75, 78, 80] and buckling of fibers in compression [8, 40, 49, 52]. Amidst this exploration, we cast a spotlight on an intriguing facet of fiber mechanics: the traces of instability that surface when fibers are subjected to compressive loads [26, 43, 76]. Finally, we touched upon how the combination of computational models and constitutive relations of fiber behavior can contribute to deepening our comprehension of ECM mechanics amidst the transformative dance orchestrated by cell-induced deformations.

Given the aforementioned context, the primary aim of this thesis is to construct models that encompass the distinctive innate traits of fiber morphology and mechanics. Through this, the thesis endeavors to unravel the intricate interplay of compression instability, shedding light on the deformation patterns entwined with ECM densification, the emergence of tethers, and the alignment of fibers.

CHAPTER 2

Scope of the thesis

τὸ γὰρ μὴ τυχόντως ἀλλ᾽ ἕνεκά
τινος ἐν τοῖς τῆς φύσεως ἔργοις
ἐστὶ καὶ μάλιστα· οὗ δ᾽ ἕνεκα
συνέστηκεν ἢ γέγονε τέλους,
τὴν τοῦ καλοῦ χώραν εἴληφεν.

Ἀριστοτέλης, *Περὶ ζῴων μορίων*

Studying Extracellular Matrix (ECM) deformations holds profound significance as it unveils the choreography of life's intricate mechanics. By delving into how this dynamic web responds to forces, we decipher the language of tissues, unveiling secrets crucial for both health and disease. Understanding ECM deformations unravels the essence of tissue development, function, and dysfunction. It paves the path to therapeutic insights, enabling us to intervene and heal when this delicate dance falters. In this exploration lies the bridge between biology and mechanics, weaving a tapestry of knowledge that enriches our grasp of life's intricacies.

Considering the unique mechanical characteristics exhibited by fibers in tension and compression —namely, strain stiffening and buckling— numerous models have been developed over recent decades [2, 24, 27, 44, 48, 52, 65, 66, 73, 82]. These models strive to replicate ECM responses under cell-induced loading and to delve into the intricate phenomena of fiber alignment, tether creation, and the far-reaching propagation of forces and displacements. Despite delving into the nonlinear facets of fiber behavior, these methodologies are constrained by their focus on stable fiber responses and occasionally modest deformations. However, it is essential to note that none of these studies have ventured to address fiber instability.

The work presented herein attempts to fill this gap. Considering the unique innate traits of fiber morphology and mechanics, our objective is to develop models that account for these features. Our aim here is to scrutinize the significance of fiber compression instabilities in shaping the deformation patterns associated with ECM densification, the emergence of tethers, and the alignment of fibers.

We introduce two distinct families of fiber constitutive relations, each possessing unique nonlinear and stability attributes. Within Family 1, stiffness exhibits a positive but decreasing trend as compression intensifies. On the other hand, Family 2 entails a stretch instability phase, where stiffness becomes negative at extreme compressions. Family 1 embodies the traditional view of post-buckling behavior and is similar with models that have been used in [2, 24, 27, 44, 48, 52, 65, 66, 73, 82], while Family 2 is a more radical model, incorporating recent experimental observations on buckling of hierarchical beams [76].

The aim of this work is to develop macroscopic models and perform simulations with the two constitutive families, in order to:

- capture the formation of *tethers* that bridge contracting centers, as well as the *wrinkles* emanating around each center, as observed in [26, 74, 77],
- capture fiber enhanced alignment,
- investigate the property of long-range mechanosensing,
- explore fiber compression instabilities and their implication in the phenomena above.

CHAPTER 3

Modelling the Extracellular Matrix

ἀρχὴ γὰρ λέγεται μὲν ἥμισυ
παντὸς ἐν ταῖς παροιμίαις
ἔργου [...] τὸ δ᾽ ἔστιν τε, ὡς ἐμοὶ
φαίνεται, πλέον ἢ τὸ ἥμισυ [...]

Πλάτων, *Νόμοι/ΣΤ'*

This chapter contains the methodology followed in order to build the proposed computational and mathematical models. The first section introduces how we construct an artificial network that represents the fibrous matrix. The next sections concentrate on the mechanical characteristics of fibers, the notion behind their modelling and introduce the model families and the mechanisms each tackles. The section closes with the formulation of the computational problem. Theoretical background is provided when necessary.

Notation:
α ... lower case letters denote a constant scalar
$\mathbf{x}$ ... bold lower case letters denote vectors
$\mathbf{X}$ ... bold upper case letters denote tensors
$\mathbf{I}$ ... identity tensor
x_i ... i component of vector $\mathbf{x}$
X_{ij} ... ij component of tensor/matrix $\mathbf{X}$
IR^n ... n-dimensional Real Vector Space
$\mathbf{G}(\cdot): IR^n \rightarrow IR^n$ ... vector function of n variables
$G(\cdot): IR^n \rightarrow IR$ ... scalar function of n variables
The definitions of various concepts are introduced according to the textbooks [1], [28], [37].

3.1 Constructing a fibrous matrix

The Extracellular Matrix (ECM) is the primary load-bearing scaffold within animal tissues. This scaffold is a complex three-dimensional network composed of collagen, elastin, and various other fibrous proteins that provide structural support and regulate various cellular functions in tissues and organs. This fibrous network possesses a geometrically intricate structure that varies among the various animals tissues and is not well established. Thus, as the in vivo geometry and topology of ECM are not clearly defined, it is frequently required to employ an artificial geometric representation of the fibrous matrix (Fig. 3.1).

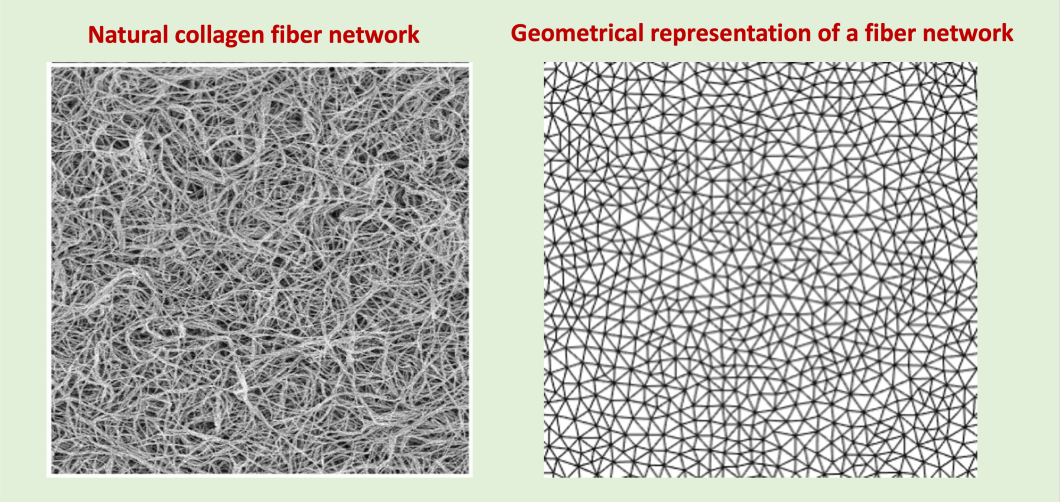

FIGURE 3.1. **Geometrical representation of a natural fibrous matrix.** In order to model the ECM, it is typical to construct geometric representations. These representations are networks of segments which correspond to fibers; the 'fibers' in these representations are assumed to have a consistent diameter, resulting in an identical force-extension behavior for each segment.
Image of the narural collagen network reproduced from [36].

We assume that the ECM is a homogeneous isotropic elastic material equivalent to a uniformly distributed network of segments which correspond to fibers as depicted in Fig. 3.1. In particular, we represent the natural ECM as a circular discretized domain which is partitioned into triangular elements (Fig. 3.5).

Let Ω be a domain, subset of $I\!R^n$ with non-empty interior. A discretization of Ω consists of subdomains which are defined as:

Definition 3.1. A subdivision of a domain Ω is a finite collection of element domains K_i. These elements must be located in such a manner that there are no empty spaces between them and that they do not overlap:

i. $\text{Int}(K_i) \cap \text{Int}(K_j) = \emptyset$, $\forall i \neq j$

ii. $\cup K_i = \Omega$

where $\text{Int}(K_i)$ is the interior, i.e. set of all points in the element K_i, except those which are located on the surface.
If P is the set of all nodes of the discretized domain Ω, then each node $p_k \in P$ has a unique global index $k = 1,\ldots,N$, where N is the number of all nodes in the whole discretized domain.

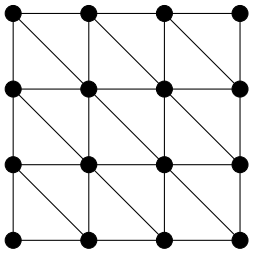

FIGURE 3.2. **Triangulation of a square domain in IR^2.**

A common discretization is a **triangulation**, in which each element is a triangle:

Definition 3.2. A triangulation of a domain Ω is a subdivision consisting of triangles having the property that no vertex of any triangle lies in the interior of an edge of another triangle.

A discrete setting adopts the physical aspects of a continuum body. In continuum mechanics materials are modelled as a continuous mass called *bodies*, which are regions $\Omega \subseteq IR^3$, where position vectors $\mathbf{x} \in \Omega$ are identified with material points. Thereby, a body consisting of material points can adopt different states in presence of stimuli, such as forces and heat. These various regions are called *configurations*. In particular, in the absence of applied forces bodies have the so-called natural state, which we call *reference configuration*. Then, the various states that a body can occupy are described using **deformations** from this natural state, defining a *deformed configuration*.

Definition 3.3. Deformation: A deformation $\mathbf{f}: \Omega \rightarrow \Omega_*$ is a mapping that maps the reference region Ω onto the deformed region Ω_*.

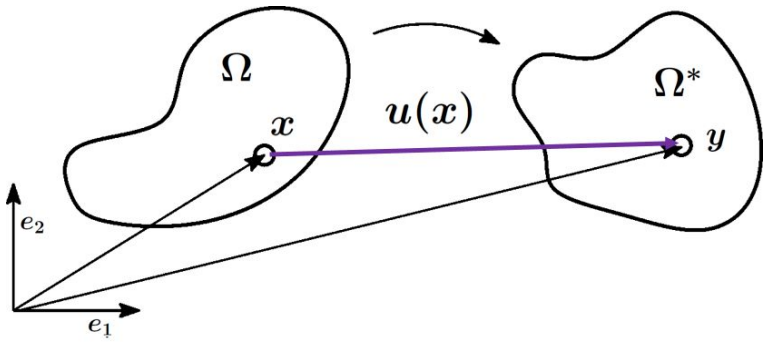

FIGURE 3.3. **Deformation of a continuum body in two dimensions.** The body occupies the regions $\Omega, \Omega_* \subseteq IR^2$ in reference and deformed configurations respectively. A material point has position vector $\mathbf{x}$ in the reference configuration, while in the deformed configuration its position is given by the position vector $\mathbf{y}$. The mapping $\Omega \to \Omega_*$ is described by the deformation $\mathbf{f}: IR^2 \to IR^2$, $\mathbf{x} \to \mathbf{y}$ or $\mathbf{y} = \mathbf{f}(\mathbf{x})$.

If $\mathbf{x} \in \Omega$ is the reference position of a material point then $\mathbf{y} = \mathbf{f}(\mathbf{x}) \in \Omega_*$ is the position vector of the same point in the deformed configuration.
The vector **u(x)** represents the **displacement** of point **x**, mathematically defined as the difference between the final and initial position of a particle:

$$\mathbf{u}(\mathbf{x}) = \mathbf{y} - \mathbf{x}$$

$$\mathbf{u}(\mathbf{x}) = \mathbf{f}(\mathbf{x}) - \mathbf{x} \tag{3.1}$$

As it appears, a discrete domain is represented by a lattice consisting of triangular elements. Each vertex corresponds to a vector with initial position $\mathbf{p_k} \in IR^n$ for a n-dimensional network, where $k = 1, \ldots, N$, with N to be the total number of vertices. A discrete setting adopts the physical aspects of a continuum body:

- The deformation function **f** is a piece-wise affine mapping from initial position $\mathbf{p_k}$ to a new position $\mathbf{p'_k}$.
- The displacement **u** is the difference between these two positions $\mathbf{p'_k} - \mathbf{p_k}$, for each node k.

For a discrete setting such our ECM representation (Fig. 3.5), forces are considered to act only at the nodes of the network so that the edges, which correspond to network's fibers, are being either pulled or compressed. Triangle vertices, where fibers terminate, are the nodes of the network, so that *fiber length* corresponds to the length of the segment between two nodes. If the deformed-position vectors of the fiber end points (nodes) are $\mathbf{x}_i$ and $\mathbf{x}_j$ and the undeformed fiber length is l_{ij}, then we define the *effective stretch* λ for a single fiber as the distance between its endpoints divided by its undeformed (reference) length (Fig. 3.4):

$$\lambda_{ij} = \frac{|\mathbf{x}_i - \mathbf{x}_j|}{l_{ij}}, \tag{3.2}$$

Hence, we have the following cases:

- $\lambda > 1$, (tensile stretch) the fiber is under tension
- $\lambda < 1$, (compressive stretch) the fiber is being compressed
- $\lambda = 1$, (undeformed) the fiber is relaxed.

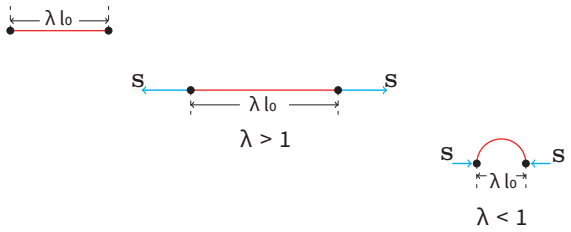

FIGURE 3.4. **Effective stretch λ of a single fiber.** λ is defined as the ratio of deformed to reference (l_0) distance of a fiber's endpoints. From left to right: a relaxed fiber with length l_0, a fiber under tension ($\lambda > 1$) and a buckled fiber under compression ($\lambda < 1$). The cyan arrows represent the applied loads at the fiber's endpoints.

3.2 Modelling the fibers

When dealing with computations, mathematical models are employed to depict the inherent mechanical characteristics of a fiber. A constitutive relation for a fiber serves as a mathematical framework that defines how the fiber responds mechanically to different types of loading. Essentially, it delineates the connection between the fiber's deformation and the applied forces. This relationship offers a quantitative insight into how fibers react to diverse mechanical situations and it is a function of the applied force on a fiber and its stretch as response to this force.

We start by defining the energy of a single fiber which can can be written as $W(\lambda)$ as a function of effective stretch λ. When the fiber is in tension, it is straight and λ equals the actual stretch, while $W(\lambda)$ equals the elastic energy due to stretching of the fiber. When the fiber is in compression, it may be buckled, in

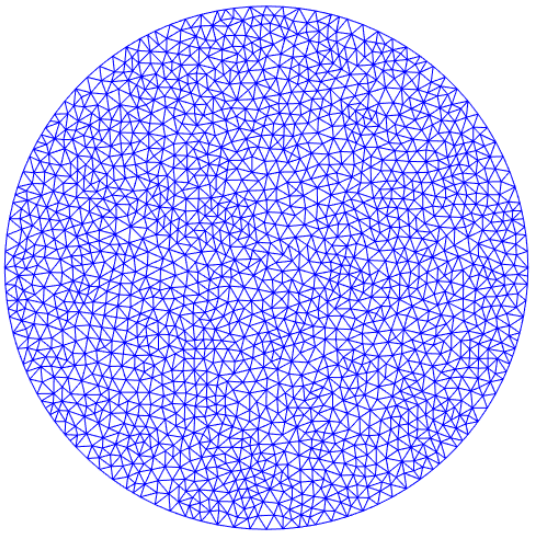

FIGURE 3.5. **ECM representation in our models.** A circular domain partitioned into triangular elements, representing the fiber network. Each of the three sides of an element represents an individual fiber.

which case the elastic (mostly bending) energy
of the fiber can still be expressed as a function $W(\lambda)$ of the distance between its endpoints, hence of the effective stretch λ (Fig. 3.4). In that case $W(\lambda)$ is chosen to embody the post-buckling response of the fiber. If the deformed-position vectors of the fiber end points (nodes) are $\mathbf{x}_i$ and $\mathbf{x}_j$ and the undeformed fiber length is l_{ij}, the energy of the fiber is

$$W\left(\frac{|\mathbf{x}_i - \mathbf{x}_j|}{l_{ij}}\right), \tag{3.3}$$

the quantity within parentheses above being the effective stretch λ of the fiber between nodes i and j. The force-stretch relation of a single fiber is given by $S = S(\lambda)$, where

$$S(\lambda) = \frac{dW(\lambda)}{d\lambda}, \tag{3.4}$$

is the fiber force which is non-dimensionalized after dividing by a coefficient with dimensions of the force.

3.2.1 Network elastic energy

Physical systems tend to a state of minimum energy. Essentially, in a discrete setting the lowest energy conformation is the set of lengths and angles between the nodes which minimize the forces that would otherwise be pulling them together or pushing them apart.

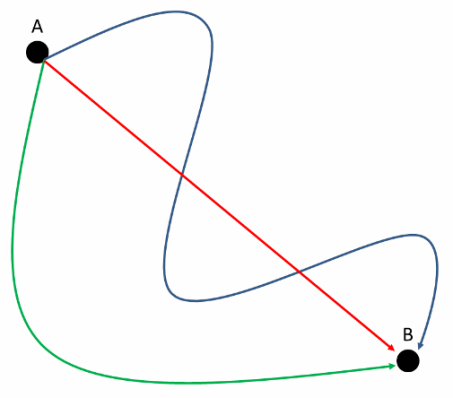

FIGURE 3.6. **Example of potential paths for a particle to move from point *A* to point *B*.** All require the same amount of work, if the exerted force is conservative. Thus, the elastic potential energy depends only on the points ***A***, ***B*** and not on the path that the particle followed.

We have defined our representation of the ECM as a finite collection of triangular elements that discretize a circular domain. In such a discretization, each node corresponds to a position vector. The coordinates of each vector are described according to a well defined vector space. This means that in n-dimensions, each node is described by a n-coordinates. The set of all coordinates in the structure correspond to *the degrees of freedom* of the particular problem.

Definition 3.4. The **degrees of freedom** for a given problem are the number of independent problem variables which must be specified to uniquely determine a solution.

Each vertex in a n-dimensional domain has n-degrees of freedom. Let $E(\mathbf{x})$ be the elastic potential energy function where $\mathbf{x}$ is a vector of all nodal positions. Thereby, if N is the total number of vertices of the domain, the vector $\mathbf{x}$ is a $n \times N$ dimensional vector and refer to the degrees of freedom set. Each $x_i, \quad i = 1, 2, \ldots, N$ is an independent variable for the minimization problem.

The **elastic potential energy** $E(\cdot)$ is the stored energy of a system that depends only on the relative position of its particles. The potential energy arises in systems with particles that exert forces on each other. It is equal to the negative of the work done by these forces which depends only on the initial and final positions of the particles. These forces, are called *conservative forces*. If the exerted force is known, and is a conservative force, then the potential energy can be obtained by:

$$E = -\int_{\mathbf{x_i}}^{\mathbf{x_f}} \mathbf{F} d\mathbf{x} \tag{3.5}$$

where $\mathbf{x_i}$,$\mathbf{x_f}$ are the reference and final position vectors of the system, respectively. In Fig. (3.6), $\mathbf{x_i}$ corresponds to the position vector of a particle at A on which a force is applied and $\mathbf{x_f}$ corresponds to the position vector the particle obtains at B, under the work of the applied force.

For a discrete system, the total network energy is a summation over the individual energy of its edges and depends solely on the reference and final positions of the nodes:

$$E(\mathbf{x}_1, ..., \mathbf{x}_N) = \sum_{k=1}^{F} W(\mathbf{x}_1, ..., \mathbf{x}_N) \tag{3.6}$$

here F is the number of edges, N the number of nodes in the network.

3.2.2 Constitutive Families

The significance of a constitutive relation for fibers lies in its capacity to capture the intricate mechanical behavior of these vital structural components. However, fibers are not simple linear materials; instead, they exhibit intricate nonlinear responses. As we discussed in the previous chapter, these responses encompass the phenomena of strain stiffening and compression softening due to buckling. Furthermore, when subjected to compression, fibers exhibit material instabilities that arise from a special nonlinearity manifested by their intricate hierarchical composition. The significant ingredients in this nonlinearity lie in the non-monotonic microscopic stress-stretch response in one dimensional elastic bars as a key feature for material phase transitions [18], as well as a transition from hardening to softening for high enough compression of hierarchical beams [76].

Driven by the aforementioned studies along with previous works that highlighted the contribution of fiber buckling under compression in ECM densification and fiber alignment [26, 52, 66],

we have developed models that accounts for the unique intrinsic features of fiber morphology and mechanics. In particular, we have implemented two different families of fiber constitutive relations with distinct nonlinearity and stability features. In particular:

- **Family 1** corresponds to the traditional view of post-buckling behavior of solid homogeneous beams as studied in [52, 66]. In homogeneous beams, stiffness decreases gradually with compression but it remains positive, marking a stable behavior in compression. When a beam is subjected to an increasing load, it initially remains in a straight, stable state. However, once a certain critical load is reached, the beam can undergo buckling, where it loses its stiffness. During post-buckling, the beam can adopt a variety of shapes and configurations, and it may still be able to carry some load.
- **Family 2** is proposed *ad hoc* and means to resemble the post-buckling behavior of structures with hierarchical assembly. It is a more radical model which considers the recent experimental observations in [76] on buckling of hierarchical elastic beams. This study highlights that, in contrast to a non-hierarchical beam, the hierarchically structured beam, when subjected to compression, displayed more catastrophic buckling modes. In particular, they documented a gradual transition from a positive to a negative slope of the stress-strain response with increasing compression. Consequently, the stress-strain response was characterized by the presence of a limit load when sudden strong softening was observed. The negative stiffness in these observations underscores an unstable behavior under compression. Another example of this instability entails a drinking straw which experiences sudden stiffness loss due to collapse of its hollow cross-section.

Each model in the proposed constitutive families arises from the one dimensional force-stretch response of a single fiber. Our models were designed as such to capture fiber stiffening in tension $(\lambda > 1)$ [32, 78], but also softening in compression $(0 < \lambda < 1)$ due to buckling [26, 52, 66].
We propose the following families of models:

$$\text{Family 1:} \quad S = S_{1k}(\lambda) = \lambda^k - 1, \quad k = 1,3,5,7 \tag{3.7}$$

which includes the linear case (k=1) and Family 2:

$$\text{Family 2:} \quad S = S_{2k}(\lambda) = \lambda^k - \lambda^{k-2}, \quad k = 5,7. \tag{3.8}$$

For all models (except for the linear one S_{11}), there is stiffening in tension. The difference between the two constitutive families lies in compression (Fig. 3.7). In all nonlinear Family 1 models, force S and stiffness $dS/d\lambda$ both increase monotonically with increasing stretch λ. For the linear model S_{11} the stiffness remains constant. However, stiffness decreases monotonically with compression — as λ decreases to zero — until it vanishes in the crushing limit $\lambda \to 0$ (Fig. 3.7a). At this limit, force reaches a plateau where it remains approximately constant as

$\lambda \to 0$. Models of Family 1 differ in how abrupt the loss of stiffness is and at which level of compressive stretch it occurs. Thus, Family-1 fibers can sustain a limited amount of compressive force even after buckling. Family-1 behavior is consistent with experiments and simulations of post-buckling in certain homogeneous nonlinear elastic beams [14]. The linear model with its constant positive stiffness is an exception, intended to model fibers that do not buckle in compression.

Family-2 models were designed to capture the material instability under compression (as discussed in Chapter 1, *When fibers bear the weight*). Stiffness decreases monotonically with decreasing $\lambda < 1$, describing a fiber that initially resists the compressive load, after which stiffness becomes negative with further compression, entering a compression instability regime (negative stiffness) up to final collapse as $\lambda \to 0$ (Fig. 3.7b).
Suppose one of the models from eq. (3.7) or (3.8) has been chosen. The corresponding elastic energy of a fiber is then given by:

$$W(\lambda) = \int_1^{\lambda} S(\gamma) d\gamma \tag{3.9}$$

with a minimum at $\lambda = 1$ when the fiber is unstretched. Let λ_j be the stretch of fiber j, where $j = 1, 2, ..., F$ and F is the total number of fibers in the network. Therefore, the total fiber network strain energy eq. (3.6) is equal to

$$E(\mathbf{x}_1, ..., \mathbf{x}_N) = \sum_{k=1}^{F} W(\lambda_k) = \sum_{i=1}^{N} \sum_{j=1}^{N} k_{ij} W\left(\frac{|\mathbf{x}_i - \mathbf{x}_j|}{l_{ij}}\right) \tag{3.10}$$

where F is the number of fibers, N the number of nodes and $k_{ij} = 1$ if there is a fiber joining nodes i and j, 0 otherwise.

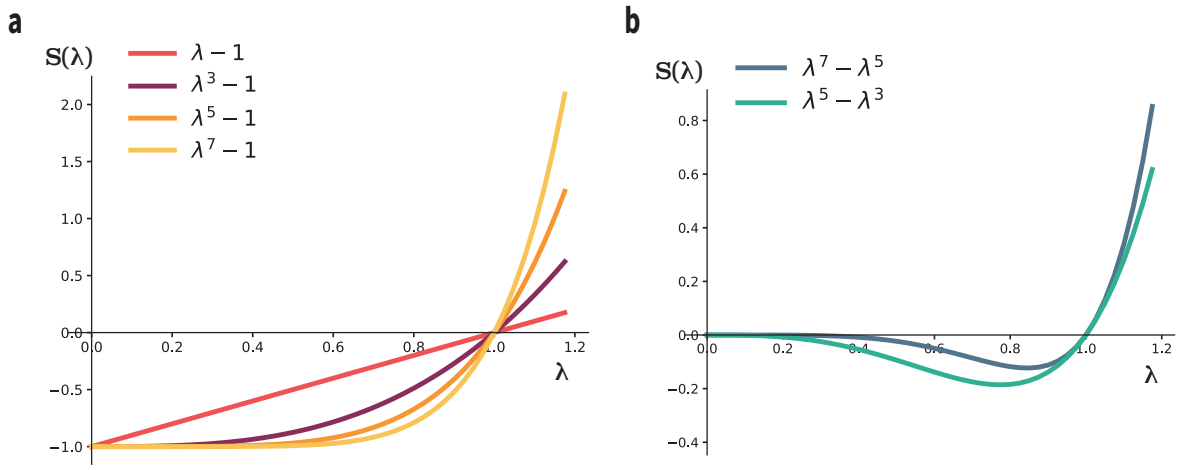

FIGURE 3.7. **Constitutive family models.** For all models (except for the linear S_{11}), there is stiffening in tension. The difference between the two constitutive families lies in compression.
(a) Family 1: $S_{1k}(\lambda) = \lambda^k - 1$, $k = 1,3,5,7$.
In all nonlinear Family 1 models, force S and stiffness $dS/d\lambda$ both increase monotonically with increasing stretch λ. Stiffness decreases monotonically with compression -as λ decreases to zero. Force reaches a plateau where it remains approximately constant as $\lambda \to 0$. Models of Family 1 differ in how abrupt the loss of stiffness is and at which level of compressive stretch it occurs. Thus Family-1 fibers can sustain a limited amount of compressive force even after buckling.
(b) Family 2: $S_{2k}(\lambda) = \lambda^k - \lambda^{k-2}$, $k = 5,7$.
Stiffness decreases monotonically with decreasing $\lambda < 1$ as the fiber initially resists the compressive load, after which stiffness becomes negative with further compression, entering a compression instability regime (negative stiffness) up to final collapse as $\lambda \to 0$.

3.3 Problem Formulation

3.3.1 Cell Models

Let us assume that a homogeneous fibrous matrix is defined within a domain Ω and is described by one of the models in (3.7) or (3.8). We motivate our model by considering cell-induced displacements within the matrix. In particular, we are interested in deformations caused by the contraction of embedded cells. Cells are modelled as circular cavities within the domain Ω. The i_{th} cavity has radius $r_i, i = \{1,2,3,...n\}$. In order to simulate cell contraction, the simplest way is to impose boundary conditions to the corresponding cavity (Fig. 3.8a). A homogeneous contraction corresponds to a radial contractile displacement of magnitude $r_i - r'_i$, where r'_i is the radius of the deformed i_{th} cavity. The vector function $\mathbf{g}_i(\mathbf{x})$ is the displacement vector for a given position vector $\mathbf{x}$ on the undeformed cell boundary. The displacements with radial

symmetry are given by:

$$\mathbf{g}_i(\mathbf{x}) = \frac{u(r_i)}{r_i}\mathbf{x} \tag{3.11}$$

where

$$u(r_i) = -u_0, \quad u_0 > 0 \tag{3.12}$$

is the inward radial displacement (cell contraction). Note that for $u_0 < 0$ the eq. (3.12) denotes an outward radial displacement and the cell expands. Simulations with n cells involve n distinct cavities with the same contractile displacement applied on the boundary of each.

As mentioned above, the natural ECM in our simulations is introduced as a circular domain partitioned into triangular elements. Let us assume the circular matrix has a radius R. The centre of the circular cavity representing the cell coincides then with the centre of the matrix (Fig. 3.7b). Thus, the domain containing the fiber network is an annulus with $r_c < r < R$, where r_c is the cell radius and $r = |\mathbf{x}|$ is the radial distance from the domain centre of the node with position vector $\mathbf{x}$. The boundary conditions in eq. (3.11) are applied on the nodes of the cavity.

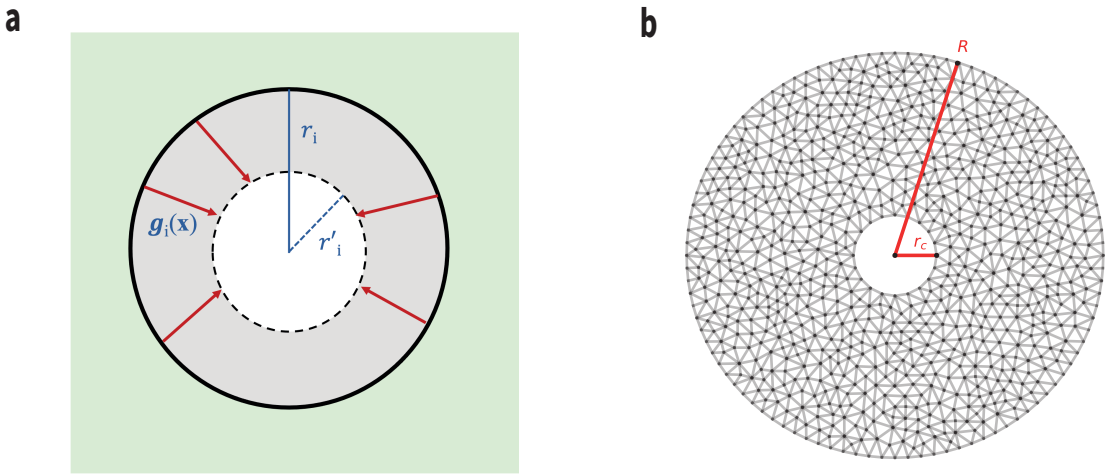

FIGURE 3.8. **Cell models in the fiber network. (a)** A circular cell with radius r_i is attached to the matrix (green area). After the cell contracts homogeneously, it occupies the area of the dashed circle with radius r'_i. For a given position vector $\mathbf{x}$ on the undeformed cell boundary (bold circle), $\mathbf{g}_i(\mathbf{x})$ denotes the radial displacement vector. **(b)** Example of our 2D discrete fiber network containing one cell. Each edge corresponds to an individual fiber. The cavity represents a cell with undeformed radius r_c.

3.3.2 Preserving Orientation

Revisiting once more the continuum theory and the deformation of bodies, recall in eq. (3.1) the vector $\mathbf{u(x)}$ representing the displacement of point $\mathbf{x}$, defined as the difference between the final and initial position of a particle, eq. (3.1): $\mathbf{u(x)} = \mathbf{f(x)} - \mathbf{x}$, where $\mathbf{f}(\cdot)$ is the deformation. If we apply the gradient with respect to $\mathbf{x}$ to the above equation, we get that:

$$\nabla \mathbf{f(x)} = \nabla \mathbf{u(x)} + \nabla \mathbf{x}$$

$$\mathbf{F} = \nabla \mathbf{u} + \mathbf{I} \tag{3.13}$$

where $\mathbf{F} = \nabla \mathbf{f(x)}$ is the **Deformation Gradient Tensor**, with components:

$$F_{ij} = \frac{\partial f_i}{\partial x_j} \quad i,j = 1,2,3 \tag{3.14}$$

The deformation gradient $\mathbf{F}$ determines local length ratios (deformed/reference length) as well as other geometric changes such as changes in angles or rotations.
Essentially, the deformation Gradient $\mathbf{F} = \nabla \mathbf{f(x)}$ is a matrix, since $\mathbf{f}$ is a vector function. Taking the determinant det$\mathbf{F}$, we have the **Jacobian Determinant** $\mathscr{J}$ of the mapping $\mathbf{f}$ which defines the **local volume ratio of the transformed volume devided by the reference volume of a small region around a material point with reference position vector $\mathbf{x}$**.

Now that we have defined the deformation gradient $\mathbf{F}$ and the geometrical meaning of its determinant, we can refer to the properties of a deformation $\mathbf{f}$ defined in domain Ω:

(i) $\mathbf{f}$ is 1-1, globally invertible, and onto.

(ii) $\mathbf{f} \in C^1(\Omega)$, i.e. is continuously differentiable.

(iii) The Jacobian Determinant $\mathscr{J} = \det \nabla \mathbf{f(x)} > 0, \forall \mathbf{x} \in \Omega$.

The positive determinant in (iii) is essential as it ensures that orientation in the deformed configuration will be preserved. In the opposite case, $\mathscr{J} = \det \nabla \mathbf{f(x)} < 0$, a deformation would include material snap-through which involve interpenetration of matter and orientation reversal, both physically unacceptable. Zero determinants are not accepted either, as they refer to matters squeezed down to zero volumes. This condition regarding orientation-preservation corresponds to a natural physical constraint in elasticity as well as in many other fields.

The Jacobian determinant is the ratio of deformed volume to the reference one, which in two dimensions is the ratio between the corresponding oriented areas. For a triangulized domain, the Jacobian determinant is defined at each triangle, given the initial and final position vectors of their respective nodes. In particular:

Consider the following domain consisting of two elements, K_1 and K_2. Assume that a force acting to a node of the network, induces changes that lead to the deformed domain on the right:

FIGURE 3.9. **Reference and deformed configurations of two triangular elements.**

As depicted in the schematic, each element is defined by nodes $\mathbf{p_k}$, each of which corresponds to a position vector with coordinates (x_k, y_k). We focus on element K_1, defined by $\mathbf{p_1}, \mathbf{p_2}, \mathbf{p_4}$. The area of K_1 will be given by the **cross product** of the vectors $\mathbf{a}, \mathbf{b}$ as defined below:

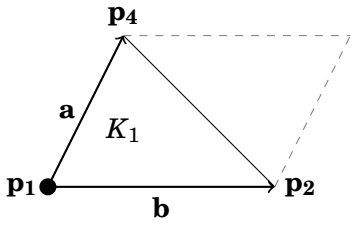

$\mathbf{a} = (a_1, a_2)$ and $\mathbf{b} = (b_1, b_2)$, where a_1, a_2, b_1, b_2 are computed by the coordinates of $\mathbf{p_1}, \mathbf{p_4}$ and $\mathbf{p_1}, \mathbf{p_2}$ as:

$$\mathbf{a} = (a_1, a_2) = (x_4 - x_1, y_4 - y_1)$$

$$\mathbf{b} = (b_1, b_2) = (x_2 - x_1, y_2 - y_1)$$

In mathematics, the cross product is a binary operation on two vectors in three-dimensional space IR^3. Given two linearly independent vectors $\mathbf{a}$ and $\mathbf{b}$, the cross product, $\mathbf{a} \times \mathbf{b}$, is a vector that is perpendicular to both $\mathbf{a}$ and $\mathbf{b}$. The *magnitude* of the resulting vector equals the area of a parallelogram with the vectors for sides, as depicted in the latter schematic.
In a two-dimension space, we introduce the cross product of two vectors, as a *scalar*:

$$\mathbf{a} \times \mathbf{b} = \epsilon_{ij} a_i b_j \tag{3.15}$$

where $i, j = 1, 2$ and ϵ_{ij} is the *altenator* or *permutation symbol*, in two dimensions, defined as:

$$\epsilon_{ij} = \begin{cases} 0, & \text{if i = j} \\ 1, & \text{if i and j are in cyclic order} \\ -1, & \text{if i and j are in anticyclic order} \end{cases}$$

In particular, we have:

$$\mathbf{a} \times \mathbf{b} = \epsilon_{11} a_1 b_1 + \epsilon_{12} a_1 b_2 + \epsilon_{21} a_2 b_1 + \epsilon_{22} a_2 b_2$$

where, from the definition above, $\epsilon_{11}, \epsilon_{22}$ are zero, while $\epsilon_{12} = 1$ and $\epsilon_{21} = -1$, so we end up with:

$$\mathbf{a} \times \mathbf{b} = a_1 b_2 - a_2 b_1$$

or equivalently,

$$\mathbf{a} \times \mathbf{b} = \begin{vmatrix} a_1 & a_2 \\ b_1 & b_2 \end{vmatrix} = A_{ab} \tag{3.16}$$

where A_{ab} is scalar and denotes the area of the parallelogram that $\mathbf{a}$ and $\mathbf{b}$ form. So, the area of the triangle K_1 will be

$$K_1 = \frac{A_{ab}}{2}$$

Accordingly, we compute the area $A_{a'b'}$ defined by the $\mathbf{a}'$ and $\mathbf{b}'$ in order to gain the area of deformed element K_1', using the formula (3.16) for $\mathbf{a}'$ and $\mathbf{b}'$.

Thus,

$$K_1' = \frac{A_{a'b'}}{2}$$

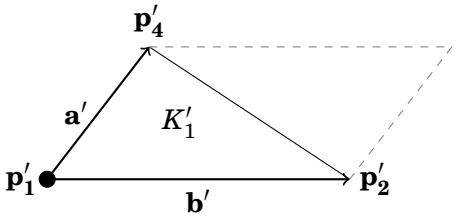

The Jacobian determinant of element K_1 will be:

$$J = \frac{K_1'}{K_1}$$

or in terms of the vector product for any triangular element with $\mathbf{a}$ and $\mathbf{b}$ be its two undeformed vector sides, and $\bar{\mathbf{a}}$, $\bar{\mathbf{b}}$ be its deformed sides, we have:

$$J = \frac{(\bar{\mathbf{a}} \times \bar{\mathbf{b}}) \cdot \mathbf{k}}{(\mathbf{a} \times \mathbf{b}) \cdot \mathbf{k}} \tag{3.17}$$

where $\mathbf{k}$ is the out-of-plane vector. Hence, we overall have the following cases:

- $J > 1$, triangle expansion
- $0 < J < 1$, triangle compression
- $J = 1$, triangle undeformed
- $J < 0$, orientation reversal, i.e. folding over and interpenetration of matter.

Our initial attempt is to impose displacements on cell boundary nodes, as defined in Section 3.11, *Cell Models* and minimize the total network energy $E(\mathbf{x}_1, \ldots, \mathbf{x}_N)$ with respect to all

positions of interior nodes $\mathbf{x}_i$, as defined in eq. (3.10). However, allowing for large cell-induced contractile deformations can result in nonphysical solutions due to interpenetration of matter. As there is no resistance to fibers crossing through one another in the model, this occurs when triangular elements fold over and snap through to the other side. Examples are shown in Fig. A.1 with rectangular triangularized structures where the fibers (edges) behave as linear springs. The orientational change is an instance of the well-known snap-through instability of structural mechanics, e.g. [55], and shows that the energy E is non-convex and likely to have multiple local minima, as well as unstable extrema, even in the case of linear models (as shown in Fig. A.1).

However, these solutions are physically unacceptable and thus, we introduce an energy penalty term to rule them out. This penalty prevents two fibers with a shared node from collapsing into each other. This situation would correspond to the oriented area of the associated triangular element approaching zero and then becoming negative when the orientation is reversed.

Penalizing the Jacobian in order to preserve orientation

We defined above in eq. (3.17) the Jacobian determinant as the *ratio of deformed to undeformed oriented triangle area.* Recall that negative J denotes orientation reversal of the respective elements, i.e. folding over and interpenetration of matter. The penalty term is chosen as a function of J,

$$\Phi(J) = e^{-Q(J-b)}, \quad b, Q > 0 \tag{3.18}$$

Thus $\Phi(\cdot) \to 0$ as $J \to \infty$ and becomes very large for $J < 0$ (Fig. A.2). Thus, it serves in maintaining positive orientation in the network, as negative orientation $(J < 0)$ is costly in energy. For elements with positive area ratio, $\Phi(J)$ is very small, thereby having essentially no contribution to the network's total energy. Physically it corresponds to fibers resisting being crushed together when network elements are on the verge of collapsing and adjacent fibers come into contact.

Consequently, the modified network potential energy in (3.10) takes the final form:

$$\hat{E}(\mathbf{x}_1, ..., \mathbf{x}_N) = \sum_{j=1}^{F} W(\lambda_j) + \sum_{k=1}^{K} A_k \cdot \Phi(J_k) \tag{3.19}$$

where F is the total number of fibers in the network, K the total number of elements, $W(\lambda_j)$ the potential energy of an individual fiber, A_k the reference area that element k occupies and J_k its oriented area ratio.

3.3.3 Instability Mechanisms

Nonconvexity due to Large Rotations
Even if the single fiber energy $W(\lambda)$ from (3.9) is strictly convex with a minimum at $\lambda = 1$, the corresponding energy in eq. (3.3) is a nonconvex function of nodal position vectors $\mathbf{x}_i$ because of rotational invariance (Fig. A.3, see also Fig. 4 in [21]). This occurs even for the linear fiber model ($k = 1$ in (3.7)). It is a source of nonconvexity of the total energy $\hat{E}$ related to geometric nonlinearity, and is typically entirely missed when small rotations are assumed.

Element Collapse Instability
Before a triangular element that consists of three fibers (Fig. 3.10a) undergoes snap-through (its oriented area changes signs) it buckles, or collapses, when a node touches the opposite side. This is actually an unstable equilibrium of the triangle energy which is thus a nonconvex function of element oriented area ratio J. Compressing an element triangle along its height (Fig. 3.10a), we observe that the energy of the triangle as a function $W(J)$ is minimal and vanishes at $J = 1$ and at $J = -1$ (Fig. 3.10b) after the triangle has snapped-through to its mirror image. Since $W(J)$ is odd it must be nonconvex with an unstable equilibrium at $J = 0$. In our model, such total collapse is prevented by the penalty term $\Phi(J)$, but bistability and noncovexity of the penalized energy $W(J) + \Phi(J)$ remains (Fig. 3.10c), with an additional, highly compressed solution for some values of compressive force (Fig. 3.10d). This occurs in both model families, even in the linear model; it is an example of the well-known snap-through instability of structural mechanics, e.g., [55].

In order to identify this instability mode in our simulations we define the *densification ratio* ϱ:

Definition 3.5. The **densification ratio** ϱ is defined for each triangular element to be the ratio of deformed to reference density of a hypothetical continuum deforming as the triangle.

This results in:

$$\varrho = 1/J. \tag{3.20}$$

We observe that the snap-through element buckling just described is attributable to the loss of convexity due to large rotations discussed before. The energy of a triangular element with fixed base as a function of the opposite nodal position is a sum of two sombrero-like energies with different centers and has precisely two global minima giving rise to the bistable form in (Fig. 3.10b).

Fiber Collapse Instability
In Family-2 networks there is an additional instability: when a fiber is compressed past the point where the slope of the $S(\lambda)$ curve becomes negative (Fig. 3.7b), it enters an unstable regime, tending to collapse to zero effective stretch. For example, the unstable regime for $S(\lambda) = \lambda^7 - \lambda^5$ is $0 < \lambda \leq 0.85$. Clearly, fiber collapse would imply area collapse of any element (triangle) with this fiber as a side (Fig. 3.10e). Eventually the penalty term eq. (3.18), (3.19) restabilizes the element (triangle) against total collapse. An unstable regime remains in general, rendering fiber compression response essentially biphasic, similar to Fig. 3.10d.
To summarize, all fiber networks are susceptible to element collapse (triangle buckling) instability. Family-2 networks suffer from an additional fiber collapse instability brought about by total loss of strength due to buckling of hierarchical fibers. Simple geometry shows that fiber collapse implies element collapse (Fig. 3.10e), but not vice versa (Fig. 3.10f).

3.3.4 Formulation, software and statistical analysis

By expressing stretches λ_j and Jacobians J_k in terms of variable nodal positions $\mathbf{x}_i$, $i = 1,...,N$, we express the total energy $\hat{E}$ in eq. (3.19) as a function $\hat{E}(\mathbf{x}_1,...,\mathbf{x}_N)$ of nodal positions. See eq. (3.10) for the first term. The boundary conditions are applied on the cell-boundary nodes and simulate cell-contraction, as described in Section 3.3.1. We then perform energy minimization on $\hat{E}$. For the energy minimization procedure the nonlinear conjugate gradient (NCG) method has been employed [51]. The choice of a NCG method is favored when dealing with non-convex functions due to their robustness in navigating complex and non-convex landscapes. Other methods, such as Newton, rely on the positive definiteness of the Hessian matrix, making them prone to convergence issues or even divergence in non-convex scenarios. In contrast, NCG algorithms exploit conjugate directions to approximate descent directions, allowing them to effectively explore non-convex spaces without requiring explicit knowledge of the Hessian or its eigenvalues. This makes NCG methods more versatile and reliable in optimizing non-convex functions, as they can gracefully handle regions of the objective function that may exhibit varying degrees of curvature or non-convexity.

The computational model has been implemented in Python [62]. The triangulation has been implemented in FEniCS [3] and the optimization method (nonlinear conjugate gradient) has been provided by SciPy [38]. The statistical analysis has been done in R [63] and for multi-group comparisons we used one-way analysis of variance (ANOVA). Illustrations and simulations visualization have been created with Python, R and ParaView [4].

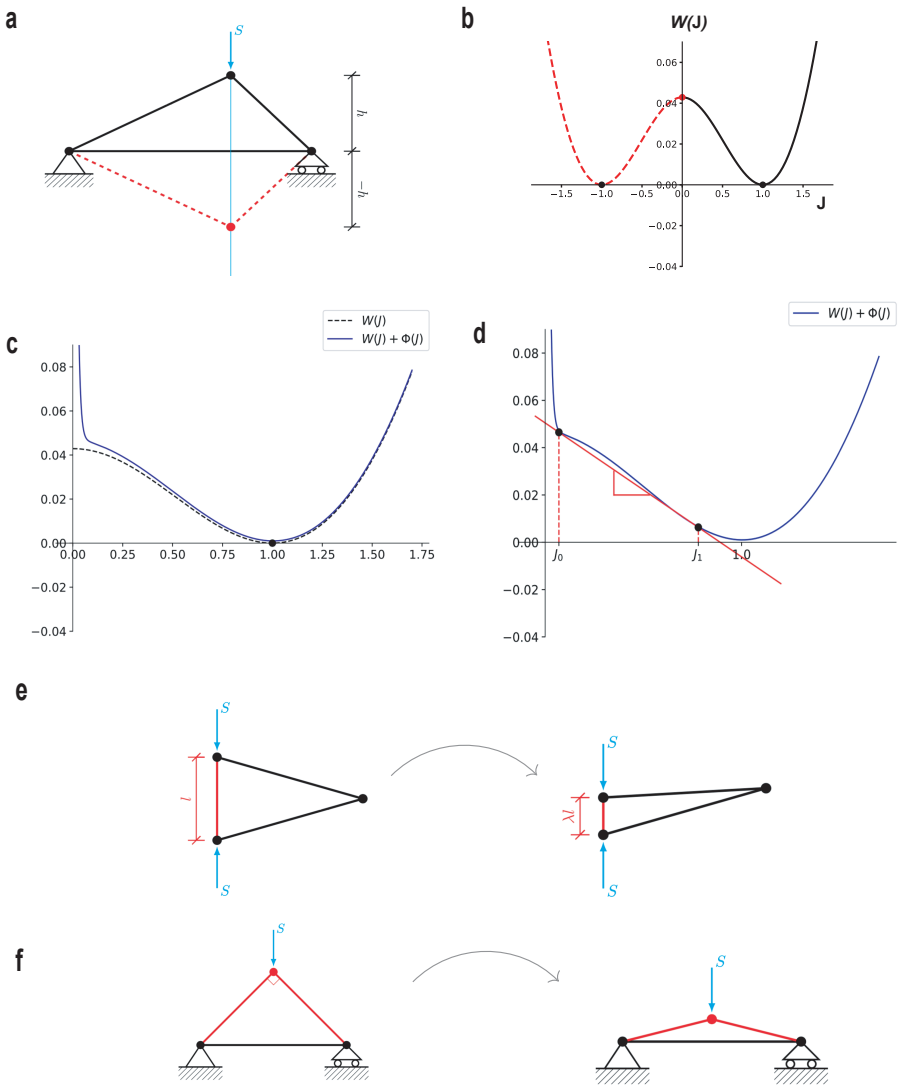

FIGURE 3.10. **Instability mechanisms. (a)** Element collapse Instability (snap-through of triangular elements) under compressive force $\boldsymbol{S}$ (cyan) **b)** Energy of a triangular element as a function of its oriented area ratio $\boldsymbol{J}$. Note nonconvexity and two-well structure. **(c)** Dotted line: as in (b) for $\boldsymbol{J>0}$. Solid line: energy with penalty $\boldsymbol{\Phi(J)}$ added. **(d)** Penalized energy has two stable equilibria $\boldsymbol{J_0}$ and $\boldsymbol{J_1}$ under suitable compressive force (equal to the slope of the red straight line) **(e)** Fiber collapse (red fiber) causes triangular element area collapse. **(f)** The converse is not true. Triangular element collapse can happen without fiber collapse.

3.4 Summary

Remodelling of the Extracellular Matrix (ECM) through cellular forces leads to unique deformation patterns, characterized by increased matrix densification and fiber alignment. These patterns play pivotal roles in intercellular communication [31, 52, 74, 77], as well as cell motility and invasion [19, 61]. To investigate these cell-induced ECM deformations, we have developed a discrete model that considers individual fibers and their inherent mechanical properties.

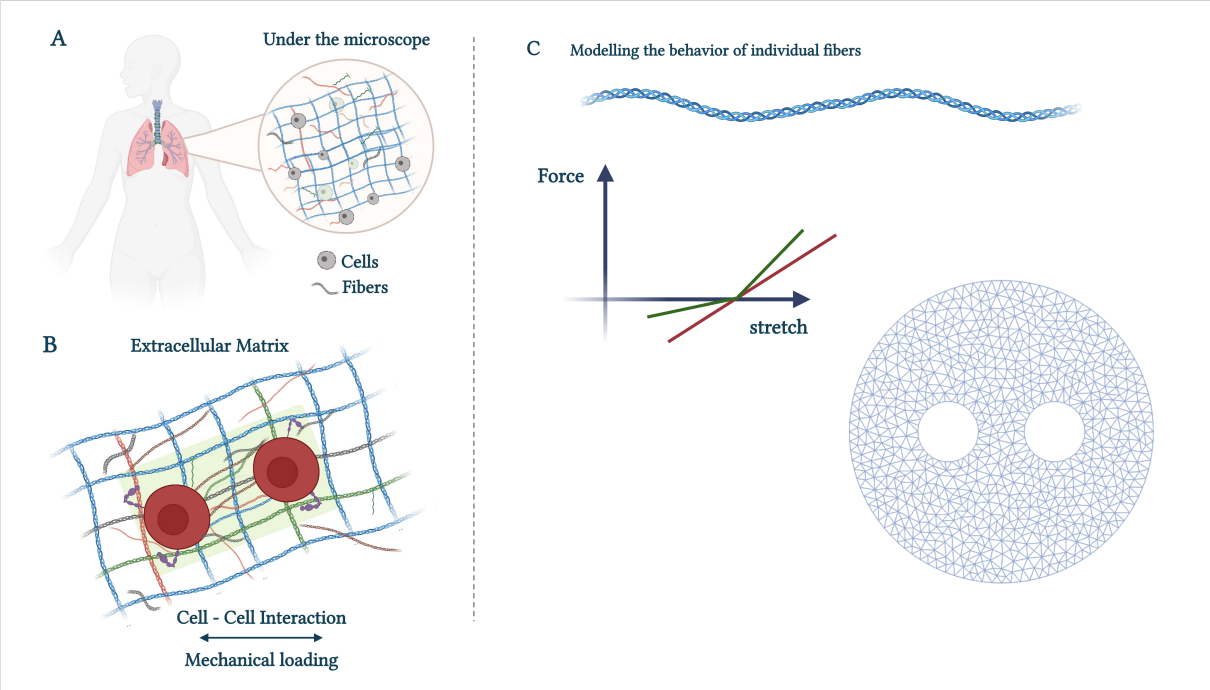

FIGURE 3.11. **Schematic summary of the current study.**

The core assumption of our study is that the mentioned phenomena result from material instabilities, primarily induced by a specific nonlinearity manifested by fiber buckling under compression. We have integrated two distinct families of fiber constitutive relations into our model, each with its unique nonlinearity and stability characteristics.
The first family (Family 1) exhibits a positive but diminishing stiffness as compression increases, representing the conventional perspective on post-buckling behavior. The second family (Family 2) introduces a more radical model, reflecting recent experimental findings related to the buckling of hierarchical beams. In this model, Family 2 includes a stretch instability phase, where stiffness turns negative at extreme compressions. We then perform extensive simulations of a fiber network containing one or more contracting circular cells, analyze the behavior of all studied models and juxtapose our results with previous models and experimental observations.

CHAPTER 4

Main Outcomes

Οὐδὲν ἀτέκμαρτον, οὐδὲν τυφλόν

Πλούταρχος

This chapter encompasses the primary results extracted from our simulations. Commencing with single contracting cell simulations, we subsequently broaden our analysis to encompass multi-cellular systems. We dissect our discoveries in alignment with the objectives of the present research. In each instance, we underline the relevance of our findings, noting instances where they harmonize or diverge from prior models and experimental investigations.

4.1 Family-2 models exhibit pronounced patterns of localized densification, while Family-1 models display more moderate variations

4.1.1 Densified bands emanate from single-contracting cells

We simulate a single cell contracting within a fibrous network for each one of the models introduced in eq. (3.7) for Family 1, and in eq. (3.8) for Family 2. Simulations at **50%** cell contraction exhibit patterns of highly localized, severe densification shown in Fig. 4.1a-c, Fig. 4.2a-c. These patterns take the form of bands, emanating from the periphery of the contracting cell into the surrounding matrix. Plotting the densification ratio of each element versus distance from the cell shows that in Family-2 models, highly densified elements have densification ratio

$\varrho \approx 3$ and reach up to six cell radii into the ECM (Fig. 4.1c). In contrast, Family-1 densified triangles are confined within two cell radii (Fig. 4.1a,b), with densification ratio ϱ at most 2.

The distribution of fiber stretches within the deformed networks illustrates similarities and differences between models (Fig. 4.1d-k, Fig. 4.2d-k). Fibers under tension ($\lambda > 1$) align roughly with the radial direction, forming continual paths that propagate a few cell diameters into the matrix (Fig. 4.1d-f, Fig. 4.2d-f). This happens regardless of the model, though in Family-2 simulations the paths extend further into the matrix (Fig. 4.1f, Fig. 4.2f). When it comes to compressed fibers, things differ significantly between models (Fig. 4.1g-k, Fig. 4.2g-k). Fibers under compression ($\lambda < 1$) are oriented close to the angular direction, forming loops around the cell (Fig. 4.1g-k). Within each of these loops, and close to the cell boundary, the stretch is nearly uniform for Family-1 models (Fig. 4.1g,h). Similar behavior is seen in [24, Fig. 6]. Simulations with Family 2 exhibit two differences: the distribution of compressive stretch around the cell is strongly inhomogeneous (Fig. 4.1k), and the maximum compression is up to twice as high as in Family-1 simulations, 60% compressive strain (or stretch $\lambda \approx 0.4$) compared to 30% ($\lambda \approx 0.7$) for Family 1 (colorbars in Fig. 4.1g-k and Fig. 4.2g-k). Compressed Family-2 fibers are still roughly in the angular direction. The most compressed fibers occur within narrow bands emanating radially from the cell and reaching as far as 6 deformed cell radii into the matrix (Fig. 4.1k,m, Fig. 4.2k,n). Furthermore, in Family 2, network triangles comprising the densified bands are excessively compressed (Fig. 4.1m), as they contain fibers that have nearly collapsed. Fibers under tension are aligned along the axis of densification bands, roughly perpendicular to fibers under compression (Fig. 4.1n). When the densification ratio of the networks in Fig. 4.1c is compared to the compressed fiber distribution of Fig. 4.1k, it becomes clear that regions of localized excessive densification ($\varrho \approx 3$) coincide with the bands containing severely compressed fibers (Fig. 4.1c,k-n, Fig. 4.2c,k).

In Family-1 simulations, severe compressive stretch is not observed at 50% contraction level, with λ remaining above 0.7, compared to 0.4 for Family 2. Densified zones are much shorter and confined to the immediate vicinity of the cell (Fig. 4.1a,b, Fig. 4.2a,b) with triangles less compressed (ϱ at most 2 compared to 3 for Family-2).

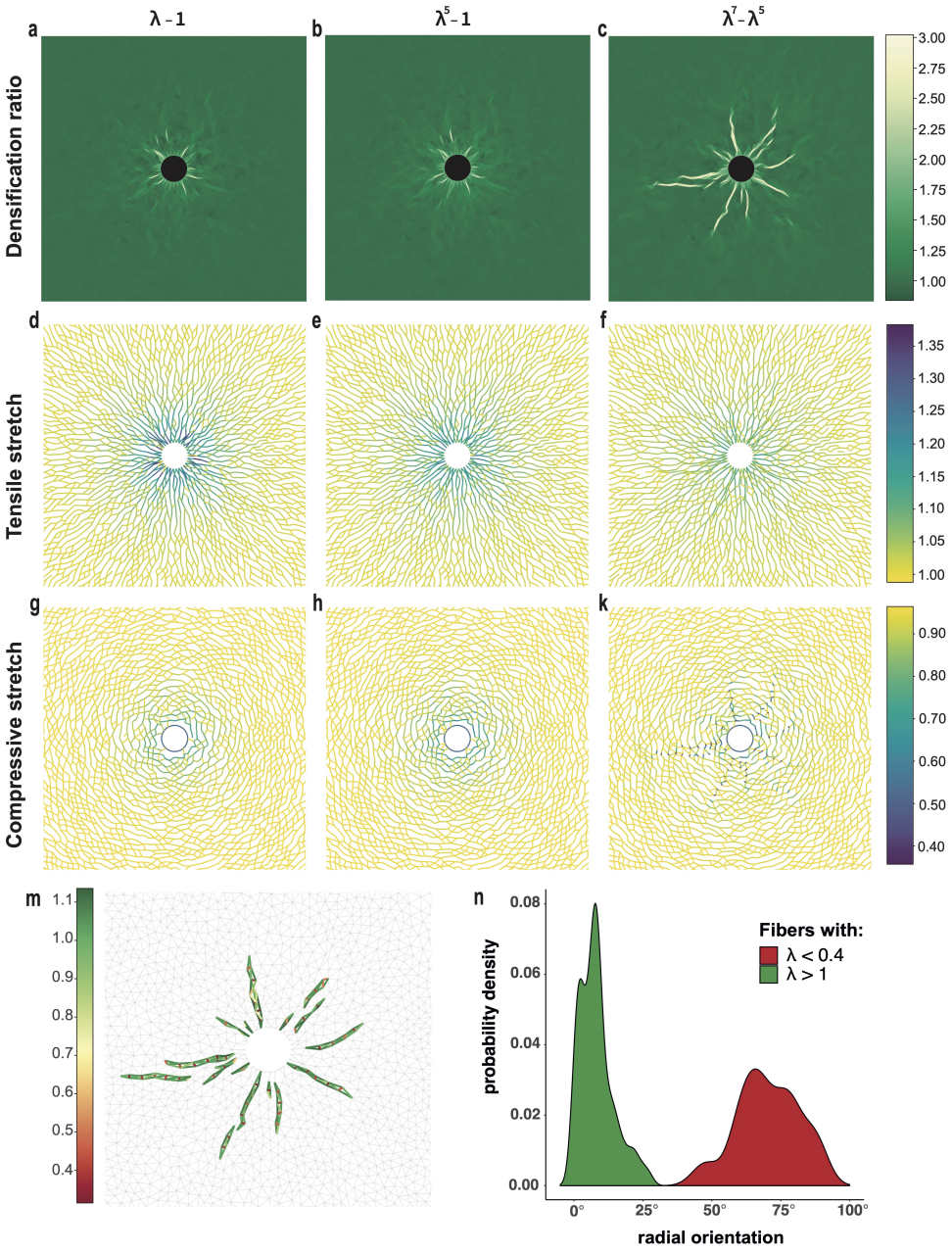

FIGURE 4.1. **Fiber collapse instability and severe localized densification - Part I.** Simulations with a single cell at 50% contraction with Family-1 models $\lambda - 1$ and $\lambda^5 - 1$ and Family-2 model $\lambda^7 - \lambda^5$. **(a-c)** Densification ratio of triangular elements (color plot) in deformed networks **(d-f)** tensile stretches and **(g-k)** compressive stretches in deformed fibers **(m)** stretch of deformed fibers and **(n)** radial orientation distribution of fibers within the densified bands in Family-2 case (c).
Colorbars: (a-c) densification ratio ρ of the deformed networks, (d-k) fiber stretch λ.

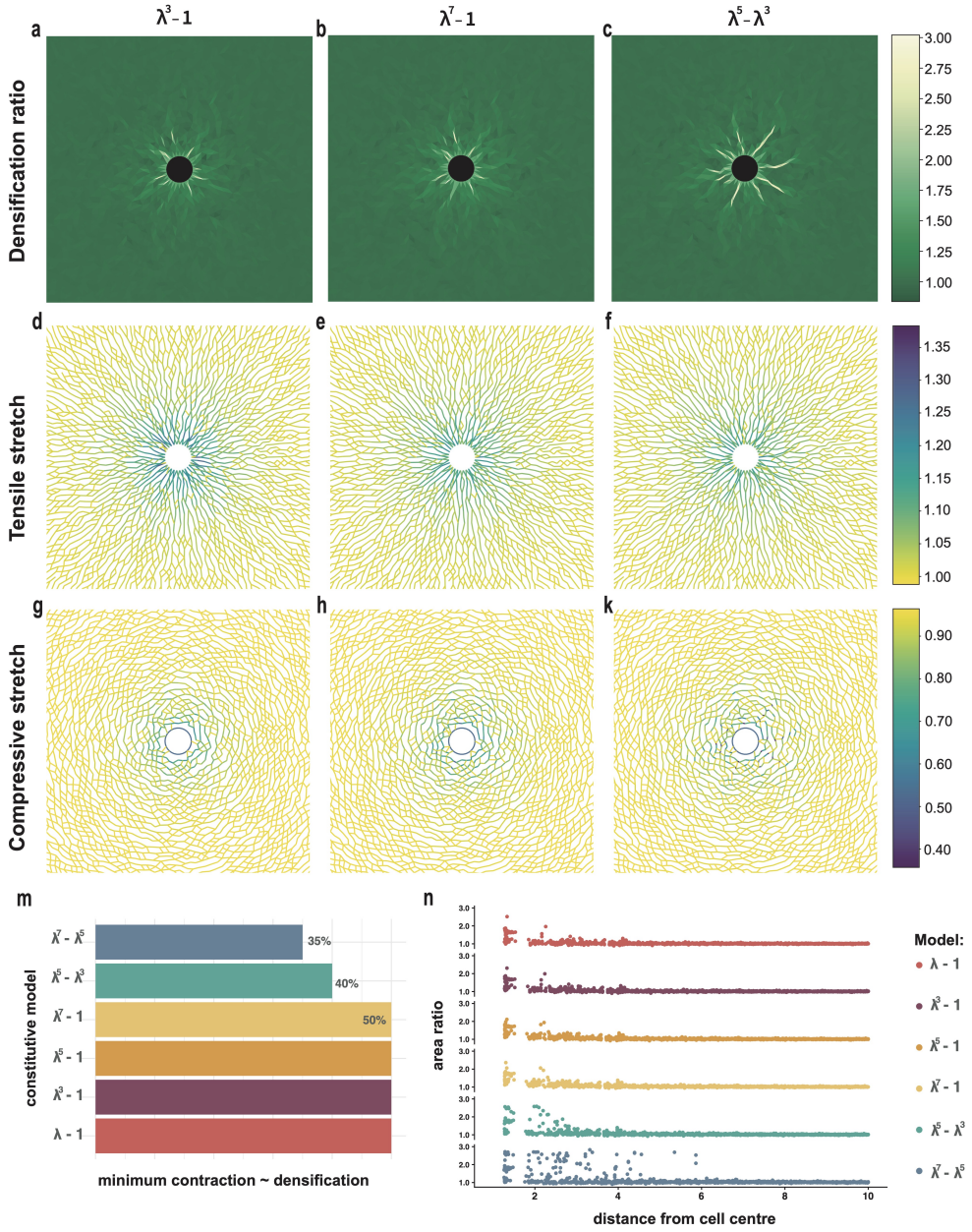

FIGURE 4.2. **Fiber collapse instability and severe localized densification - Part II.** Complementary to Fig. 4.1 containing simulations of a single cell at **50%** contraction with Family-1 models $\lambda^3 - 1$ and $\lambda^7 - 1$ and Family-2 model $\lambda^5 - \lambda^3$. **(a-c)** Densification ratio of triangular elements (color plot) in deformed networks. **(d-f)** Tensile stretches and **(g-k)** compressive stretches in deformed fibers. **(m)** Minimum contraction required for densification to be evident for each one of the models studied. **(n)** Simulations with various models of one cell contracting at **50%**; *x axis:* triangular element distance from cell center, *y axis:* element densification ratio.
Colorbars: (a-c) densification ratio ρ of the deformed networks, (d-k) fiber stretch λ

4.1.2 Intercellular tether formation in multi-cellular systems

We report on simulations involving a pair of cells contracting at 50% of their initial radius, separated by either $6r_c$ or $4r_c$, where r_c is the cell radius (Fig. 4.3, Fig. 4.4, Fig. 4.5). What distinguishes these from singe-cell simulations is the spontaneous appearance of intercellular tethers, composed of thin, roughly parallel bands of high densification and fiber alignment, that connect the two cells (Fig. 4.3c, Fig. 4.4c). When cells are separated by a larger distance, $6r_c$, tethers are generated only with Family-2 models. Additional densified bands emanate radially from each cell (Fig. 4.3c, Fig. 4.4c) as before. In contrast, in Family-1 simulations, matrix densification is limited close to the cell boundary and cells remain isolated and disconnected (Fig. 4.3a,b, Fig. 4.4a,b). When cells are closer together, tethers are generated by all models, even the linear one (Fig. 4.5). In this case, we observe that they are substantially stronger in Family-2 simulations, as they extend from one cell to the other and are noticeably wider compared to Family-1 tethers (Fig. 4.5a-c).

When tethers form, we observe a fraction of fibers, located almost entirely in the intercellular region, to be highly stretched (Fig. 4.5d-f). These fibers are densely packed and aligned with the horizontal direction passing through the cell centers, generating straight paths of fibers connecting the two cells. These paths comprise the tether. At the same time, fibers under extreme compression occupy the same region as the tensile ones, but their orientation is nearly perpendicular to the paths of the tensed and aligned fibers (Fig. 4.5g-k). This is true for all models, though fiber compression magnitude is almost twice as large with Family 2, reaching approximately 70% compression (Fig. 4.5k). This indicates that in Family-2 tethers, compressed fibers are well within the regime of the fiber collapse instability. In addition, we observe highly compressed fibers within the densified bands that emanate radially from the cell periphery (Fig. 4.5k).

When cells are separated by a greater distance, $6r_c$, and tethers are generated only with Family-2 models, fiber stretches highlight a significant difference between families (Fig. 4.3d-k, Fig. 4.4d-k). In Family-2 simulations, fiber distributions and orientations within the tether are the same as for shorter distances (Fig. 4.3f,m, Fig. 4.4f,k). For Family-1 models, this is no longer true, as the fiber paths are disrupted and tensile stretches are distributed in a broader region between cells, without the strong alignment we have with Family-2 models (Fig. 4.3d,e, Fig. 4.4d,e). This is reflected in angle distributions of the tensile fiber orientation, which are substantially different across models within the intercellular region (Fig. 4.4m). This distribution is more localised for Family-2 models, consistent with greater alignment.

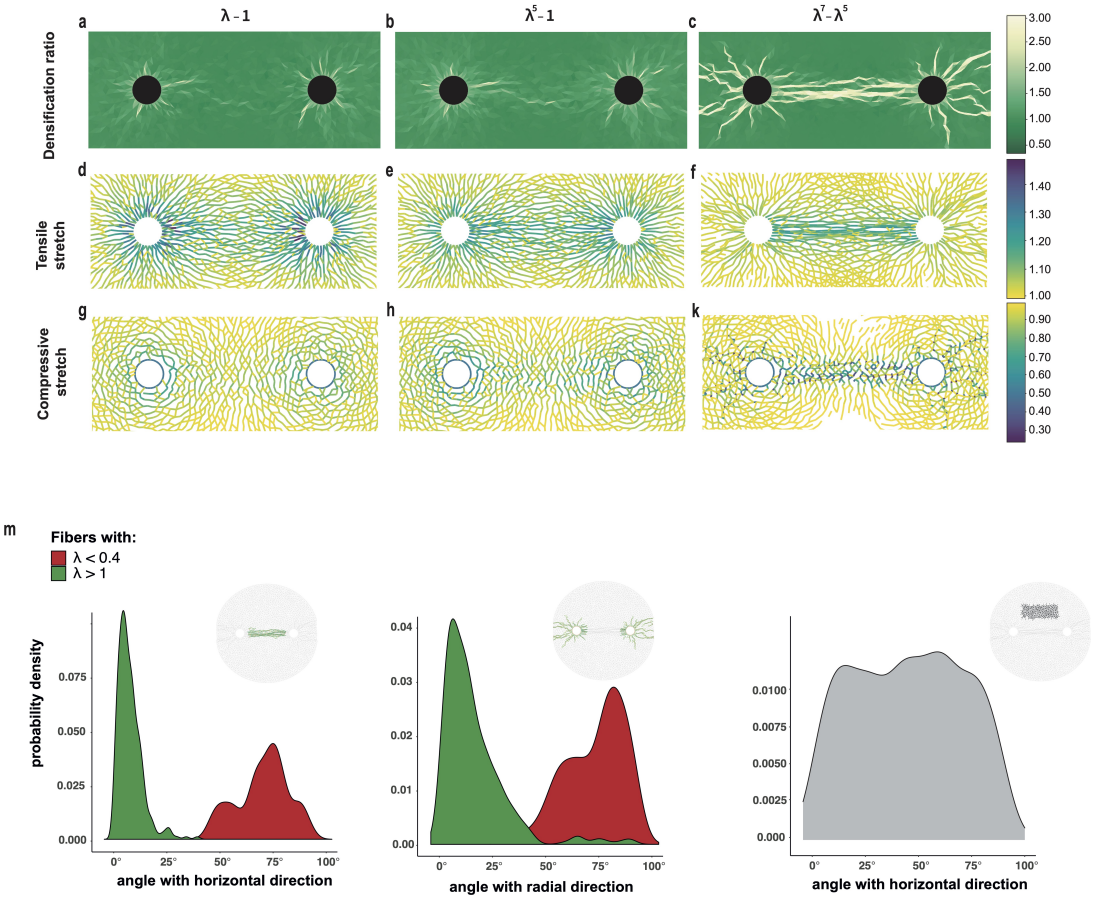

FIGURE 4.3. **Intercellular tether formation - Part I.** Simulations with two cells contracting at **50%**, for three different models (three columns in **a-k**). Cell centers are separated by $\mathbf{6}r_c$, where r_c is the undeformed cell radius. **(a-c)** densification ratio of triangular elements (color plot) in deformed networks **(d-f)** tensile stretches and **(g-k)** compressive stretches of deformed fibers **(m)** orientation distribution of deformed fibers within the densified zones (tether and radial bands) in Family-2 case (c) and within the highlighted non-densified zones. Horizontal direction is the one parallel to the axis connecting the cell centres. Radial direction is the one passing through the cell centre.
Colorbars: (a-c) densification ratio ϱ of the deformed networks, (d-k) fiber stretch.

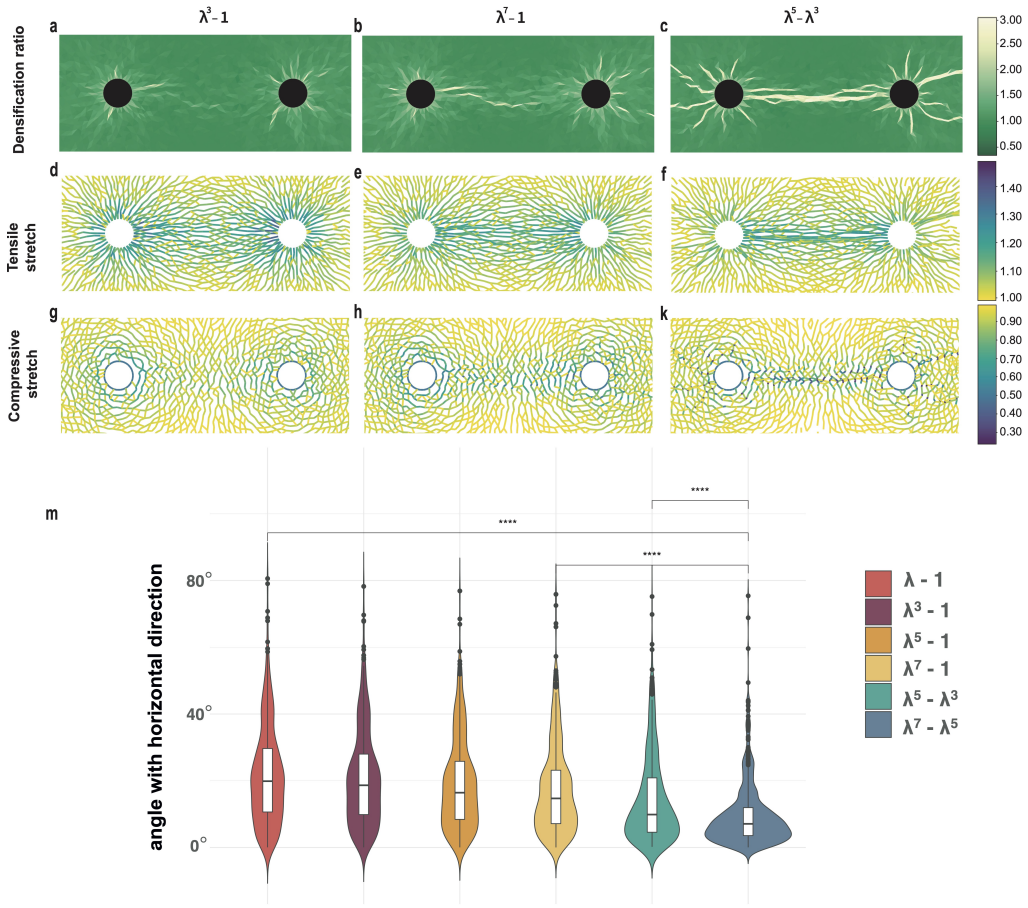

FIGURE 4.4. **Intercellular tether formation - Part II.** Complementary to Fig. 4.3 containing predictions for the remaining models. Simulations with two cells contracting at **50%**. Cell centers are separated by $6r_c$, where r_c is the undeformed cell radius. **(a-b)** densification ratio of triangular elements (color plot) in deformed networks **(d-f)** tensile stretches and **(g-k)** compressive stretches of deformed fibers. **(m)** Orientation distribution of fibers under tension (stretch $\lambda > 1$) within the intercellular region across all models. Each violin corresponds to each one of the models studied and shows the distribution of fiber horizontal direction (in degrees), $^{***}p-value < 0.001$
Colorbars: (a-c) densification ratio of the deformed networks, (d-k) fiber stretch.

Excessively tensed fiber angles within the densified region are narrowly distributed about zero (horizontal direction through cell centers) (Fig. 4.3m). Compressed fibers are distributed about $80-90^{\circ}$ within the densified region, compared to a uniform distribution in non-densified regions (Fig. 4.3m). On the contrary, compressive stretches in Family-1 models are confined to concentric loops around each individual cell instead of the region between cells, and oriented in the circumferential direction (Fig. 4.3g,h, Fig. 4.4g,h).

The previous findings hold for 50% contraction. When cells contract more, tethers are eventually generated for Family-1 models as well. In Fig. 4.6 we present the case of Family-1 model $S(\lambda) = \lambda^5 - 1$ (eq. (3.7), Fig. 3.7c) with two cells separated by $6r_c$ at four contraction levels 45%, 55%, 65% and 75%. We observe that densification between the two cells progressively strengthens. Fiber compression in the cell-cell vicinity is ever-increasing with contraction level, resulting finally in a solid tether at 75% contraction (Fig. 4.6d).

Working in the same manner for each model separately, we have tested different contraction levels ranging from 5% to 80% decrease in cell radii, for multiple distances separating the two cells. Results are summarized in Fig. 4.6e. In particular, for each model we obtain a curve that indicates the minimum contraction cells should undergo to produce a tether, expressed as a function of cell distance. That is, above each curve a tether is predicted to form for the respective model. Clearly, Family-2 models are able to sustain tether formation for moderate contraction levels $\leq 50\%$, and for relatively large cell-cell distances (up to $11r_c$). On the contrary, regarding Family-1 models for the same contraction levels $\leq 50\%$, a full tether is formed when cells have a distance at most $5r_c$.

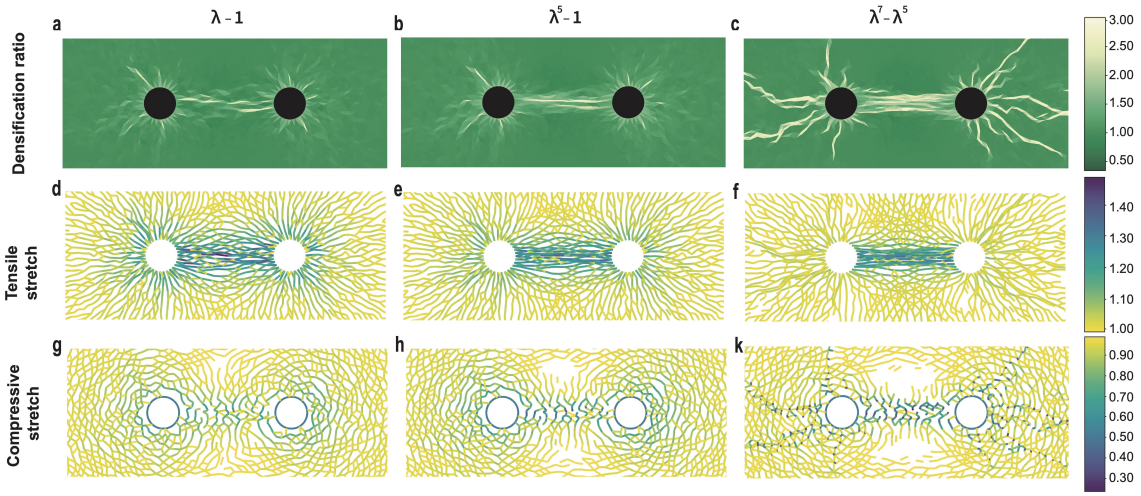

FIGURE 4.5. **Intercellular tether formation - Part III.** Simulations with two cells contracting at **50%**. As in Fig. 4.3, Fig. 4.4 except that cell centers are separated by $4r_c$, where r_c is the undeformed cell radius. **(a-b)** densification ratio of triangular elements (color plot) in deformed networks **(d-f)** tensile stretches and **(g-k)** compressive stretches of deformed fibers. We observe densification around each cell boundary, which extends towards the neighboring cell. Tethers are rather weak for Family-1 cases (a-b) and significantly stronger with Family-2 (c). Within tethers, densification ratio is three times larger than the rest of the matrix. In the intercellular region, fibers under tension are directed towards the neighboring cell so that they form continual paths connecting the two cells. In these paths, fibers under tension are almost perfectly aligned with the horizontal line connecting the two cells. In Family-2 case (f) excessive tensile stretches are concentrated only within the tether-region. Severely compressed fibers (g-k) locate in the intercellular domain, being roughly perpendicular to fibers under tension.
Colorbars: (a-c) densification ratio of the deformed networks, (d-k) fiber stretch.

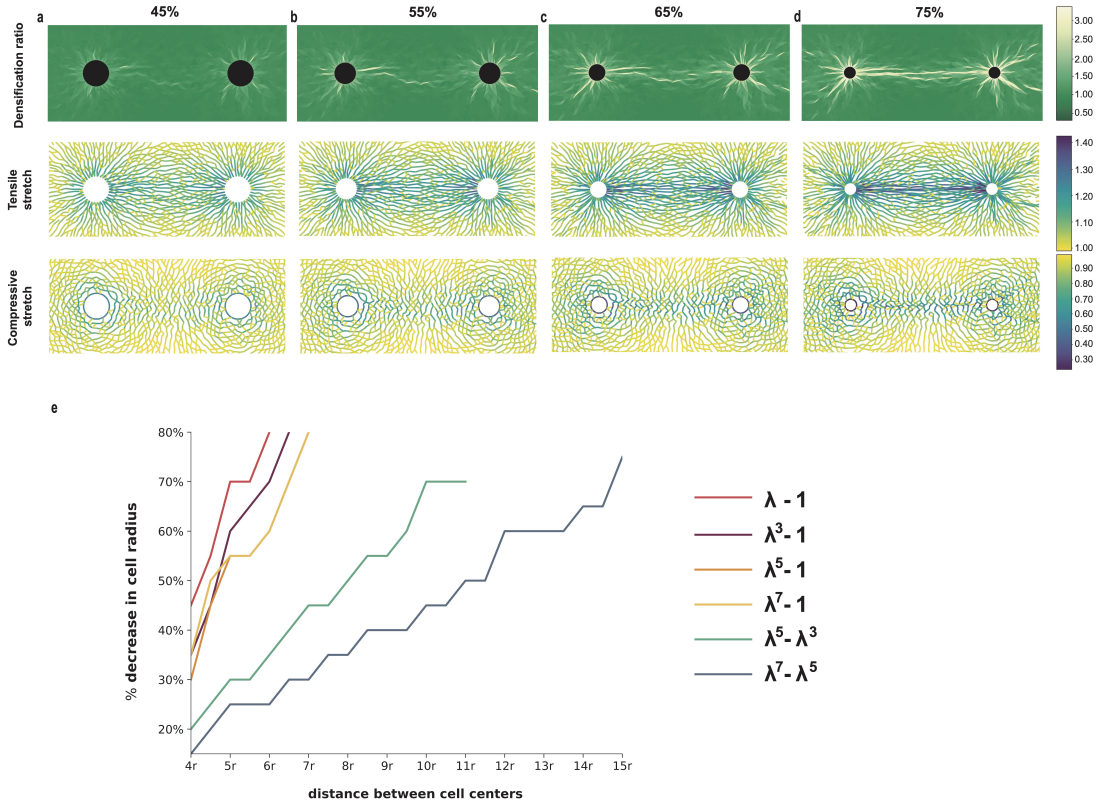

FIGURE 4.6. **Tether formation in Family-1 networks.** Simulations with two cells contracting at different levels in a Family-1 network (model $S(\lambda) = \lambda^5 - 1$). Cell centers have distance $6r_c$, where r_c is the undeformed cell radius. **(a-d)** Densification ratio color plot of triangular elements (up), tensile (middle) and compressive (bottom) stretches of deformed fibers at each contraction step. **(e) Contraction versus cell-cell distance required for tether formation in various models.** Simulations with two cells contracting in the range $5\% - 80\%$ decrease in cell radius (*y axis*). Cells are separated by a distance proportional to cell undeformed radius r (*x axis*). Each curve corresponds to a different model and depicts the minimum contraction level required for a solid tether joining the cells as a function of distance separating them.

4.1.3 Bridges across multi-cellular systems

We proceed by exploring simulations with more than two cells contracting in regard to matrix densification. We start with two cells separated by a certain distance (Fig. 4.7a) and consecutively induce cells in the matrix, with the same level of contraction as the reference pair. The distance between the initial cells is kept constant for all ensuing simulations (Fig. 4.7, b to e). Starting with the initial pair (Fig. 4.7a), we observe matrix densification between the two contractile cells and radial densified emanations around each one of them. When a third cell is added to the contractile pair, it attracts the matrix away from the tether bridging the original pair and, thus, the tether becomes less intense (Fig. 4.7b). As more cells are progressively induced, matrix densification between the first pair decreases accordingly, until it is finally vanished (Fig. 4.7, b to e). In addition, these simulations depict the preference of each cell to bond with the nearest adjacent cell. For example, when a third cell is induced in the matrix (Fig. 4.7b), it interconnects with the nearest neighbouring cell, while we observe a weak yet visible tendency towards the cell located further. But when a cell is added in the vicinity of these non-connected cells, we see tethers formed between the new entry and each one of the cells in concern, as the former is close enough to apply pulling forces that induce matrix densification (Fig. 4.7d).

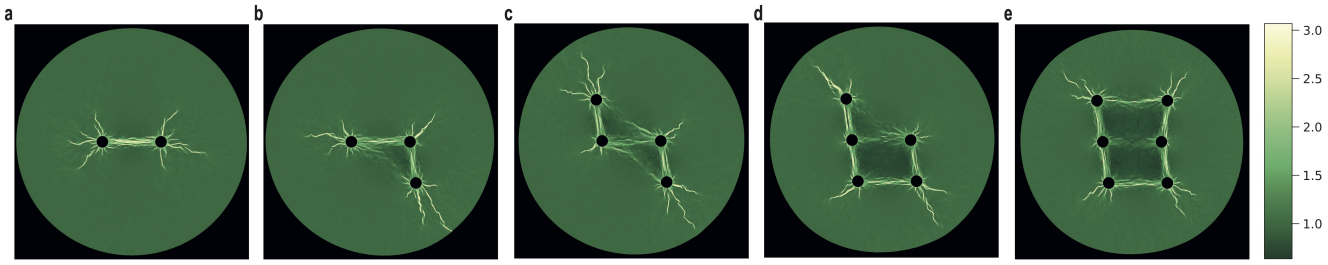

FIGURE 4.7. **Axial fields of densification which interconnect nearest neighbors.** Simulations with identical cells at 50% contraction and model $S(\lambda) = \lambda^7 - \lambda^5$. We start with two cells separated by $5r_c$, where r_c is the undeformed cell radius **(a)** and sequentially add one cell at a time **(b-e)**. The initial tether in **(a)** weakens as more and more cells are introduced in the system, until it vanishes **(e)**. Cells show preference to their nearest neighbour in order to interconnect.
Colorbar: densification ratio of the deformed networks.

4.2 Contrasting the threshold levels for the emergence of densification within the two model families

4.2.1 Fiber collapse instability is accountable for the sudden growth of localized densification bands

Given that the primary disparity between the two model families lies in the unstable compression regime in Family-2 models, where the $S(\lambda)$ curve has negative slope (Fig. 3.7b), the outcomes in Section 4.1 imply that fiber collapse instability is accountable for the sudden growth of localized densification bands. To assess this conjecture, we employ simulations to explore the network's response under incremental cell contraction, and capture the onset of densified band formation.

Figure 4.8a-e presents a Family-2 network with a cell undergoing contraction at five successive stages, spanning from **20%** to **40%** reduction in the cell reference radius. Initially, as contraction progresses, the densification ratio of essentially the same few triangles proximal to the cell increases linearly with cell contraction (Fig. 4.8a-d) up to **35%**. Remarkably, at the next level of (**40%**) contraction, densified bands around the contracting cell have appeared, extending noticeably further into the matrix (Fig. 4.8e). Below each plot of Fig. 4.8a-e, in a "tree diagram", we plot the stretch of each individual fiber (abscissa) versus distance from the cell center (ordinate) for each contraction level; color indicates orientation relative to the radial direction. The evident asymmetry near the base of each tree at larger contractions shows the difference of compressive versus tensile stretches. Tensile stretches $\lambda > 1$ grow gradually with increasing contraction. In fibers under compression ($\lambda < 1$), the stretch first decreases slowly, with only a few fibers in the unstable regime $\lambda < 0.85$ (red dotted line), all of whom are close to the cell up to **30%** contraction. At **35%** there is a steep increase in the number of fibers below the threshold, with stretches down to 0.4 and reaching more than 6 cell radii into the network by **40%** contraction. Going back to the respective densification ratio configurations, we observe that the jump in fiber compressive stretch and the abrupt appearance of densified bands occur at the same contraction level between **35%** and **40%**.

This trend in densification localization is reflected in plots of the maximum over the network of the densification ratio inverse $1/\varrho_{max}$, and the minimum stretch λ_{min}, at each contraction level (Fig. 4.8f). We note that $1/\varrho_{max} = J_{min}$, the minimum area ratio, corresponding to the most compressed triangular element. The densification ratio first increases slowly with contraction, then there is a steep rise between 35 and **40%** contraction, the level at which extensive localized densification is spotted (Fig. 4.8e). The minimum fiber stretch follows exactly the same behavior as $1/\varrho_{max}$, the two curves in Fig. 4.8f being nearly identical. Initially, λ_{min} decreases approximately linearly with contraction, namely the minimum stretch occurs at the cell boundary as dictated by the boundary conditions

$$\lambda_{min} = 1 - \gamma, \tag{4.1}$$

with γ the fractional cell diameter decrease. Then there is a sudden drop in stretch magnitude at $\mathbf{35-40\%}$ contraction, exactly the level of sudden $\mathbf{1/\varrho_{max}}$ drop in Fig. 4.8f and band growth in Fig. 4.8e. This shows that element densification is driven by fiber collapse as explained in Fig. 3.10f. We recall also Fig. 4.1m showing a collapsed red fiber within each densified green triangle (see Section 3.3.3., *Fiber collapse instability*)

The behavior of Family-1 networks is different (Fig. 4.8g, Fig. 4.9, Fig. 4.10). The minimal stretch λ_{min} follows (4.1) all the way up to the largest simulated contraction (red line in Fig. 4.8g), occurs on the cell boundary, and is equal to cell boundary contraction prescribed by boundary conditions. This shows that fiber collapse is not observed, as expected. In contrast, the maximal densification ratio does undergo a sudden leap ($\mathbf{1/\varrho_{max}}$ drop in Fig. 4.8g) as in Family-2 models, albeit at a higher contraction level of $\gamma \approx \mathbf{45\%-50\%}$. This is evidence of an element collapse instability (see Section 3.3.3.) that is weaker and requires higher cell contraction than the fiber collapse instability of Family-2 models. Notably, this instability occurs in the linear fiber model $\mathbf{S(\lambda)=\lambda-1}$ (Fig. 4.9) as well as the nonlinear ones (Fig. 4.10).

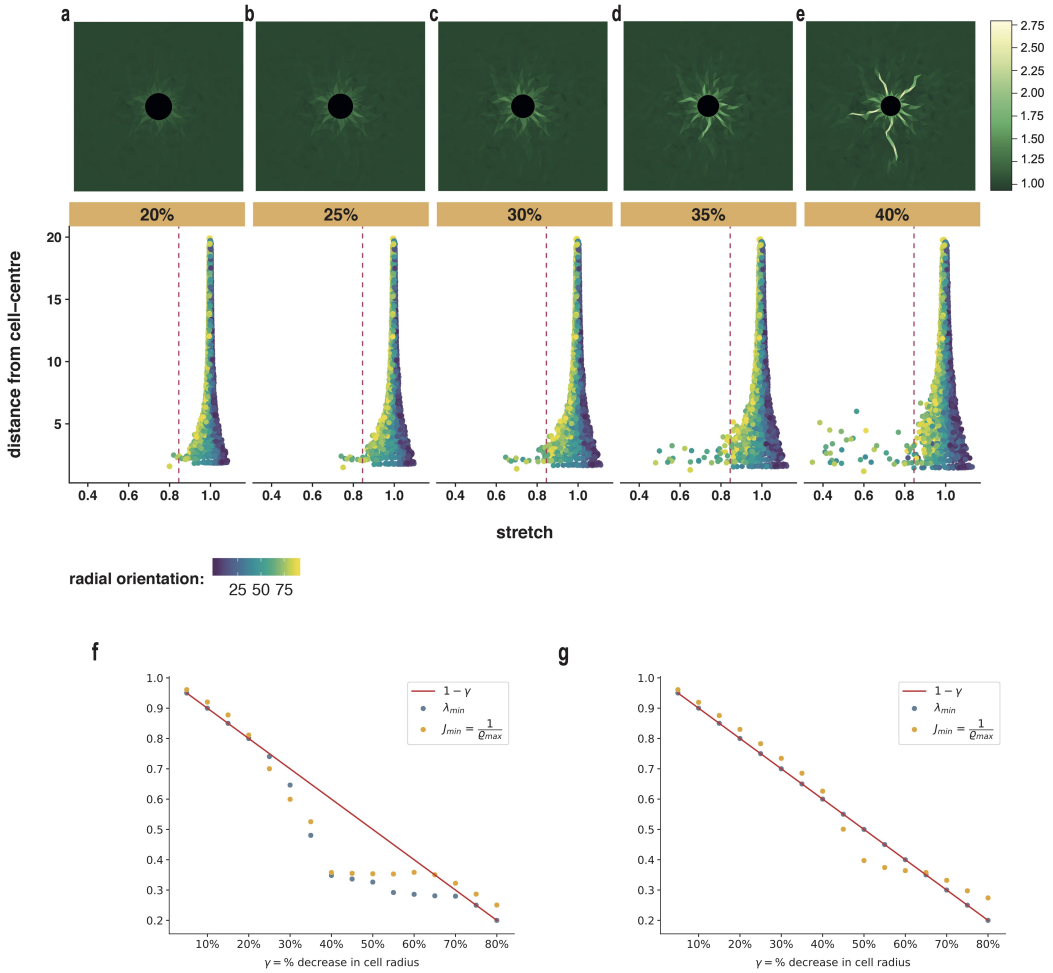

FIGURE 4.8. **Progressive cell contraction and densification localization - Family 2.** **(a-e)** Simulations with Family-2 model $S(\lambda) = \lambda^7 - \lambda^5$ of a cell contracting in the range $5\% - 80\%$. Top: densification ratio ϱ color plot at each indicated contraction step. Bottom: tree diagrams, fiber distance from cell center versus fiber stretch for all fibers in the network at each contraction step, *x axis*: fiber stretch, *y axis:* fiber distance from cell center. **(f,g)** Maximum densification ratio inverse $1/\varrho_{max}$ and minimum stretch value λ_{min} over the network at each contraction level, for **(f)** Family-2 $S(\lambda) = \lambda^7 - \lambda^5$ and **(g)** Family-1 $S(\lambda) = \lambda - 1$. Note that $1/\varrho_{max} = J_{min}$. Red solid line: cell boundary stretch imposed by boundary conditions.
Colorbars: Densification ratio ϱ and fiber radial orientation (in degrees).

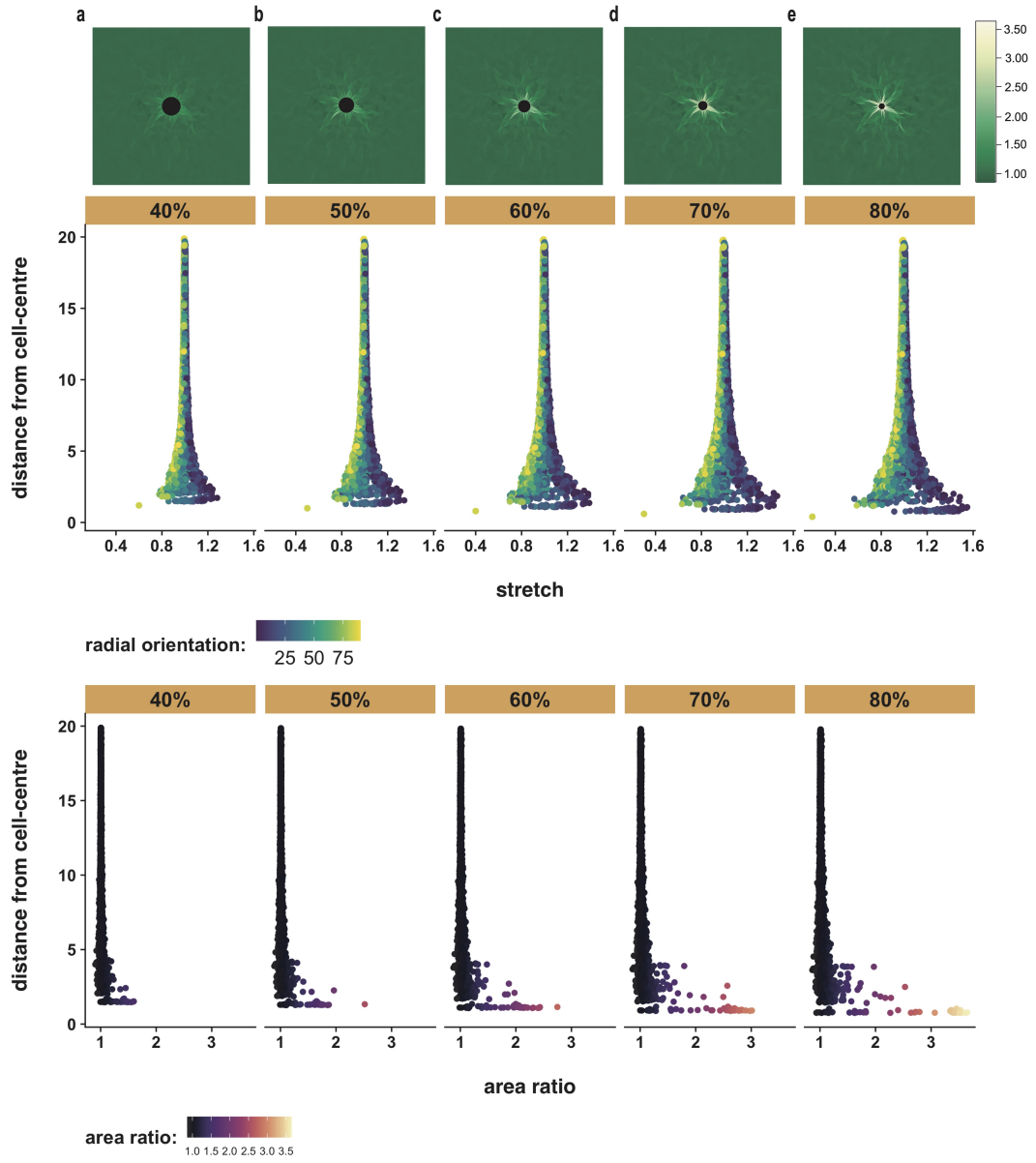

FIGURE 4.9. **Progressive cell contraction and densification localization - Family 1.** Complementary to Fig. 4.8. Simulations with the linear Family-1 model $S(\lambda) = \lambda - 1$ of a cell contracting in the range $5\% - 80\%$. *Top:* densification ratio ϱ color plot at each indicated contraction step. *Middle:* tree diagrams, fiber distance from cell center versus fiber stretch for all fibers in the network at each contraction step, x axis: fiber stretch, y axis: fiber distance from cell center. *Bottom:* triangular element distance from cell center versus densification area ratio, *x axis:* densification area ratio ϱ, *y axis:* triangular element distance from cell center.

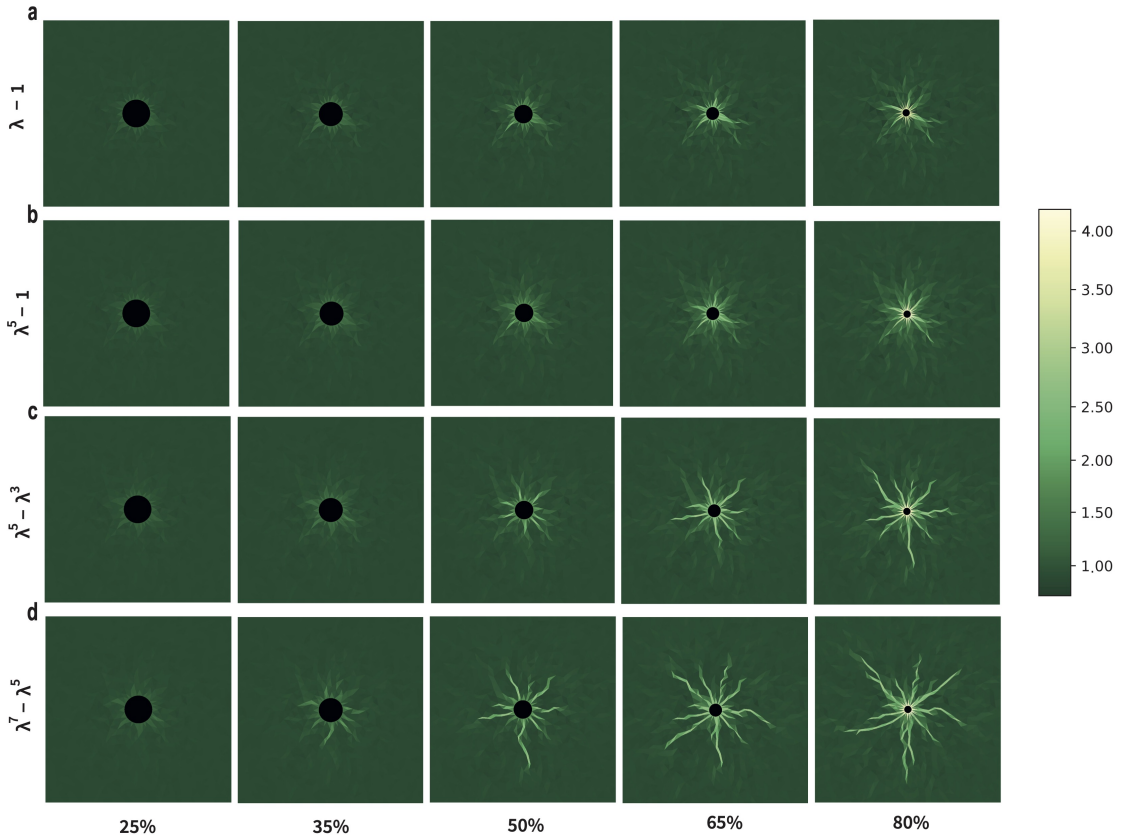

FIGURE 4.10. **Progressive contraction and densification in single-cell simulations.** As contraction level rises, densification strengthens in the close proximity of the cell for Family-1 models in **(a-b)**. The bands consisting of densified elements do not propagate far from the cell boundary, reaching as far as 3 deformed cell radii at **80%**. On the contrary, in Family-2 simulations **(c-d)** densification is evident at much lower contraction levels, **35%**. With increased contraction, more densified bands are generated and extend substantially further into the matrix. Colorbar: densification ratio ϱ of deformed networks.

4.2.2 Identifying instabilities in the emergence of tethers

What are the mechanisms responsible for the significant differences between tethers in the two Family models? We have witnessed how fiber and element collapse instabilities emerge due to single-cell contractions. Following the prominent differences between the two families with respect to tether formation, we report here observations of pairs of cells undergoing progressive cell contraction. Extremely compressed fibers occur in Family-2 tethers ($\lambda_{min} \approx 0.3$) but not in Family 1, where $\lambda_{min} \approx 0.6$ (Fig. 4.11a,b). In Family 2, fiber collapse (extreme fiber compression, sudden λ_{min} drop in Fig. 4.11b) occurs at the same time as extreme densification (sudden $1/\varrho$ drop , Fig. 4.11b). On the contrary, in Family 1, we see extreme densification without fiber collapse (Fig. 4.11a). In Family 2, most collapsed triangles within the tether contain a highly compressed fiber, oriented within $45°$ of the vertical (Fig. 4.11d as in Fig. 3.10e). In contrast, in Family-1, collapsed triangles have nearly horizontal bases, while the other two sides are under moderate compression, and are closer to horizontal than vertical after collapse (Fig. 4.11c as in 3.10g). These findings indicate that fiber collapse instability is the main player in Family-2 tethers, whereas the dominant role in Family-1 tethers is played by element (triangle) collapse instability.

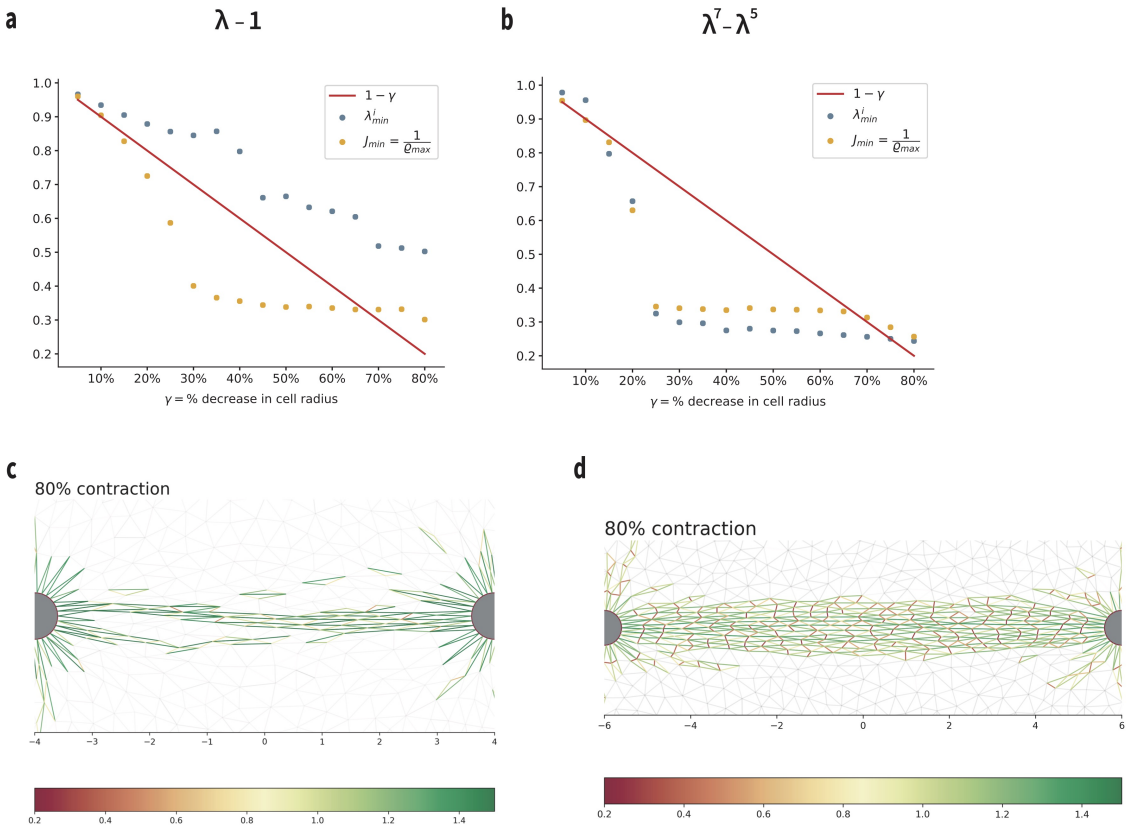

FIGURE 4.11. **Mechanisms of densification within tethers in the two Families.** **(a-b)** Maximum densification ratio inverse $1/\varrho_{max}$ and minimum stretch value λ^i_{min} over the network at each contraction level excluding fibers on the cell boundary, for Family-1: $S(\lambda) = \lambda - 1$ and Family-2: $S(\lambda) = \lambda^7 - \lambda^5$ respectively. Note that $1/\varrho_{max} = J_{min}$. Red solid line: cell boundary stretch imposed by boundary conditions. **(a)** Element area collapse (yellow dots) occurs without fiber collapse (blue dots), indicating element collapse instability. **(b)** Densification (yellow dots) occurs simultaneously with fiber collapse (blue dots), suggesting fiber collapse instability. **(c-d)** Stretch of fibers (red: compression; green: tension) at 80% contraction within a Family-1 tether (c) and Family-2 tether (d). Note scarcity of compressed fibers despite presence of collapsed triangles in (c), indicating element collapse instability. In contrast, in (d) most collapsed triangles contain a highly compressed fiber, pointing towards fiber collapse instability.

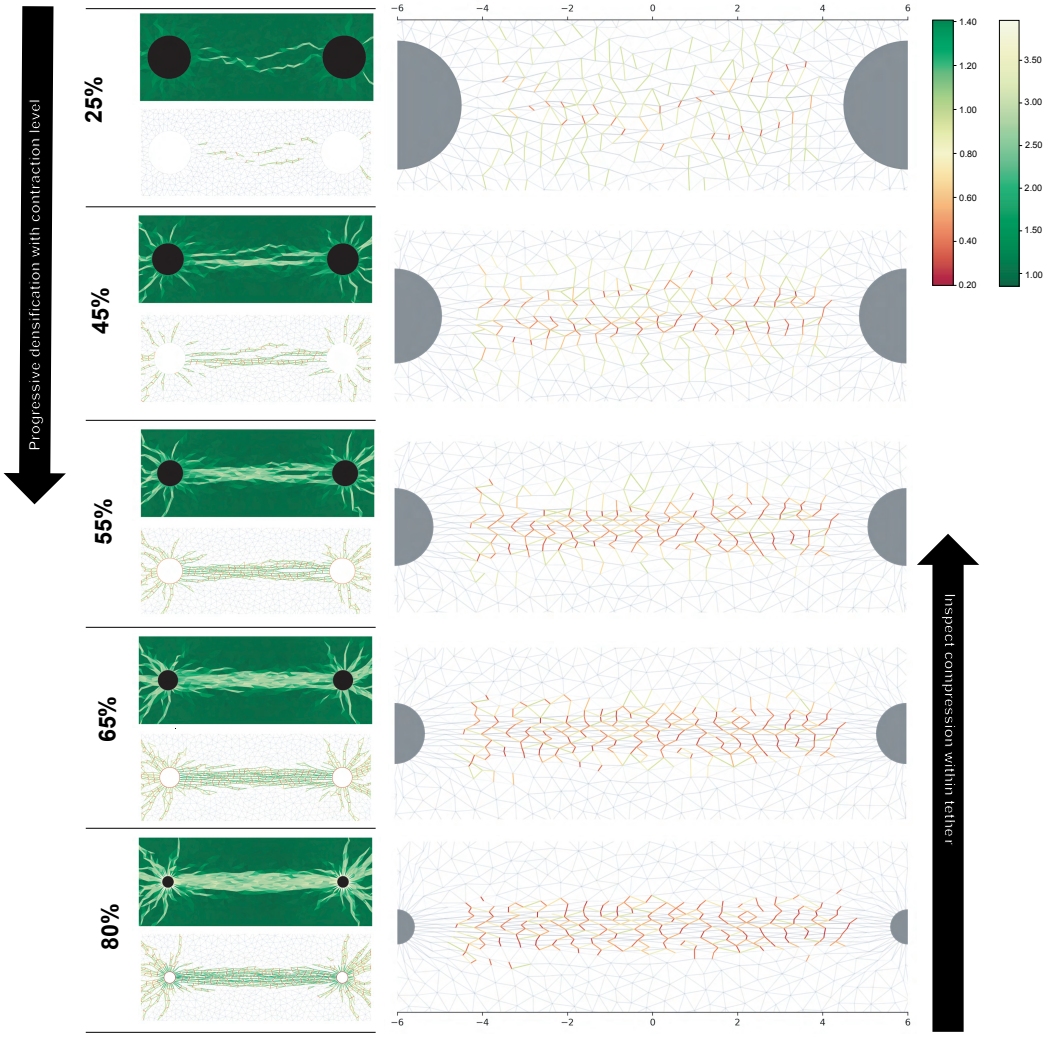

FIGURE 4.12. **Compression instability as dominant mechanism in ECM deformations.** Progressive contraction of two cells with Family-2 model $S(\lambda) = \lambda^7 - \lambda^5$. In the left column, we observe the emergence of the tether bridging the cells (color plots of densification ratio). At each contraction state, and beneath each of the densification plots, we depict the stretches of the fibers comprising the densified elements. Note the excessive fiber alignment within the densified regions (horizontal alignment across the tether, radial alignment around the contracting cells). In the right column, we depict the fibers of the solid tether in reverse order, i.e. at each state, we mark the fibers that comprise the tether at the final contracted state **80%**, to inspect the behavior of individual fibers as the contraction intensifies. With increased contraction, more individual fibers appear to be extremely compressed, $\lambda < 0.6$, which means that they are well within the regime of fiber collapse instability. As compressed fibers and subsequent triangles collapse, fibers under tension align almost perfectly in the horizontal direction, forming well-defined fiber paths that bridge the cells. These observations reveal that (i) the formation of the densified zones is a direct consequence of fiber compression instability, and (ii) fiber instability leads to the close alignment of fibers within the densified regions. Overall, alignment and densification are observed to be integral components of the same underlying mechanism.

4.3 Long-range mechanosensing

4.3.1 Two fields of displacement propagation

In order to further characterize the deformations due to a single contracting cell, it is essential to explore how fast or slow the induced displacements decay for each one of the proposed constitutive models. The quantification of displacements propagation over the disk provides an insight into cell's zone of influence, its relevance to cell-contraction and the possible effects of network's size. Thereby, we consider cell contractions in the range of 5% to 80% at different domain sizes, ranging from $5r_c$ to $15r_c$, where r_c is the cell radius, and fit the radial displacements of the network vertices to:

$$u(r) \propto Ar^{-n} \tag{4.2}$$

where $u(r)$ is the radial component of displacement for each node and r denotes its distance from the center of the contracting cell. Parameters A and n are constants and $n > 0$ is the decay power. Linear elasticity predicts $n = 1$ in two dimensions, therefore we expect n to deviate from the linear elastic solution, providing evidence that our model captures the slow decay of displacements in natural ECM networks. Indeed, we report the decay power n to be substantially lower than one, regardless the constitutive model. Previous studies predicted the presence of two [24] or more [82] distinct domains of the decay scaling. These domains were defined such as to discriminate between a near-field regime, where the displacements decay slow with $n < 1$ in (4.2), and a far-field regime, where displacements were generally considered to decay with $n = 1$, pointing out a transition from a nonlinear to a linear ECM elastic behavior. Here, we argue that this transition cannot be arbitrarily considered at the same distance from the contracting cell at all cases, i.e. ruling out the domain size and the magnitude of cell-contraction. Thus, we devise an iterative method to find the radius R_* at which the total mean squared error of the fitted displacements is minimized, with displacements at distance $r \leq R_*$ fitted to eq. (4.2) while for those at distance $r > R_*$ we explore the following cases:

$$u(r > R_*) \propto A_2 r^{-1} \tag{4.3}$$

$$u(r > R_*) \propto A_2 r^{-1} + Br \tag{4.4}$$

$$u(r > R_*) \propto A_2 r^{-m} + Br \tag{4.5}$$

While the aforementioned studies, used solely eq. (4.3) to describe the far-field as linear elastic, here we examine the behavior of the material at this regime using the general elastic solutions in eq. (4.4), (4.5). In Fig. A.5 and Fig. 4.13, we summarize our results when exploring the decay power in either one regime, i.e. the whole matrix, or in two regimes, using the method described above and each of the eq. (4.3-4.5) for the radial displacements in the second regime. We identify two regimes to describe better the propagation of displacements, as the errors of fits with any of the above cases are significantly lower ($P < .0001$) than the ones gained when

we considered the whole domain with eq.(4.2). Results discussed here concern Family-2 model $S(\lambda) = \lambda^5 - \lambda^3$, however they are common for all constitutive models. More importantly, we report the significance of eq. (4.4), (4.5) in describing the behavior in the far-field compared to previously reported eq. (4.3). Even if the difference between these two fitting power-laws is not statistically significant, it is remarkable to note the behavior of decay power m in the far-field. The decay power m in the far-field (Fig. 4.13c), is greater than 0.8 or close to linear elastic solution $m = 1$, mainly for the largest domains, with clear dependence on cell-contraction. As domain size decreases and for contraction levels $\geq 40\%$ power m shows a denoting decrease. These findings, demonstrate the importance of exploring the decay parameter m in the far-field rather than assuming linear elastic behaviour at all cases. We note that even though the main zone of influence of the contracting cell appears to be the highly nonlinear near-field, the magnitude of contraction apparently affects the far-field as well.

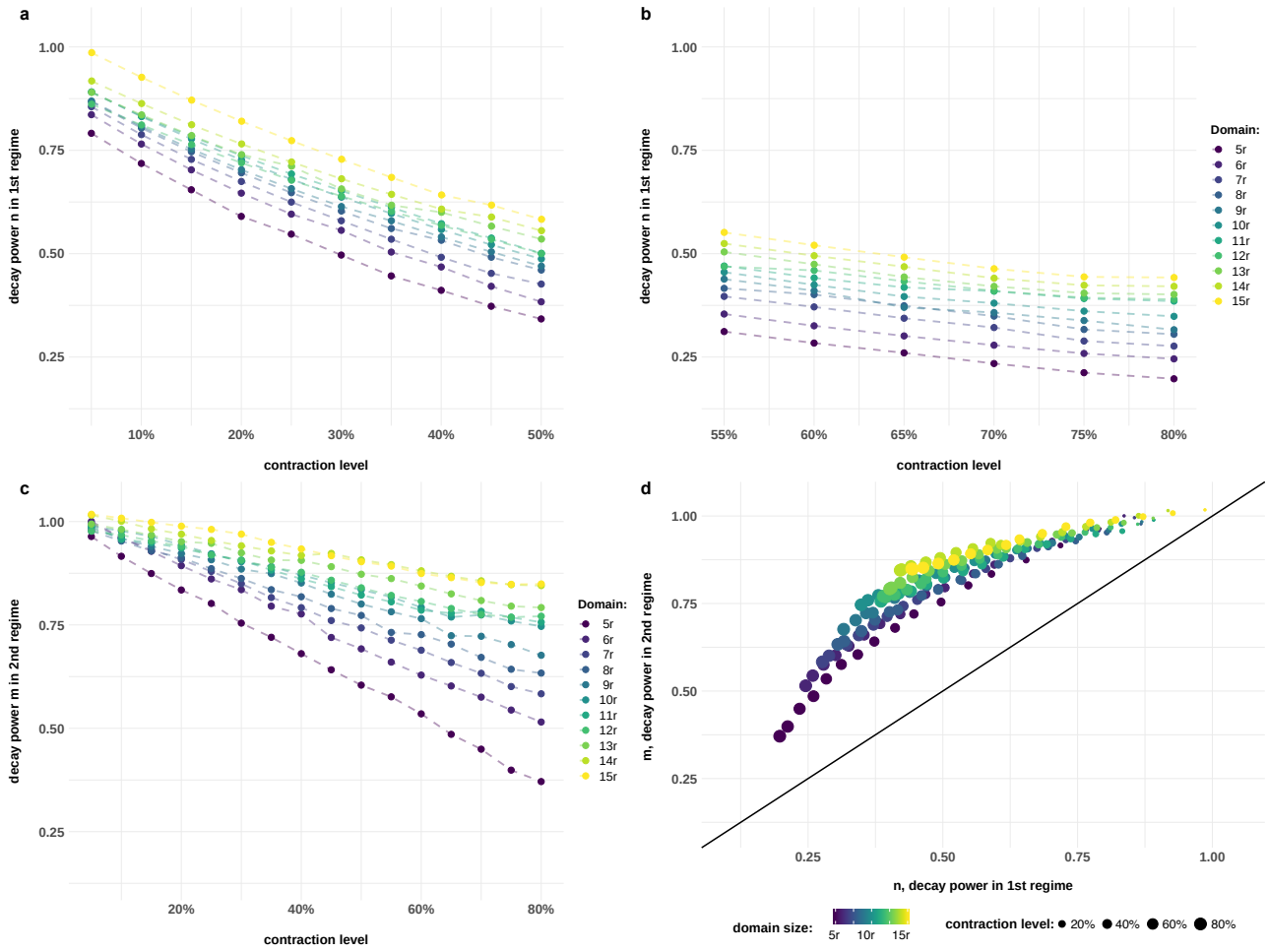

FIGURE 4.13. **Cell contraction and displacements decay. (a-b)** Decay power in near-field at contraction levels ranging from 5% to 80%, for 16 network (domain) sizes. We observe a monotonic decrease in the decay as contraction progresses, regardless the domain size, for contractions $\leq 50\%$ **(a)** while at more extreme contraction levels **(b)** displacements' propagation does not show the same variation. **(c)** Decay power m in the far-field. As the domain size increases, the decay power m is close to elastic solution $m = 1$. **(d)** *x-axis*: decay power n in near-field, *y-axis*: decay power m in far-field. The mark size denotes the contraction levels in the range discussed above. We observe that the two decay powers tend to be equal at small contraction levels in large domain sizes and at large contraction levels in small domain sizes, which denotes that in the former case the matrix resembles a linear material while in the latter exhibits high nonlinearity in its whole domain. Colormap in all subfigures denotes the matrix radius.

Focusing on the nonlinear near-field, we report that decay power decreases linearly with contraction for the linear case $S(\lambda) = \lambda - 1$ and contraction levels $\leq 50\%$. This linearity is also evident, yet vaguely disrupted, for family-1 models $S(\lambda) = \lambda^k - 1$, with $k = 3, 5$. For models $\lambda^7 - 1$, $\lambda^5 - \lambda^3$ and $\lambda^7 - \lambda^5$ the linearity is evidently lost, and we have a monotonic decrease in decay

power. This behavior is the same regarding the domain size. For extreme contraction levels, $>50\%$, the monotonic decrease is lost and we observe a plateau in decay n, as it deviates only slightly. This is true for any constitutive relation. These observations are summarized in Fig. 4.14, by taking the mean decay value over all simulated domain sizes at each contraction level.

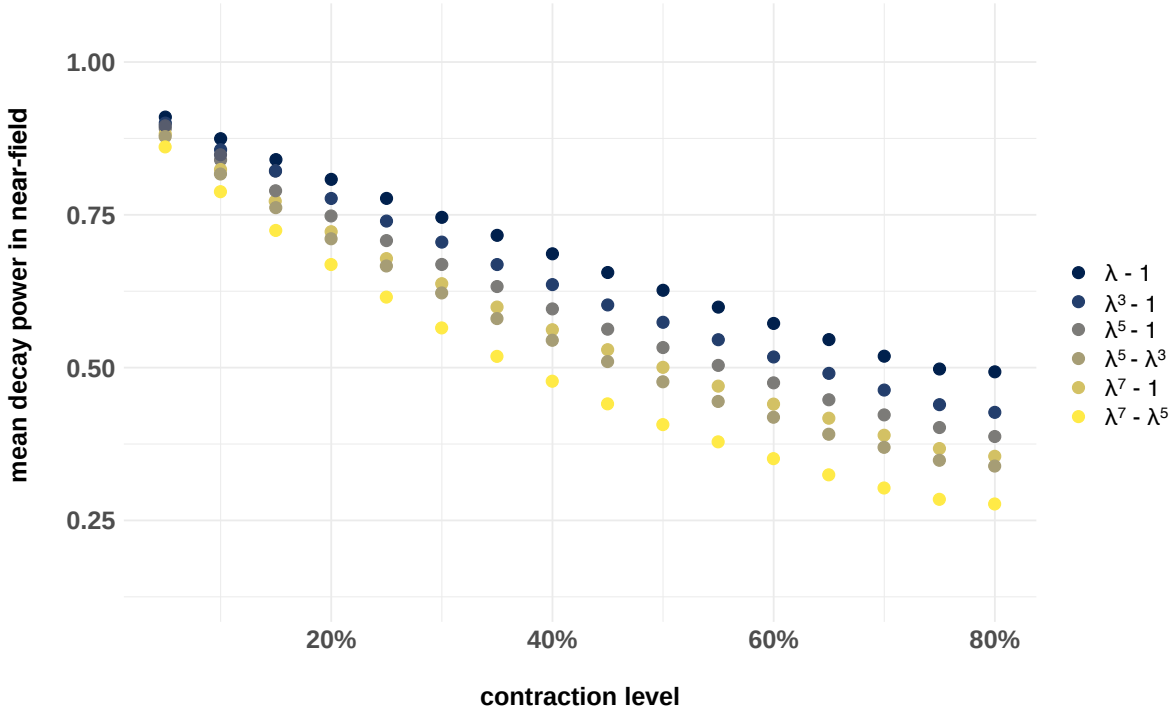

FIGURE 4.14. **Cell contraction and mean decay power in the near-field.** Mean decay power in near-field over 16 domain sizes at contraction levels ranging from 5% to 80%. Decay power decreases linearly with contraction, at least for contraction levels that reach 50%, for Family-1 models apart from $S\lambda = \lambda^7 - 1$. For the latter along with the Family-2 models there is a monotonic decrease in the decay power. In general, the decay is substantially lower than one (linear elastic solution) even for the linear case.

CHAPTER 5

Adding another dimension

οὐ δεῖ τὰς λεωφόρους βαδίζειν
ὁδούς

Πυθαγόρας

Expanding upon the foundation laid in Chapter 3, we took the initial two-dimensional model and extended it to three dimensions. The 3D model retains the same assumptions regarding individual fiber mechanics. Before we embark on an exploration of the intricacies of this extended model, let us first illuminate the rationale guiding its inception.
The ECM in biological tissues is inherently three-dimensional. Using a 3D model allows us to represent the complex spatial arrangement of ECM fibers and their interactions with cells in a way closer to reality. The advantages of going beyond two-dimensions can be summarized as:

- Biological tissues have intricate architectures with cells embedded within a 3D ECM network. This complexity cannot be fully captured in a 2D model, which assumes a flat, planar structure.

- Many biological processes, such as cell migration, tissue development, and wound healing, occur in three dimensions. Studying ECM deformations in 3D provides a more physiologically relevant context for understanding these processes.

- The mechanical behavior of ECM fibers, can vary significantly in different directions. A 3D model allows for the accurate representation of anisotropic (direction-dependent) material properties.

- Creating functional tissues or organs in the lab requires 3D models to mimic the natural tissue environment. Understanding ECM deformations in three dimensions is critical for designing and optimizing tissue engineering strategies.

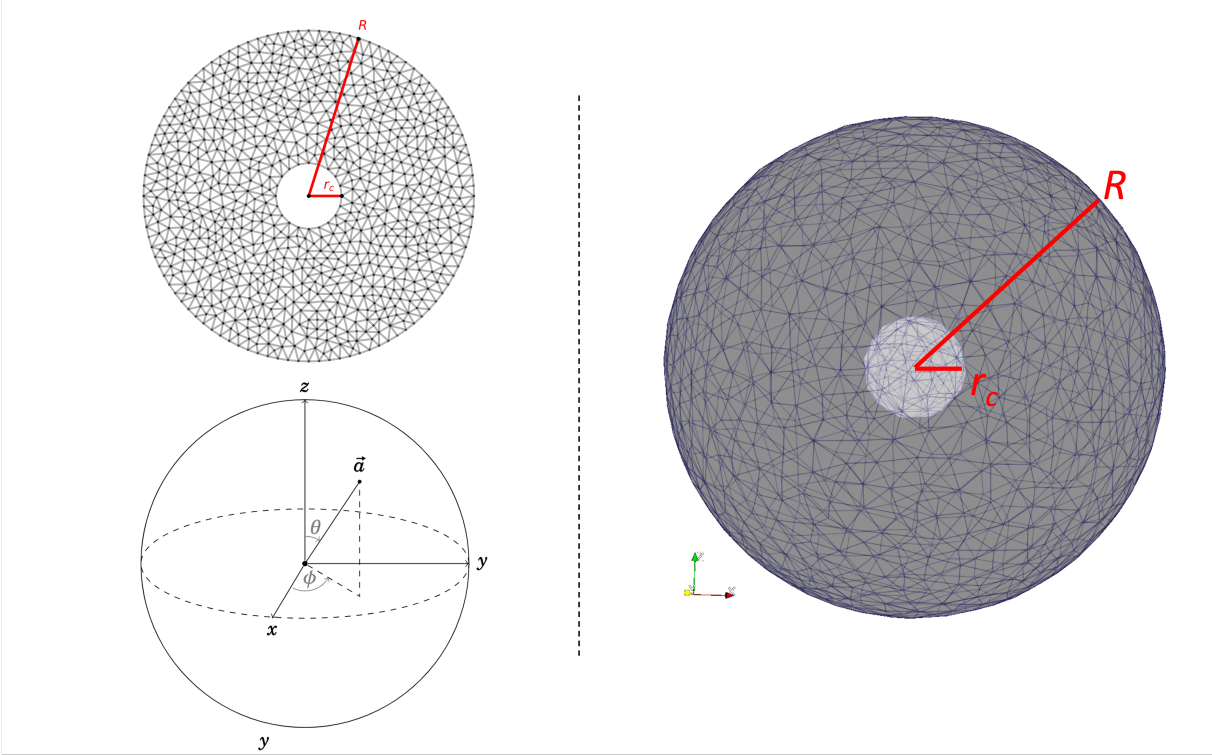

FIGURE 5.1. **ECM representation in three dimensions.** A two-dimensional fibrous matrix has been represented as a circle of radius $\boldsymbol{R}$ discretized into triangular elements whose edges correspond to individual fibers. In this network, each cell is modelled as a circular cavity of radius r_c. Consequently, in order to expand our networks to three dimensions, we define the ECM as a sphere of radius $\boldsymbol{R}$ where cells are modelled as smaller spheres (with radius $r_c << \boldsymbol{R}$) embedded in the 3D network. Just like our 2D networks, the 3D representations are networks of segments which correspond to fibers; recall that the 'fibers' are assumed to have a consistent diameter, resulting in an identical force-extension behavior for each segment.

The ECM in three dimensions

We have represented the two-dimensional ECM as a discrete domain, represented by a circular lattice of radius $\boldsymbol{R}$ consisting of triangular elements (Fig. 3.5). Expanding this setting to three-dimensions involves a geometrical rearrangement that keeps the initial $\boldsymbol{2D}$ symmetry. Thus, the $\boldsymbol{3D}$ representation of the natural ECM is a three-dimensional analogue to a two-dimensional circle: a *sphere* of radius $\boldsymbol{R}$ where cells are modelled as smaller spheres of radius r_c (Fig. 5.1).

The discretization of a spherical domain corresponds to its division into *tetrahedral elements.* Each tetrahedron is a polyhedron composed of four triangular facets, six straight edges, and four vertices (Fig. 5.2).

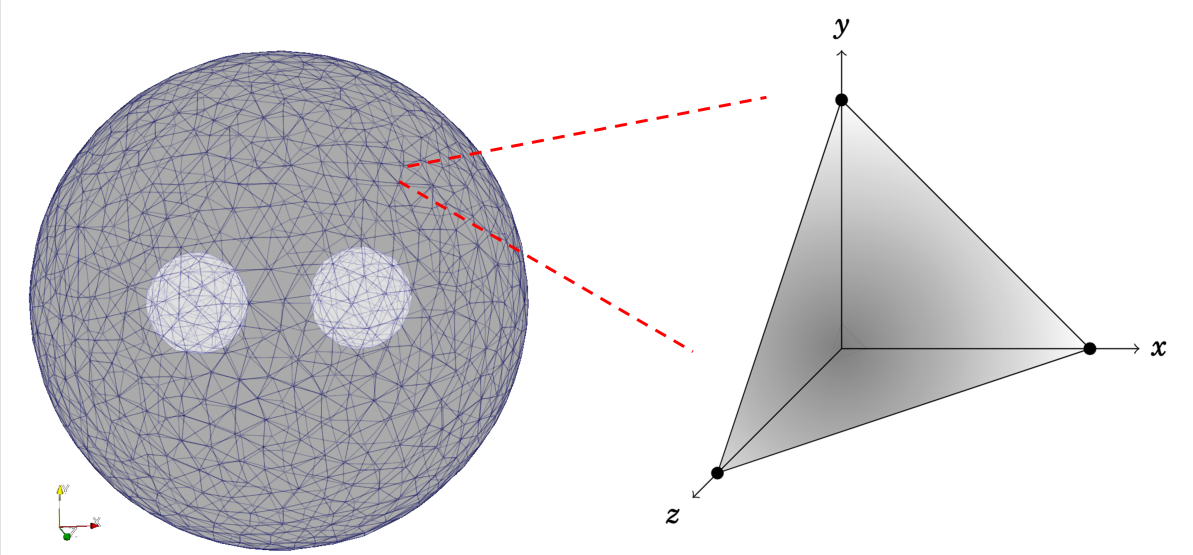

FIGURE 5.2. **Network discretization in three dimensions.** A three-dimensional fibrous matrix is represented as a sphere of radius R discretized into tetrahedral elements. Each tetrahedron is composed of four triangular facets, four vertices and six edges which correspond to individual fibers.

Each vertex corresponds to a vector with initial position $\mathbf{p_k} \in IR^3$, where $k = 1,\ldots,N$, with N to be the total number of vertices. Just like the two-dimensional problem, forces are considered to act only at the nodes of the network so that the edges, corresponding to network's fibers, are being either pulled or compressed. Recall that:

- $\lambda > 1$, (tensile stretch) the fiber is under tension
- $\lambda < 1$, (compressive stretch) the fiber is being compressed
- $\lambda = 1$, (undeformed) the fiber is relaxed.

The $3D$ problem formulation follows the two-dimensional as described in Chapter 3. In particular, we impose boundary conditions on the boundary nodes of the cell-spheres in order to simulate cell-contraction and the optimization problem minimizes the total energy of the system, as defined in eq. (3.19):

$$\hat{E}(\mathbf{x}_1,\ldots,\mathbf{x}_N) = \sum_{j=1}^{F} W(\lambda_j) + \sum_{k=1}^{K} A_k \cdot \Phi(J_k) \tag{5.1}$$

where F is the total number of fibers in the $3D$ network, K the total number of tetrahedral elements, $W(\lambda_j)$ the potential energy of an individual fiber, A_k the reference volume that element k occupies and J_k its volume ratio.

Recall that the Jacobian determinant J was defined in $2D$ eq. (3.17) as the *ratio of deformed to undeformed oriented triangle area.* Accordingly, in three-dimensions J is defined as *ratio of deformed to undeformed oriented tetrahedral volume.* In order to keep consistency between the two approaches — two and three dimensions — in maintaining positive orientation in the network, we make use of the same penalty term as a function of J, as defined in eq. (3.18):

$$\Phi(J) = e^{-Q(J-b)}, \quad b, Q > 0 \tag{5.2}$$

5.1 Preliminary results

Adhering to the same methodology employed in two dimensions, we proceed to conduct simulations involving either a singular cell or pairs of cells undergoing contraction within a fibrous network for each of the models introduced in eq. (3.7) for Family 1, and in eq. (3.8) for Family 2. When considering solitary cells, it is pertinent to note that the centers of both the cell-sphere and the domain-sphere coincide. In case of pairs of cells, the centers of the cell-spheres coincide with the plane that passes through the center of the domain-sphere. It is worth mentioning that visualizing simulations in a three-dimensional matrix proves to be quite intricate. To delve into the phenomenon of matrix densification, we captured planes of the deformed matrix. Each of these planes intersected through the centers of both the domain and the cells, effectively bisecting the entire network.
Starting with single cells at 50% contraction, we present results with linear model $\lambda - 1$ and Family-2 model $\lambda^7 - \lambda^5$. Interestingly, simulations with Family-2 model (Fig. 5.3a-b) do not resemble the irregular and extended hair-like densified bands we had in $2D$ (Fig. 4.1). However, the distribution of fiber stretches (Fig. 5.3c-d) within the deformed network depicts an important similarity. When subjected to tension $(\lambda > 1)$, fibers tend to align approximately in the radial direction, as illustrated in Fig. 5.3d. This results in the formation of continuous fiber paths that extend several cell diameters into the surrounding matrix. However, it is important to note that this alignment is notably heterogeneous around the contracting cell, leading to varying path lengths in different directions. Conversely, fibers experiencing compression $(\lambda < 1)$ tend to orient themselves closer to the angular direction, giving rise to loops around the cell-sphere, as depicted in Figure 5.3c. The distribution of compressive stretch around the cell

exhibits significant heterogeneity, mirroring observations made in the two-dimensional networks (Figure 4.1). Notably, the phenomenon of matrix densification also displays a similar level of inhomogeneity. In the accompanying Fig. 5.4, we illustrate matrix densification by examining four different planes of the sphere, as previously described. Two key observations emerge from this analysis: (i) the densification ratio exhibits considerable heterogeneity and irregularity around the contracting sphere at each plane, and (ii) the distribution of densification ratio at each slice is distinct and varies across the different planes.

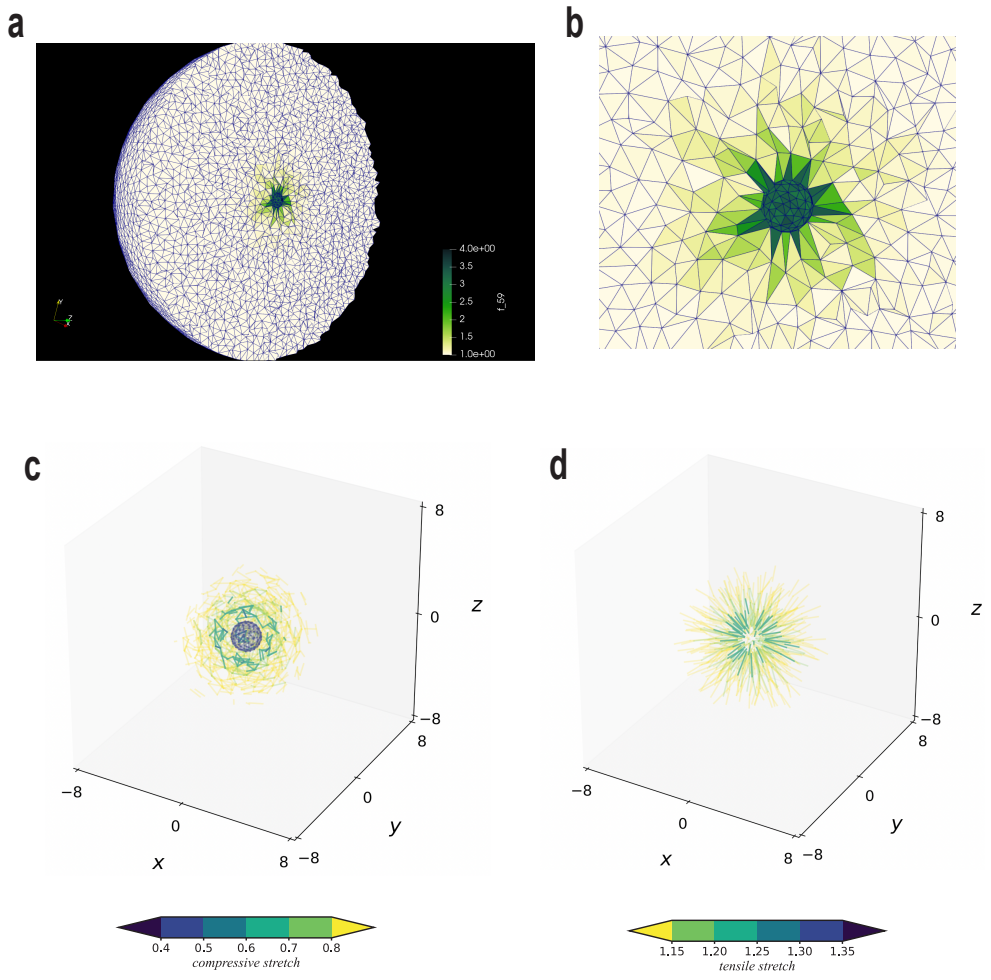

FIGURE 5.3. **Matrix densification and fiber stretches in three dimensions - Part I.** Simulation with Family-2 model $\lambda^7 - \lambda^5$ and a single cell contracting at **50%** of its reference volume. **(a)** Representation of the deformed **3*D*** matrix. Colorbar: densification volume ratio ρ of tetrahedral elements. **(b)** Close-up of the contracting cell. **(c)** Compressive stretches in deformed fibers ($\lambda < 1$). **(d)** Tensile stretches in deformed fibers ($\lambda > 1$).

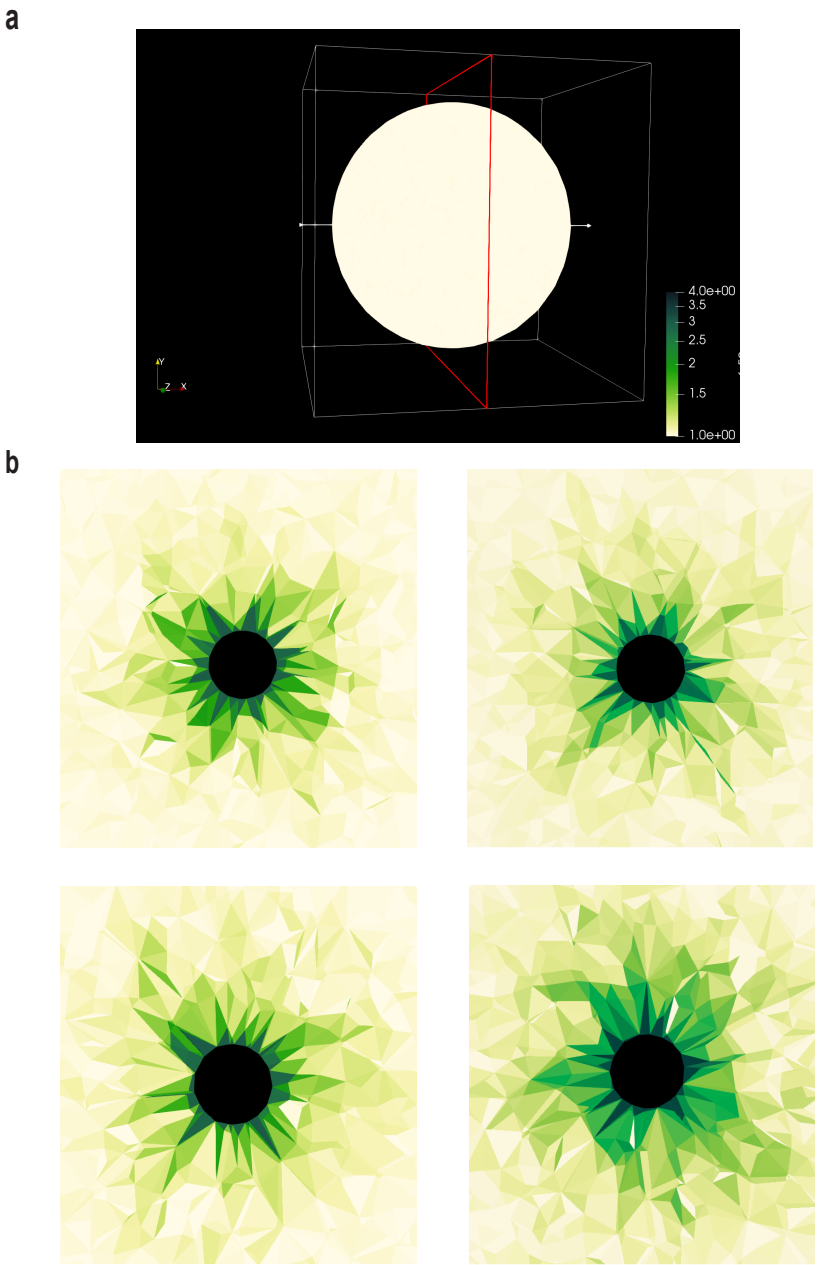

FIGURE 5.4. **Densification heterogeneity around contracting spheres.** Complementary to Fig. 5.3. Simulation with Family-2 model $\lambda^7 - \lambda^5$ and a single cell contracting at **50%** of its reference volume. We depict densification ratio ϱ at four different planes of the network. **(a)** Example of how a plane is chosen. The red rectangular defines where the particular plane bisects the $3D$ network. **(b)** At each plane, the densification ratio exhibits considerable heterogeneity and irregularity around the contracting sphere. In addition, the distribution of densification ratio at each slice is distinct and varies across the different planes.

We replicate the analysis using simulations involving the linear Family-1 model, denoted by $\lambda - 1$. Similar to the predictions in the two-dimensional model, densification appears to be concentrated in proximity to the cell boundary (Fig. 5.5, 4.1). Fibers under compression ($\lambda < 1$) are oriented close to the angular direction, just like in the Family-2 case discussed above, forming loops around the cell. However, within each of these loops, and close to the cell boundary, the stretch is nearly uniform for the linear case in contrast to the Family-2 case (Fig. 5.3c, Fig. 5.5c). In addition, the maximum compression is up to twice as high as in Family-1 simulations, 60% compression (or stretch $\lambda \approx 0,4$) compared to 30% ($\lambda \approx 0,7$) for Family 1. Once more, these discoveries align with the observations in the two-dimensional model, where compressive stretches display a comparable uniform distribution around the contracting cell and the difference in compressive magnitude is similarly noticeable. Fibers under tension ($\lambda > 1$) align roughly with the radial direction, forming again continual paths that propagate a few cell diameters into the matrix. One important difference with Family-2 prediction is that, fibers overall reach higher levels of tension with the linear model compared to Family-2 (Fig. 5.3d, Fig. 5.5d).

When it comes to matrix densification, distinctions arise between the two models. As depicted in Figure 5.6, we analyze matrix densification using the same four planes of the sphere that were employed for the Family-2 model. Two notable observations come to light from this examination: (i) the densification ratio displays a more uniform and regular pattern around the contracting sphere, and (ii) the distribution of densification ratio remains consistent across the various planes, with pronounced densification observed only in very close proximity to the cell boundary. Both of these observations stand in sharp contrast to the findings in the Family-2 model.

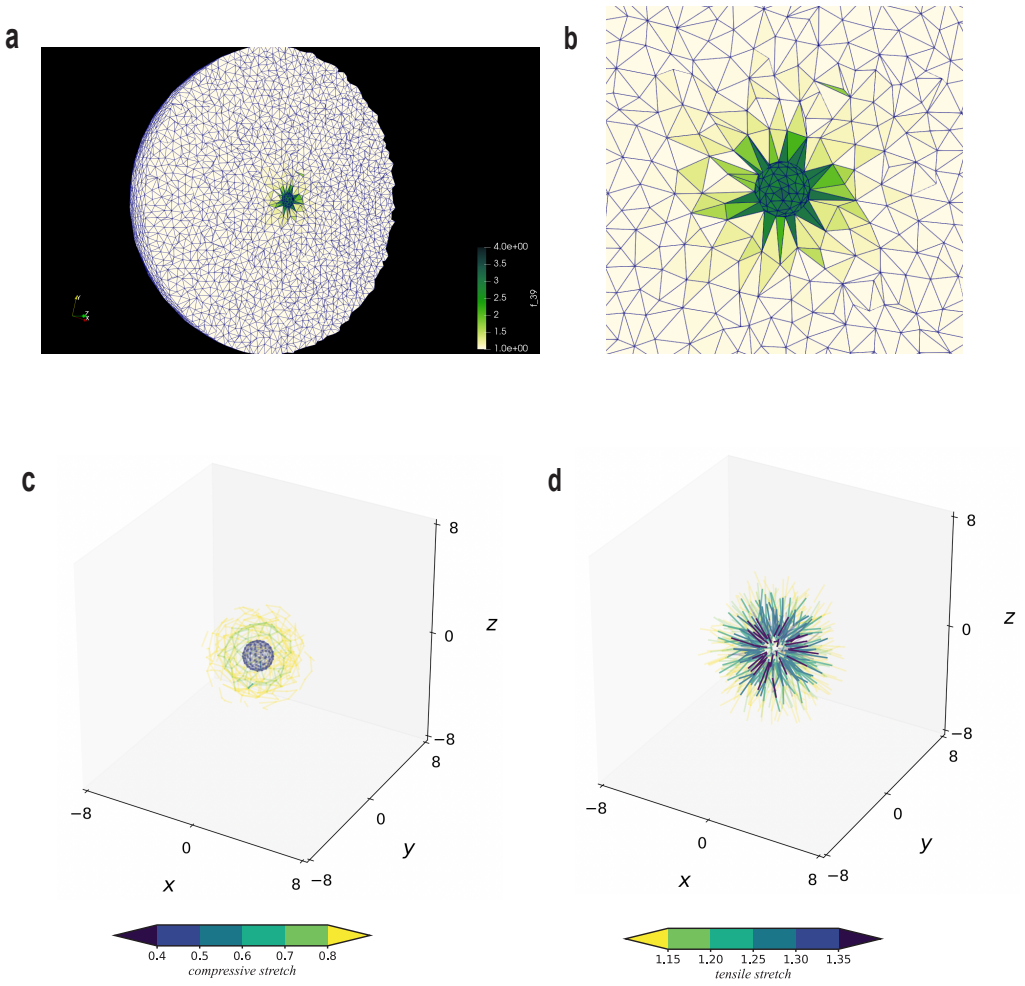

FIGURE 5.5. **Matrix densification and fiber stretches in three dimensions - Part II.** Simulation with Family-1 model $\lambda - 1$ and a single cell contracting at 50% of its reference volume. **(a)** Representation of the deformed $3D$ matrix. Colorbar: densification volume ratio ρ of tetrahedral elements. **(b)** Close-up of the contracting cell. **(c)** Compressive stretches in deformed fibers ($\lambda < 1$). **(d)** Tensile stretches in deformed fibers ($\lambda > 1$).

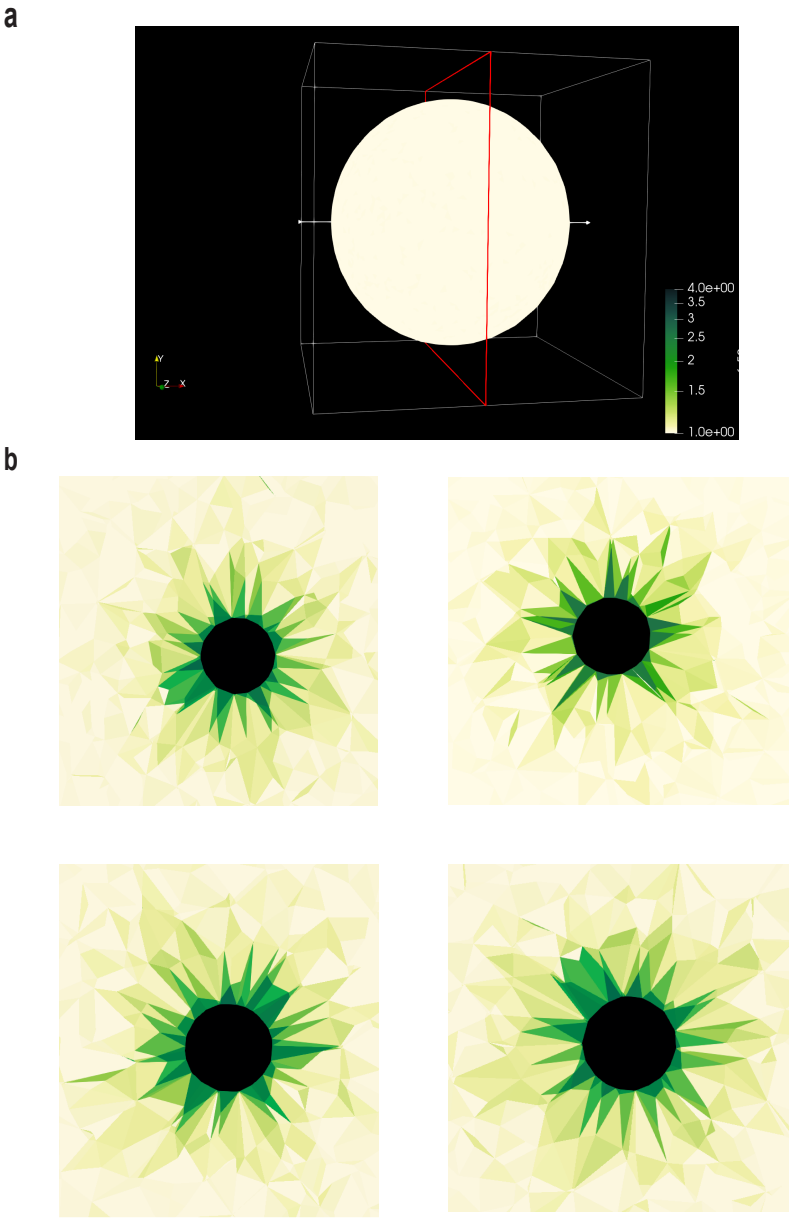

FIGURE 5.6. **Densification distributes uniformly around contracting spheres in linear networks.** Complementary to Fig. 5.5. Simulation with Family-1 model $\lambda - 1$ and a single cell contracting at **50%** of its reference volume. We depict densification ratio ρ at four different planes of the network. **(a)** Example of how a plane is chosen. The red rectangular defines where the particular plane bisects the $3D$ network. **(b)** The densification ratio displays a more uniform and regular pattern around the contracting sphere. Additionally, the distribution of densification ratio remains consistent across the various planes, with pronounced densification observed only in very close proximity to the cell boundary.

Tethers in three dimensions

In Chapter 4 we reported on simulations featuring a pair of cells undergoing contraction, with each cell reduced to **50%** of its initial radius. These cells were positioned at separations of either 6 times the cell radius ($6r_c$) or 4 times the cell radius ($4r_c$), where r_c denotes the cell radius (see Fig. 4.3, Fig. 4.4, Fig. 4.5). Notably, we observed the spontaneous emergence of intercellular tethers. These tethers were characterized by slender, roughly parallel bands exhibiting heightened densification and fiber alignment, effectively linking the two cells together. When cells were separated by larger distances, tethers were generated only with Family-2 models. In contrast, for Family-1 models, cells necessitated a significantly higher degree of contraction to initiate tether formation. Additional densified bands emanated radially from each cell (Fig. 4.3c, Fig. 4.4c). In Family-1 simulations, matrix densification is limited close to the cell boundary and cells remain isolated and disconnected (Fig. 4.3a,b, Fig. 4.4a,b). Repeating simulations with pairs of cells with the $3D$ network, we observe the same behavior. We report on simulations with cells separated by $5r_c$, involving the linear Family-1 model, denoted by $\lambda - 1$ and Family-2 model $\lambda^7 - \lambda^5$, Fig. 5.7. We observe a tether connecting the two cell-spheres with Family-2 model, while in Family-1 case the cells appear to be isolated with densification restricted only in the close proximity of the cells. Additionally, we report the intense densification around each contracting cell in Family-2 case, which sharply contrasts with the more modest densification levels observed in the Family-1 case. Focusing on the tether that formed (Fig. 5.7b), we depict its structure at the midpoint between the cells by examining two planes that intersect through the center, Fig. 5.8. Remarkably, the tether exhibits a notably irregular and disrupted structure, aligning with predictions from 2D networks. We see densification extending towards various directions with no certain preference. Additionally, we note that its geometry does not adhere to any specific pattern, such as a cylindrical shape, but rather, it appears entirely irregular. When tether is formed (Family-2 model), we observe a fraction of fibers, located almost entirely in the intercellular region, to be highly stretched (Fig. 5.9b). These fibers are aligned with the horizontal direction passing through the cell centers, generating straight paths of fibers connecting the two cells. These paths comprise the tether. At the same time, fibers under extreme compression occupy the same region as the tensile ones, but their orientation is nearly perpendicular to the paths of the tensed and aligned fibers (Fig. 5.9b). Fiber compression magnitude is almost twice as large with Family 2, reaching approximately **70%** compression. This indicates that in Family-2 tethers, compressed fibers are well within the regime of the fiber collapse instability. In addition, we observe highly compressed fibers within loops surrounding the cells. In these loops, the distribution of fiber stretch is inhomogeneous, as we discussed in single-cell simulations. For Family-1 model $\lambda - 1$, the are no fiber paths and tensile stretches are distributed in a broader region between cells, without the strong alignment we have with Family-2 model. In addition, compressive stretches in Family-1 prediction are confined to concentric loops around each individual cell instead of the region between cells, and

oriented in the circumferential direction.

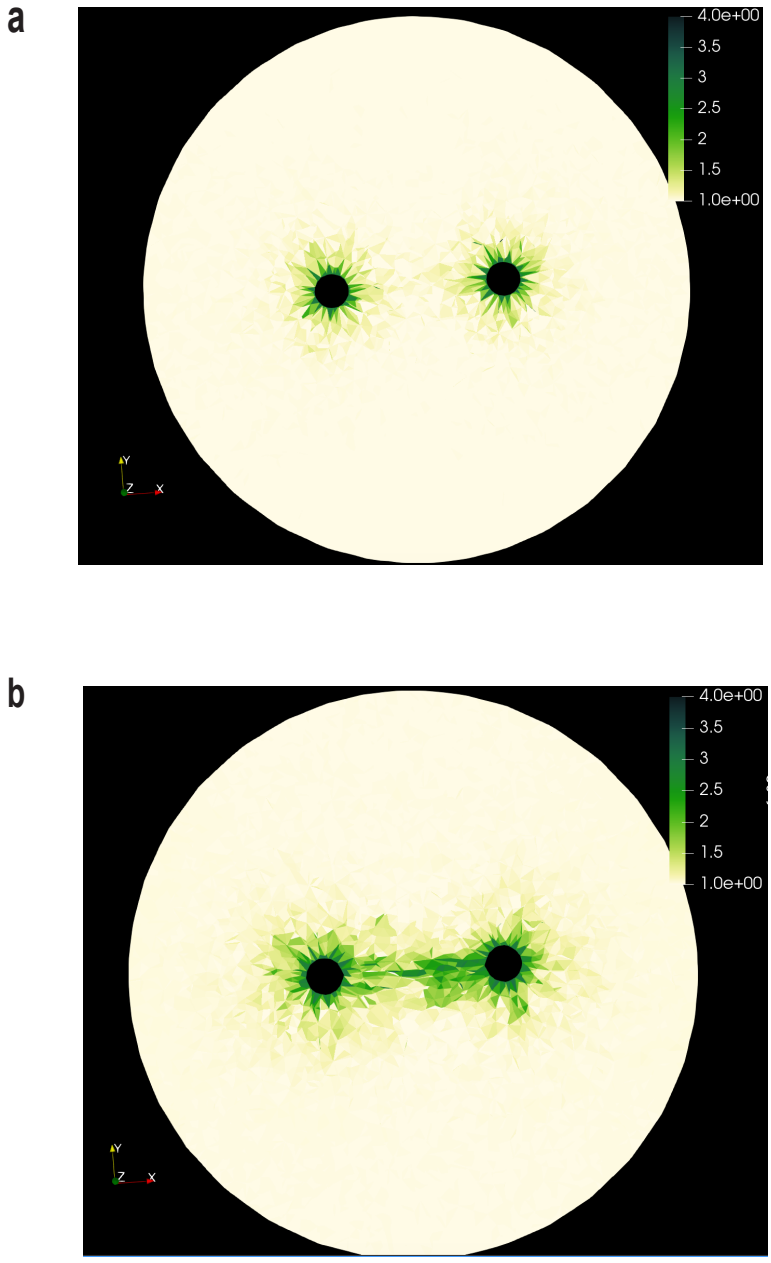

FIGURE 5.7. **Tethers in three dimensions.** Simulations with two cells contracting at **50%**. Cell centers are separated by $5r_c$, where r_c is the undeformed cell radius. Color plot of densification ratio ϱ of tetrahedral elements in deformed networks with **(a)** Family-1 model $\lambda - 1$ and **(b)** Family-2 model $\lambda^7 - \lambda^5$.

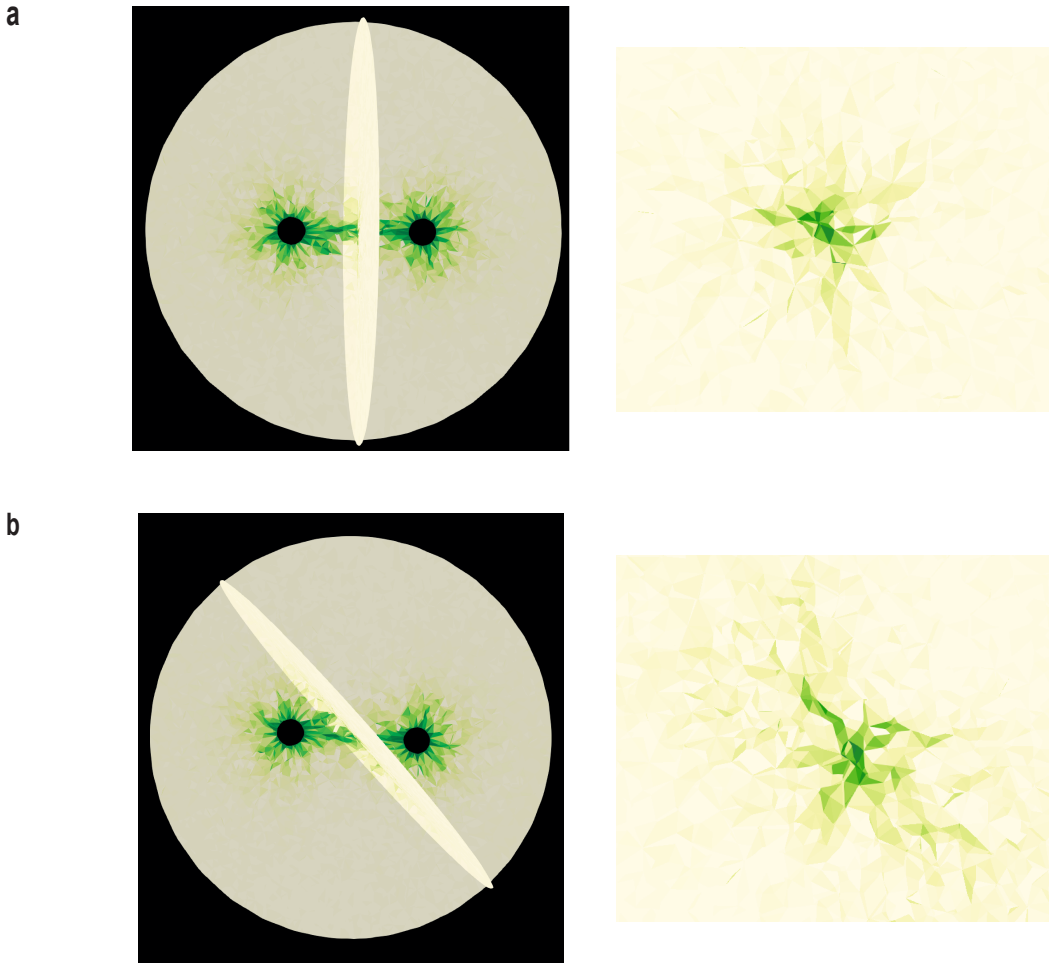

FIGURE 5.8. **The geometry of a 3*D* tether.** Complementary to Fig. 5.7. Tether structure at the midpoint between the contracting cells at two highlighted planes that intersect through network's center. The tether exhibits a notably irregular and disrupted structure. We see densification extending towards various directions with no certain preference.

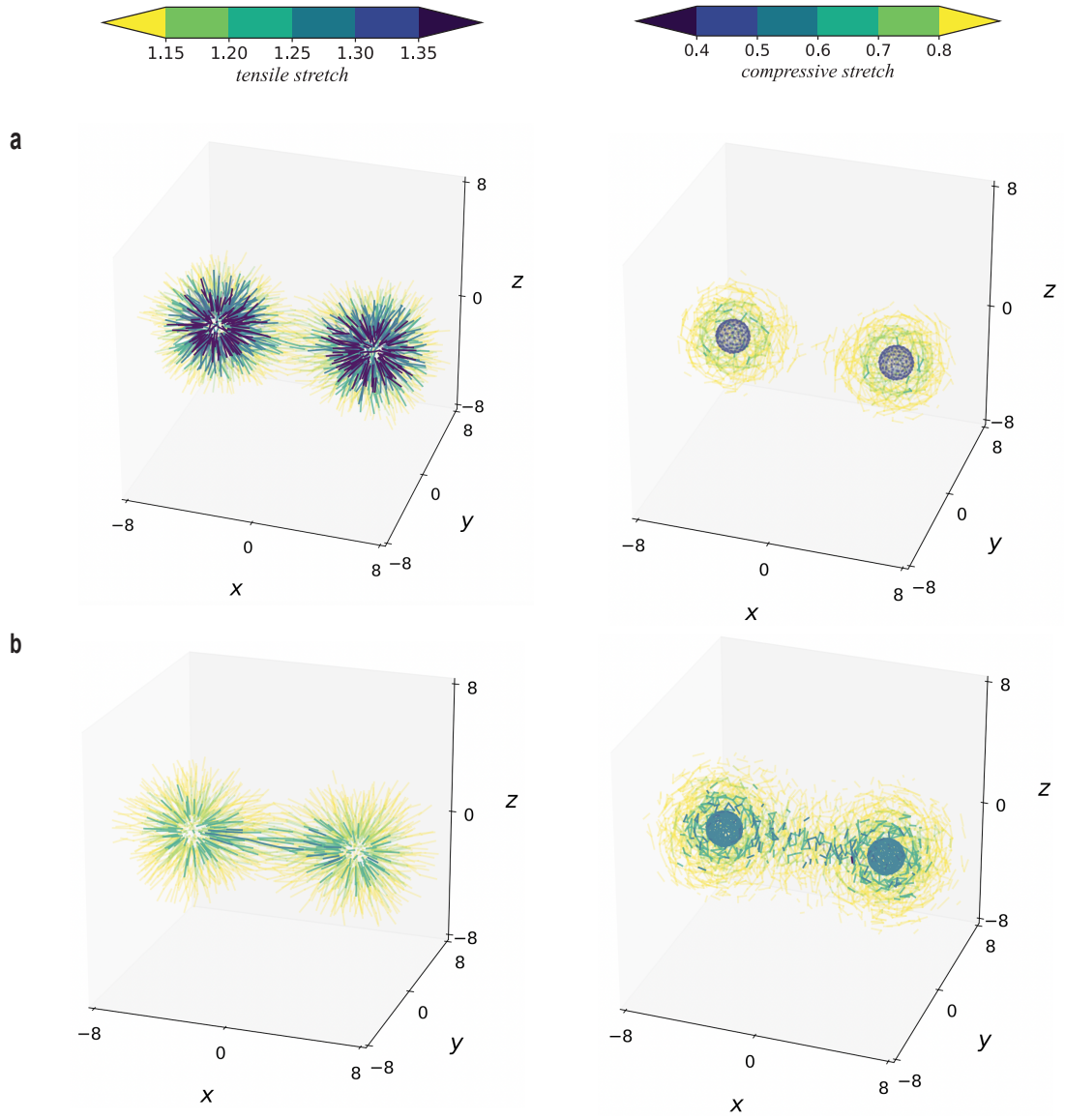

FIGURE 5.9. **Fiber stretch distributions in 3*D* networks.** Tensile and compressive stretches of deformed fibers in **(a)** Family-1, $\lambda - 1$ and **(b)** Family-2, $\lambda^7 - \lambda^5$. In Family-2, fibers under tension are aligned with the horizontal direction passing through the cell centers, generating straight paths that connect the two cells. These paths comprise the tether, Fig. 5.7. Notably, fibers experiencing extreme compression occupy the same spatial domain as those undergoing tension. Furthermore, we observe highly compressed fibers forming loops around the cells. Within these loops, the distribution of fiber stretch displays significant heterogeneity. In the case of the Family-1 model with $\lambda - 1$, there are no discernible fiber paths, and tensile stretches are dispersed across a broader region between cells without the pronounced alignment observed in the Family-2 model. Additionally, compressive stretches in the Family-1 model are primarily confined to concentric loops around each individual cell, as opposed to being distributed across the intercellular region.

5.2 Brief discussion and challenges

Developing a three-dimensional fiber network to explore tether formation and fiber alignment is a significant undertaking. Introducing the intricacies of various family models, along with the associated geometric complexities and computational demands, further amplifies the level of challenge. However, this study underscores the existence of material instabilities under compression. The outcomes derived from the three-dimensional model, even preliminary, provide additional support for our initial hypothesis. Simulations with either one or two cells, depict the difference between the two family models and, in particular, the mechanism for fiber buckling induced in Family 2. These preliminary results highlight the presence of severely compressed fibers in the majority of tetrahedral elements within densified network regions. This compellingly suggests that the mechanism responsible for densification in Family-2 networks is the instability associated with fiber collapse, aligning with predictions from the $\mathbf{2}\boldsymbol{D}$ model. Notably, fiber collapse is not encountered in the case of Family-1 simulations. Additionally, a significant observation pertains to fiber alignment. Irrespective of the model employed, our simulations reveal that excessive fiber alignment coincides with the same locations within the ECM where densification takes place (Fig. 5.9). This phenomenon holds true for both single-cell and two-cell scenarios. In Family 2, particularly within tethers and bands, we note a consistent alignment of the stretched sides of densified elements with each other. Conversely, the highly compressed side exhibits a rough perpendicular orientation to them. This observation provides further evidence that the instability leading to fiber collapse is responsible for the alignment of stretched fibers within densified regions.

The above overall add to our $\mathbf{2}\boldsymbol{D}$ analysis and the interconnection of fiber collapse instability with matrix densification and fiber alignment. Complementary to these findings, the $\mathbf{3}\boldsymbol{D}$ simulations shed light on a crucial aspect of natural ECM: anisotropy. Fibers within a network often exhibit anisotropic properties, meaning their mechanical characteristics vary along different directions. The outcomes of our $\mathbf{3}\boldsymbol{D}$ analysis unveil a notable heterogeneity in matrix densification surrounding contracting cells. Particularly noteworthy is the significant heterogeneity observed across the tether connecting two contracting cells (Fig. 5.8). This irregularity and the disrupted structure of the densified tether are attributed to the pronounced anisotropic behavior of the fibers.

When modelling the mechanical properties of a collagen network, transitioning from two dimensions to three dimensions introduces several distinct challenges:

- **Increased Computational Complexity:** In three dimensions, the computational requirements significantly increases. The number of elements, nodes, and computations grows significantly, demanding more computational resources.

- **Additional Degrees of Freedom:** Three-dimensional models have additional degrees of freedom, as they account for deformation in three spatial directions, requiring more

comprehensive and sophisticated modelling techniques.

- **Variability:** Three-dimensional collagen networks tend to exhibit greater variability in fiber density, orientation, and arrangement. Capturing this complexity in the model is more challenging.
- **Visualization and Interpretation**: Visualizing and interpreting results from three-dimensional models is more complex compared to two-dimensional models due to the added spatial dimension.

While the results presented here are preliminary, they unmistakably showcase the potential and significance of expanding the model into three dimensions. This expansion introduces added complexity, but concurrently, it unveils a new avenue for comprehending material instabilities. Moreover, it paves the way for the exploration of larger-scale instabilities.

CHAPTER 6

Discussion

Ἡ δ᾽ αὐτάρκεια καὶ τέλος καὶ βέλτιστον

Ἀριστοτέλης, *Πολιτικά I*

Through modelling and simulations, we demonstrate that material instabilities play a central role in shaping the mechanical behavior of the fibrous collagen Extracellular Matrix (ECM) when subjected to deformation by contractile biological cells. We have compared two distinct families of fiber network models: Family 1, characterized by stable force-stretch responses of individual fibers, and Family 2, exhibiting unstable responses in compression, akin to the post-buckling behavior observed in hierarchical structures like beams.

Our simulations unveil distinct compression instabilities within each family. In Family 2, we observe fiber collapse (buckling), while in Family 1, there is the collapse of fiber elements (snap-through). These instabilities result in the formation of densely packed regions comprising highly aligned fibers, emanating either from individual contractile cells or connecting neighboring cells, mirroring observations in experimental settings.

Despite the significant differences in the behavior of the two families, our study underscores the critical role of buckling and compression instabilities in shaping the characteristics of fibrous biological tissues. These findings hold implications for our understanding of processes like cancer invasion and metastasis.

6.1 Material instabilities play a dominant role in ECM deformations

Our simulation results have unveiled instability mechanisms that were not previously recognized in prior research. Specifically, all nonlinear networks are susceptible to an instability termed as *element collapse* (triangle buckling), as explained in Chapter 3. Notably, this susceptibility extends to linear networks when significant rotations are considered. In the case of Family-2 networks, there is an additional instability termed as *fiber collapse*. This instability arises when the fibers lose their strength due to buckling under compression, as detailed in Chapter 3. Simple geometry reveals that fiber collapse implies element collapse (as depicted in Fig. 3.10e), but not vice versa. Consequently, both instabilities can occur within Family-2 networks. In contrast, Family-1 networks can experience element collapse, even though individual fibers exhibit stable behavior. This distinction between these different instabilities is a consequence of the discrete nature of our model and is not captured by continuum models, even those that allow instability [26].

In the Family-2 models, we observe a sudden increase in densification occurring concurrently with the abrupt collapse of fibers, evident in both single-cell and two-cell simulations (as shown in Fig. 4.8f and Fig. 4.11b). The majority of elements within these densified regions contain severely compressed fibers (indicated by the red fibers in Fig. 4.11d). This compellingly suggests that the mechanism responsible for densification in Family-2 networks is the instability associated with fiber collapse, as explained in Chapter 3 and depicted in Fig. 3.10e. Densification also occurs in Family-1 networks but requires higher levels of cell contraction. Notably, fiber collapse is not encountered in this case (as shown in Fig. 4.8g and Fig. 4.11a). Instead, the densification observed in Family-1 networks is attributed to the collapse of triangular elements (as illustrated in Fig. 4.11c). Element collapse instability, as detailed in Chapter 3 and depicted in Fig. 3.10f, plays a central role in the emergence of densified regions within Family-1 networks. These observations apply to both intercellular tethers and densified zones around single contracting cells.

An important discovery pertains to the alignment of fibers. Regardless of the model used, our simulations reveal that excessive fiber alignment occurs concomitantly with densification and at the same locations within the ECM. This phenomenon is consistent in both single-cell and two-cell cases (as depicted in Fig. 4.1-Fig. 4.5).

In particular, within Family 1, we observe that severe element compression leads to the alignment of all sides of densified triangles with each other (as shown in Fig. 4.11c). This alignment is a direct consequence of the element collapse instability, as illustrated in Fig. 3.10f. Especially in two-cell simulations, we detect a moderate tendency for fibers to align before tethers form, particularly evident in Fig. 4.6a and Fig. 4.6b. Once tethers are established, the fibers within them align almost perfectly (as seen in Fig. 4.6d), and it is within these tethered elements that

we observe extreme densification.

Within Family 2, in tethers and bands, we observe that the stretched sides of densified elements align with each other, while the highly compressed side is roughly perpendicular to them (as depicted in Fig. 4.1m and Fig. 4.11d), evidence that fiber collapse instability brings about the alignment of stretched fibers within the densified regions.

These significant findings collectively indicate that ECM compression instabilities are responsible for both matrix densification and fiber alignment.

In general, it is notably easier to establish a tether using Family-2 models compared to Family-1 models. When considering the same distance between two cells, a tether formation requires significantly less compression with Family-2 models than with Family-1 models. For example, for a distance $6r_c$, where r_c is cell radius, the linear model necessitates a substantial 80% compression to initiate tether formation, while a mere 25% compression suffices with the $\lambda^7 - \lambda^5$ model (Fig. 4.6e). To put it differently, given a fixed level of compression, let's say 50%, a Family-1 tether is established when cells are in very close proximity, less than $5r_c$. On the contrary, a Family-2 tether can take shape when cells are separated by more than twice that distance from each other (as demonstrated in Fig. 4.6e).

Our most noteworthy prediction centers around the creation of densified tethers connecting two cells, accompanied by the emergence of densified radial bands emanating from each cell. Experimental evidence has shown the existence of high-density zones (tethers) linking clusters of contractile cells [5, 31, 71, 74]. Furthermore, thinner bands were observed extending from each cluster [31, 74], and gradually diminishing within the matrix. In a related study [26], densified tethers and radial bands were also observed, using contracting active particles instead of living cells, thereby eliminating non-mechanical causes for densification. Fibers within these tethers exhibit pronounced alignment along the tether axis. Notably, individual cells from each explant [31, 74] or acinus [71] have been observed to initiate migration along these tethers in an effort to reach neighboring clusters. Moreover, isolated fibroblasts extended protrusions towards each other along the tethers formed following their contraction [52]. These studies underscore the critical role of tethers and radial bands in processes such as cell migration, motility, and intercellular communication.

Our simulations reveal that the formation of these densified zones is a direct consequence of compression instabilities. Furthermore, these instabilities lead to the close alignment of fibers within the densified regions. As a result, alignment and densification are observed to be integral components of the same underlying mechanism.

The most crucial application of this research pertains to cancer invasion and metastasis. Studies involving tumor explants cultured within initially randomly organized matrices have revealed a fascinating phenomenon. As these tumor explants contract, they induce the alignment of collagen fibers in the surrounding matrix. This alignment provides individual cancer cells with

"highway paths" composed of these aligned fibers, enabling them to invade the Extracellular Matrix (ECM) [59, 61]. In fact, both densification [60] and fiber alignment [59] are considered prognostic biomarkers for breast carcinoma [12], specifically referring to the presence of "bundles of straightened and aligned collagen fibers that are oriented perpendicular to the tumor boundary" [12]. The development of these features relies on the contractility of cells [61]. It is important to highlight that these observations apply to both tethers and radial densified bands. In the case of expanding tumors, a different phenomenon is observed. The densified layer surrounding them consists of fibers that are parallel (rather than perpendicular) to their boundary [12]. Remarkably, our simulations of expanding cells align with this observation (as depicted in Appendix, Fig. A.4). Additionally, the alignment of collagen fibers facilitates the transportation of biochemical molecules between cells [23].

By focusing on the elevated fiber alignment within the tethers, our predictions underscore the contribution of compression instability in mechanisms related to cancer related ECM mechanisms.

6.2 Contribution to literature

Family-2 models, characterized by unstable stretch responses, yield clearly defined tethers that exhibit highly localized densification and fiber alignment in close proximity to the tether axis. These outcomes align qualitatively with experimental findings [26, 71, 74]. Conversely, in models featuring a stable stretch response (Family 1), tethers are diffused and lack localization, while fibers under tension are dispersed throughout the broader intercellular region. Additionally, tethers in Family 2 models form under physiological levels of cell contraction, approximately around **50%**, as observed experimentally [26, 52, 71]. In contrast, Family-1 models require extreme levels of contraction for tether formation. Considering these observations, Family-2 models prove to be more suitable than Family-1 models as they better replicate experimental observations. The instability in the response of Family-2 fibers finds justification in recent research [76] on the post-buckling behavior of hierarchical structures like ECM fibers [57] (detailed in Chapter 3).

Significant efforts have been dedicated to modeling the Extracellular Matrix (ECM) in previous studies [2, 24, 27, 44, 48, 52, 65, 66, 73, 82]. In these investigations, ECM fibers are typically represented as Timoshenko beams [2, 27], or they are modeled as elements exhibiting asymmetric elastic responses to extension and compression. These responses are often described using piecewise linear stress-strain curves or combinations of strain-stiffening and compression softening intended to simulate fiber buckling [24, 44, 48, 52, 66, 73, 82]. While these approaches have explored various nonlinear aspects of fiber behavior, they are constrained by stable stretch responses, typically exhibiting monotonic behavior, and are sometimes limited to small deformations. In terms of the stretch response, all of these models are conceptually similar

to our Family-1 models. Notably, none of these previous works explicitly address the role of instability. In our study, we recognize that instability plays a central role in the emergence of ECM densification and fiber alignment. Importantly, we demonstrate that instability can occur even in models with a stable stretch response, such as Family 1, but this instability necessitates unreasonably high levels of cell contraction. Consequently, we introduce models within Family 2, characterized by stretch responses that become unstable under compression. This specific instability enables the formation of tethers and fiber alignment under experimentally observed levels of cell contraction.

Previous studies have indeed explored the concept of fiber alignment within the ECM, as noted in references [73] and [24]. However, these studies typically considered fiber alignment as a distinct ECM mechanism, often in relation to intercellular force transmission [73] or matrix elastic anisotropy [24]. For instance, Sopher et al. [73] proposed that elevated tension within the intercellular region compels fibers to stretch and align. In our simulations, we observe a sudden and substantial increase in both densification and fiber alignment compared to the aforementioned works. This transition occurs when a compression instability is triggered. In the case of models with stable stretch responses (Family 1), this transition would require much higher levels of cell contraction than those considered in previous studies [24, 44, 48, 52, 66, 73, 82]. In contrast, our Family-2 models not only require moderate cell contraction levels but also exhibit much stronger densification. Additionally, the tethers formed are solid and significantly wider, while the fibers align almost perfectly with the tether axis. These differences highlight the distinctive characteristics of our proposed models.

The concept of deformation-induced anisotropy has been explored in previous studies [24] as a potential mechanism for facilitating long-range cell communication. It's important to note that the compressive instabilities we investigate in this study lead to a robust form of anisotropy within the densified state of the network. This anisotropy arises because these instabilities generate a highly aligned and dense uniaxial distribution of fibers from an initially roughly isotropic random fiber distribution. Our findings emphasize a significant point: there exists a single underlying mechanism that unifies densification, fiber alignment, and matrix anisotropy, and that mechanism is compression instability. These phenomena occur concurrently within the same localized zones as soon as compression instability is triggered, whether due to fiber buckling (collapse) or element collapse (snap-through buckling). This observation underscores the interrelated nature of these ECM responses when subjected to compressive forces. Compression instability stemming from the buckling of elastic fibers within networks was initially identified in [43] as a mechanism responsible for localized densification. Similarly, the continuum model presented in [25] and further developed in [26], also exhibits a compression instability. This continuum model predicts the formation of highly localized densified tethers and radial bands, sharing a qualitative similarity with the results presented in our study. The advantage of our model lies in its ability to capture the discrete nature of actual fibrous networks.

Consequently, it can distinguish between different types of compression instabilities, buckling of fibers versus the collapse of fiber elements. Furthermore, our model elucidates the close relationship between instability, fiber alignment, and densification, providing a comprehensive understanding of these interconnected phenomena.

6.3 Limitations of the study

Our model has several noteworthy limitations that should be kept in mind when interpreting the results. Firstly, like many previous models in the field [2, 24, 26, 27, 44, 48, 52, 65, 66, 73, 82], we have adopted a specific network geometry to represent the fibrous Extracellular Matrix (ECM). In our case, we have assumed the ECM to be a uniform, isotropic elastic material represented by a uniformly distributed network of segments, akin to fibers, as shown in Figure 3.5. While these modelling approaches have enhanced our understanding of discrete fiber networks, the choice of network geometry raises questions about the generalizability of our results [33]. Another structural aspect of representing a fiber network refers to its connectivity, meaning the mean number of fibers that meet at a node. For instance, collagen gels have typically connectivity of 3.5 - 4 [6, 36, 52]. A fully connected two-dimensional network in our model has a mean connectivity of 6. Therefore, it is important to explore different network geometries and connectivities, in order to establish a more versatile methodology.

Moreover, the ECM is a highly intricate structure composed of various proteins, fibers, and other components. Fibrous proteins often interact with one another and with other biomolecules. Accurately modelling these interactions, including both attractive and repulsive forces, is a complex task that demands specialized models and experimental observations. In this study, as well as in most related studies in the literature, we have not accounted for this variability in macromolecular composition. However, modelling this intricate architecture accurately can be challenging, thus simplifications are often necessary, even though they may not capture the full complexity.

Complementary to this, another limitation concerns fiber modelling at different scales, from the nanoscale to the macroscale, which can be difficult. As a result, some models may not capture the interactions and behaviors that occur at specific scales. For instance, many fibrous proteins undergo post-translational modifications that can affect their structure and function and their interaction with other proteins. Incorporating the effects of these modifications into models can be extremely challenging. In addition, achieving molecular-level detail in models of fibrous proteins can be computationally intensive and may not be feasible for large-scale simulations. Thus, simplified models are often used to strike a balance between accuracy and computational efficiency.

Finally, our methodology could benefit from enhancements in predictive capabilities, such as incorporating strain-dependent degradation of collagen [16, 68] and accounting for viscoelastic

effects in ECM deformations. Viscoelasticity arises from the ECM's combination of viscous (fluid-like) and elastic (solid-like) components [46], and addressing these effects could improve the accuracy of our predictions or even challenge our hypothesis.

6.4 Research Outlook

The limitations highlighted above open up several promising avenues for future research. Among the most significant opportunities are:

- *Exploration of Diverse Network Geometries:* Investigating a broader range of network geometries to understand how different representations of the fibrous ECM impact mechanical deformations. This can provide insights into the generality of results and help develop a more versatile modeling framework.
- *Incorporation of Macromolecular Variability:* Developing models that consider the complex macromolecular composition of the ECM, accounting for interactions between various proteins, fibers, and biomolecules. This could involve capturing both attractive and repulsive forces, reflecting the real-world diversity of ECM components.
- *Viscoelasticity Consideration:* Investigating the role of viscoelastic effects in ECM deformations by developing models that account for the viscous and elastic components of the ECM. This can provide a more realistic representation of ECM behavior under various mechanical scenarios.
- *More sophisticated modelling of joints and crosslinking between fibers:* Modelling crosslinking allows for a more accurate assessment of the material's ability to withstand forces, and can be essential for capturing the material's viscoelastic properties.

Additionally, given that the current study primarily centers on unraveling the origins of instabilities in fiber mechanical responses, a prospective expansion of our research could encompass the exploration of larger-scale instabilities. These could either stand alone or integrate with some of the strategies outlined above.

Exploring these avenues for further research has the potential to foster a more profound and all-encompassing comprehension of the mechanical attributes inherent to the Extracellular Matrix and its significance in diverse biological phenomena.

Chapter 7

Epilogue

ἐντελέχεια < ἐν + τέλος + ἔχω

Ἀριστοτέλης

Cell-generated forces within the Extracellular Matrix (ECM) result in distinctive deformation patterns, characterized by pronounced densification of the matrix and alignment of its fibers. These patterns are pivotal in intercellular communication, as well as cell motility and invasion. In this thesis, the primary goal was to explore how the discrete nature of the fiber network combined with the intricate intrinsic fiber mechanics manifest the emergence of such patterns. To achieve this, we introduced two distinct families of fiber constitutive relations, each characterized by unique nonlinearity and stability features. Family 1 exhibits a positive but diminishing stiffness as compression increases, representing the conventional perspective on post-buckling behavior. On the other hand, Family 2 introduces a more radical model, as it incorporates a stretch instability phase which to stiffness becoming negative at extreme levels of compression.

In conclusion, the significant points of this thesis are:

- **Model Distinctions:** The thesis highlights the differences between two model families, Family 1 and Family 2, in the context of simulating ECM behavior and the emergence of matrix densification and fiber alignment. Regardless of the model used, simulations reveal that excessive fiber alignment occurs concomitantly with densification and at the same locations within the ECM. These phenomena are direct consequences of element collapse instability regarding Family 1 and fiber collapse instability regarding Family 2.

- **Family-2 Model Features:** Family-2 models, characterized by unstable stretch response

under compression, result in well-defined tethers with highly localized densification and fiber alignment near the tether axis.

- **Comparison with Previous Models:** Previous ECM modelling efforts primarily utilized stable stretch responses (similar in spirit to Family 1) and did not explicitly address the role of instability. The work presented herein emphasizes that the instability is crucial in explaining ECM densification and fiber alignment.
- **Dominant Role of Compression Instability:** Compression instability due to fiber buckling (Family 2) or element collapse (Family 1) plays a central role in the ECM densification, fiber alignment, and matrix anisotropy. It unifies these phenomena and allows them to occur simultaneously.
- **Unique Contribution of the Model:** The advantage of the presented model lies in its ability to capture the discrete nature of fibrous networks, enabling the distinction between different types of compression instabilities and clarifying their relationship with fiber alignment and densification.
- **Relevance to ECM Research:** The study's outcomes have implications for understanding the behavior of the ECM in response to mechanical forces and offer insights into phenomena like cell-cell communication, tumor invasion, and metastasis.

Gaining a more precise comprehension and modelling capability regarding the intricate mechanics of ECMs holds the potential to advance our exploration of crucial biological processes like fibrosis, morphogenesis, and cancer cell invasion. Theoretical modelling of disease states may offer opportunities to investigate various treatment strategies, forecast disease progression, and eventually tailor treatment approaches to individual patients. The outcomes of this study shed light on the broader implications of these mechanical phenomena in intercellular biomechanical interactions, cancer metastasis, and cell motility. The models implemented here highlight the role of material instability, specifically the nonlinearity induced by fiber buckling under compression. The evidence and analysis presented in this thesis emphasize the significance of compression instability caused by buckling as a fundamental nonlinear mechanism that governs the mechanical behavior of fibrous ECM. These findings offer new perspectives on delving into the characteristics of cell-induced deformations responsible for matrix densification and fiber alignment. Finally, the incorporation of different families of fiber constitutive relations, ranging from traditional post-buckling behavior to more radical models, has expanded our understanding of how the discrete nature of fiber networks influences ECM mechanical responses. This multifaceted approach provides valuable insights into the mechanical properties of fibrous materials and their significance in diverse biological contexts, offering a comprehensive foundation for future investigations in the field.

... and as these fibers navigate the labyrinth of forces, they teach us that strength is not just measured in resistance, but in the ability to adapt, to transform, and to weave tales of unyielding tenacity, proving that within the embrace of innate structure lies the resilience to weather life's storms.

— Chrysovalantou Kalaitzidou

List of Figures

Appendix A

Appendix

A.1 Supplementary figures

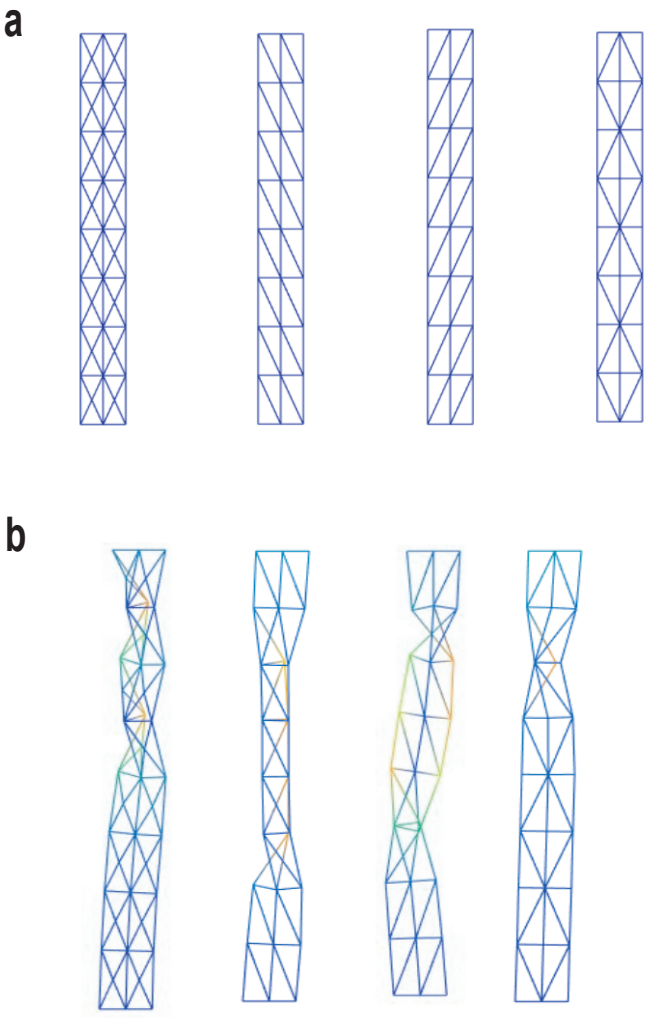

FIGURE A.1. **Interpenetration of matter. (a)** Various representations of triangulated rectangular elements. Each edge in the structures represents a linear spring. Boundary conditions were applied on the upper boundary nodes by imposing a displacement u = (h, 0.0), h being the scale to x direction. **(b)** Deformed structures contain triangles that have changed orientation, resulting in interpenetration of matter. We see triangles folded over and also snap-through one into the other.

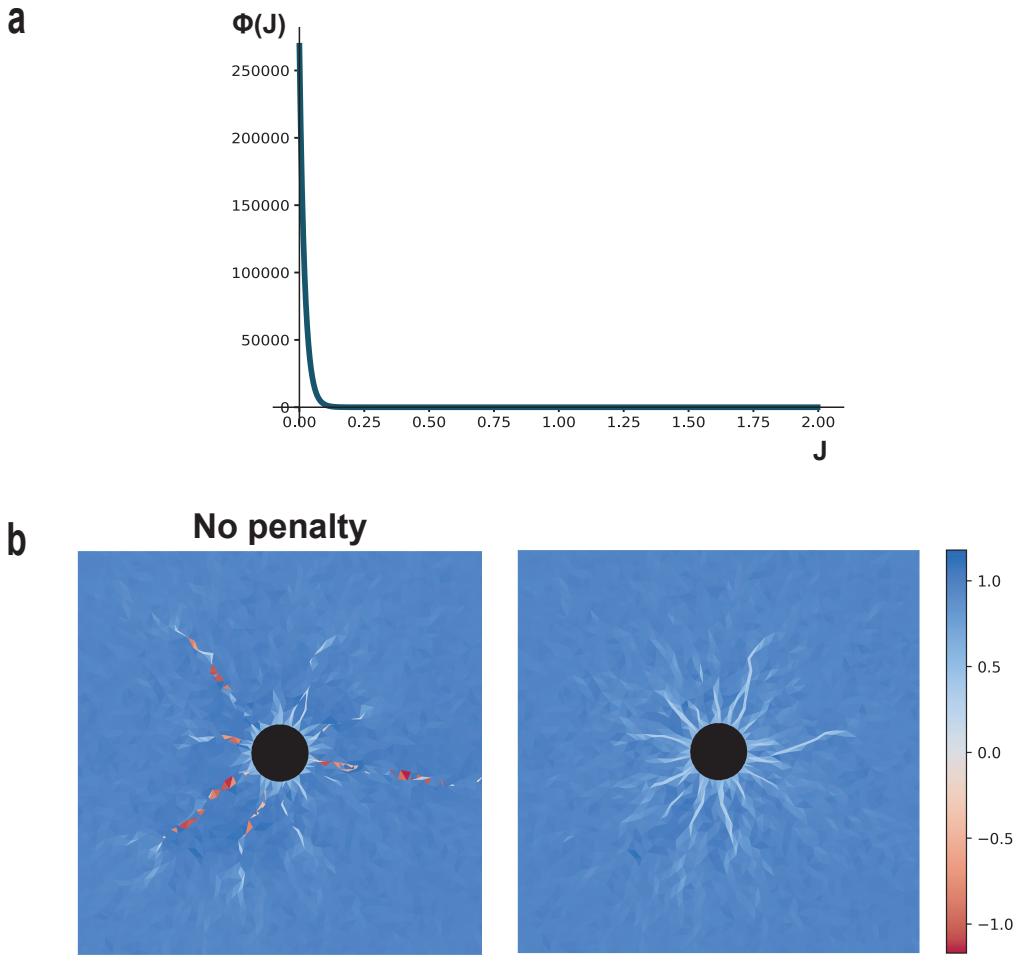

FIGURE A.2. **Penalizing the Jacobian in order to preserve orientation. (a)** Penalty term $\Phi(J) = exp(-Q(J-b))$, where J is *ratio of deformed to undeformed oriented triangle area*. $Q > 0$ is large and $b > 0$ is small constant. As a result, negative values of J have high energy cost, whereas positive values have negligible contribution to the network's total energy. **(b)** Simulations of a cell contracting by 50%, either with or without the penalty term for the area ratio J. Without penalizing J, the optimizer finds solutions that are physically unacceptable, as $J < 0$ corresponds to elements (red) that changed orientation. Colorbar: J values.

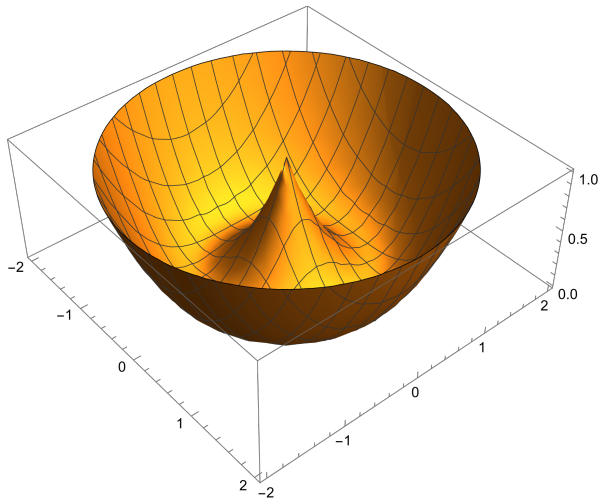

FIGURE A.3. **Nonconvex energy of a linear fiber. (a)** Energy (3.3) of single linear fiber with one end $\mathbf{x}_j$ fixed at the origin, as a function of the position vector $\mathbf{x}_i$ of the other end (nonconvex surface of revolution of a convex parabola with minimum at $\mathbf{1}$).

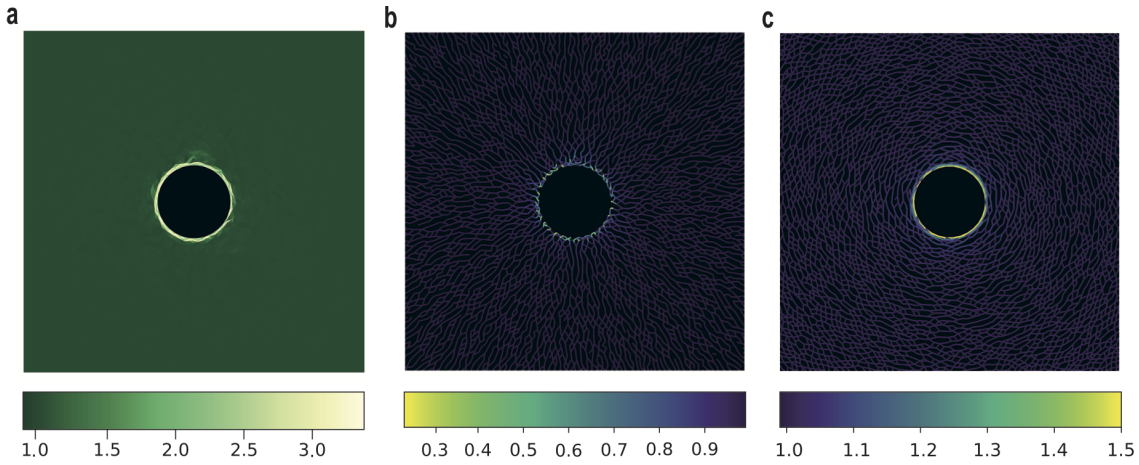

FIGURE A.4. **Cell expansion.** Simulation with $S(\lambda) = \lambda^5 - \lambda^3$ of a single cell radially expanded by 50%.**(a)** Densification ratio of triangular elements in deformed networks **(b)** compressive stretches and **(c)** tensile stretches of deformed fibers. Note that the densified layer surrounding the expanding cell consists of tensed fibers, aligned in the circumferential direction.

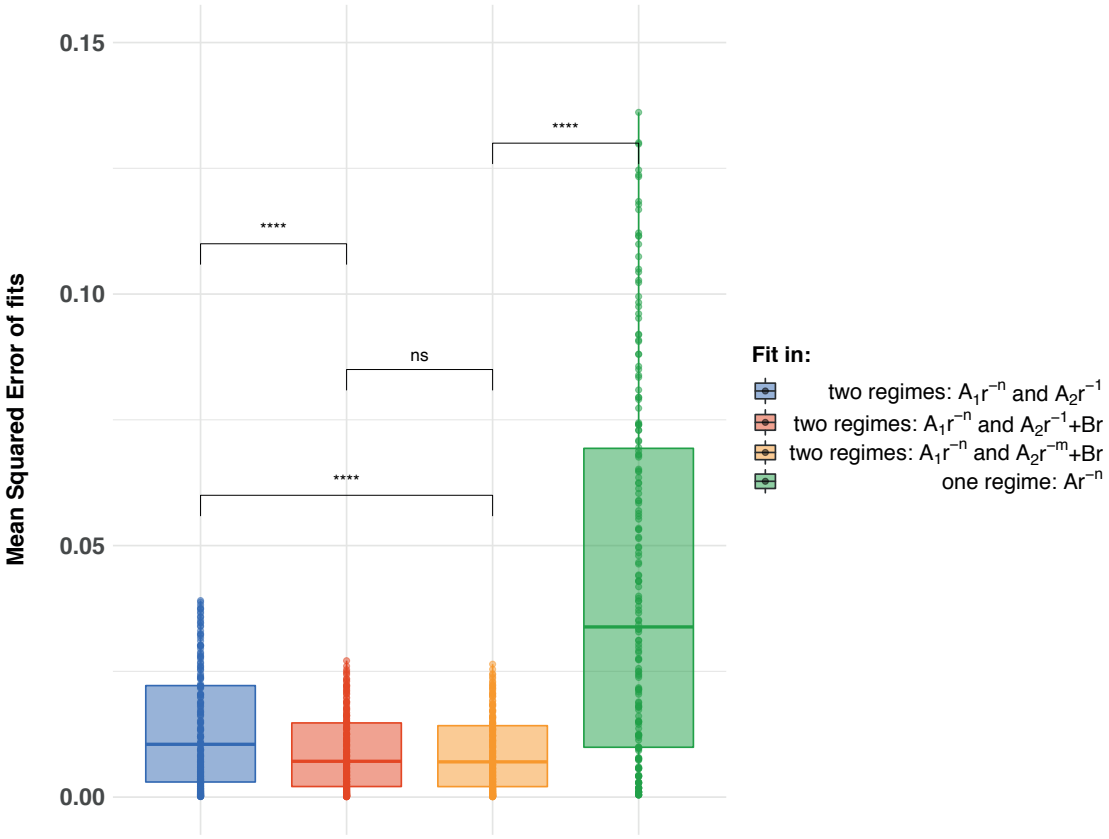

FIGURE A.5. **Boxplots of mean squared errors of the different fitting methods.** Each dot within the boxplots correspond to the mean squared error between the fitted radial displacement values and the corresponding simulated radial displacements, for a particular contraction level and domain size. The first three boxes (blue, red and orange) correspond to fits in two regimes, where the near-field displacements were fitted to $A_1 r^{-n}$ and the far-field displacements were fitted to $A_2 r^{-1}$, $A_2 r^{-1} + Br$ or $A_2 r^{-m} + Br$, respectively. The green box includes fits of the whole domain with Ar^{-n}. The difference between any two-regime fit and the last case is statistically significant. The same applies between the fits with $A_2 r^{-1}$ for the second regime (blue box) and teach one of the other two-regime cases (red and orange), yielding in the importance of exploring the decay power in the far field with regard to contraction level and domain size.
***P < 0.0001, ns: not significant

Bibliography

[1] R. Abeyaratne, *Lecture Notes on The Mechanics of Elastic Solids*, `http://web.mit.edu/abeyaratne/lecture_notes.html`, 2006.

[2] A. S. Abhilash, B. M. Baker, B. Trappmann, C. S. Chen, and V. B. Shenoy, *Remodeling of fibrous extracellular matrices by contractile cells: Predictions from discrete fiber network simulations*, Biophysical Journal, 107 (2014), pp. 1829–1840.

[3] M. S. Alnæs, J. Blechta, J. Hake, A. Johansson, B. Kehlet, A. Logg, C. Richardson, J. Ring, M. E. Rognes, and G. N. Wells, *The FEniCS Project Version 1.5*, Archive of Numerical Software, 3 (2015), pp. 9–23.

[4] Ayachit and Utkarsh, *The ParaView Guide: A Parallel Visualization Application*, Kitware, 2015, ISBN 9781930934306.

[5] E. Ban, J. M. Franklin, S. Nam, L. R. Smith, H. Wang, R. G. Wells, O. Chaudhuri, J. T. Liphardt, and V. B. Shenoy, *Article Mechanisms of Plastic Deformation in Collagen Networks Induced by Cellular Forces*, Biophysj, 114 (2018), pp. 450–461.

[6] E. Ban, H. Wang, J. M. Franklin, J. T. Liphardt, P. A. Janmey, and V. B. Shenoy, *Strong triaxial coupling and anomalous poisson effect in collagen networks*, Proceedings of the National Academy of Sciences, 116 (2019), pp. 6790–6799.

[7] A. Brown, R. Litvinov, D. Discher, P. Purohit, and J. Weisel, *Multiscale Mechanics of Fibrin Unfolding and Loss of Water*, Science, 741 (2009).

[8] B. Burkel and J. Notbohm, *Mechanical response of collagen networks to nonuniform microscale loads*, Soft Matter, 13 (2017), pp. 5749–5758.

[9] ——, *Mechanical response of collagen networks to nonuniform microscale loads.* , Soft Matter, (2017).

[10] F. Burla, B. E. Vos, and A. A. Roberts, *From mechanical resilience to active material properties in biopolymer networks*, Nature Reviews Physics, (2019).

[11] O. Chaudhuri, S. H. Parekh, and D. A. Fletcher, *Reversible stress softening of actin networks*, 445 (2007), pp. 20–22.

[12] M. W. Conklin, J. C. Eickhoff, K. M. Riching, C. A. Pehlke, K. W. Eliceiri, P. P. Provenzano, A. Friedl, and P. J. Keely, *Aligned collagen is a prognostic signature for survival in human breast carcinoma*, Am J Pathol, 178 (2011), pp. 1221–1232.

[13] E. Conti and F. C. MacKintosh, *Cross-linked networks of stiff filaments exhibit negative normal stress*, Phys. Rev. Lett., 102 (2009), p. 088102.

[14] C. Coulais, J. T. B. Overvelde, L. A. Lubbers, K. Bertoldi, and M. van Hecke, *Discontinuous buckling of wide beams and metabeams*, Phys. Rev. Lett., 115 (2015), p. 044301.

[15] D. E. Discher, P. Janmey, and Y.-L. Wang, *Tissue Cells Feel and Respond to the Stiffness of Their Substrate*, Science, 310 (2005), pp. 1139–1143.

[16] A. Dittmore, J. Silver, S. K. Sarkar, B. Marmer, G. I. Goldberg, and K. C. Neuman, *Internal strain drives spontaneous periodic buckling in collagen and regulates remodeling*, Proc Natl Acad Sci U S A, 113 (2016), pp. 8436–8441.

[17] A. J. Engler, F. Rehfeldt, S. Sen, and D. E. Discher, *Microtissue Elasticity: Measurements by Atomic Force Microscopy and Its Influence on Cell Differentiation*, in Cell Mechanics, vol. 83 of Methods in Cell Biology, Academic Press, 2007, pp. 521–545. ISSN: 0091-679X.

[18] J. L. Ericksen, *Equilibrium of bars*, Journal of Elasticity, 5 (1975), pp. 191–201.

[19] J. Ferruzzi, M. Sun, A. Gkousioudi, A. Pilvar, D. Roblyer, Y. Zhang, and M. H. Zaman, *Compressive Remodeling Alters Fluid Transport Properties of Collagen Networks – Implications for Tumor Growth*, Scientific Reports, 9 (2019), p. 17151.

[20] C. Frantz, K. M. Stewart, and V. M. Weaver, *The extracellular matrix at a glance*, J Cell Sci, 123 (2010), pp. 4195–4200.

[21] Friesecke and Theil, *Validity and Failure of the Cauchy-Born Hypothesis in a Two-Dimensional Mass-Spring Lattice*, Journal of Nonlinear Science, 12 (2002), pp. 445–478.

[22] F. Gattazzo, A. Urciuolo, and P. Bonaldo, *Biochimica et Biophysica Acta Extracellular matrix : A dynamic microenvironment for stem cell niche*, BBA - General Subjects, 1840 (2014), pp. 2506–2519.

[23] D. Gomez, S. Natan, Y. Shokef, and A. Lesman, *Mechanical Interaction between Cells Facilitates Molecular Transport*, Adv. Biosyst., 1900192 (2019), pp. 1–12.

[24] S. Goren, Y. Koren, X. Xu, and A. Lesman, *Elastic anisotropy governs the range of cell-induced displacements*, Biophysical Journal, 118 (2020), pp. 1152–1164.

[25] G. Grekas, *Modelling, analysis and computation of cell-induced phase transitions in fibrous biomaterials*, PhD thesis, University of Crete, 2019.

[26] G. Grekas, M. Proestaki, P. Rosakis, J. Notbohm, C. Makridakis, and G. Ravichandran, *Cells exploit a phase transition to mechanically remodel the fibrous extracellular matrix*, J. R. Soc. Interface, (2021).

[27] P. Grimmer and J. Notbohm, *Displacement Propagation in Fibrous Networks Due to Local Contraction*, Journal of Biomechanical Engineering, 140 (2018).

[28] M. Gurtin, *An Introduction to Continuum Mechanics*, Mathematics in Science and Engineering, 1981.

[29] M. S. Hall, F. Alisafaei, E. Ban, X. Feng, C.-Y. Hui, V. B. Shenoy, and M. Wu, *Fibrous nonlinear elasticity enables positive mechanical feedback between cells and ecms*, Proceedings of the National Academy of Sciences, 113 (2016), pp. 14043–14048.

[30] A. M. Handorf, Y. Zhou, M. A. Halanski, and W.-J. Li, *Tissue stiffness dictates development, homeostasis, and disease progression*, Organogenesis, 11 (2015), pp. 1–15.

[31] A. K. Harris, D. Stopak, and P. Wild, *Fibroblast traction as a mechanism for collagen morphogenesis*, Nature, 290 (1981), pp. 249–251.

[32] N. E. Hudson, J. R. Houser, E. T. O'Brien, R. M. Taylor, R. Superfine, S. Lord, and M. R. Falvo, *Stiffening of individual fibrin fibers equitably distributes strain and strengthens networks*, Biophysical Journal, 98 (2010), pp. 1632–1640.

[33] D. L. Humphries, J. A. Grogan, and E. A. Gaffney, *Mechanical Cell-Cell communication in fibrous networks: The importance of network geometry*, Bull Math Biol, 79 (2017), pp. 498–524.

[34] P. A. Janmey, M. E. M. C. Cormick, S. Rammensee, J. L. Leight, P. C. Georges, and F. C. M. A. C. Kintosh, *Negative normal stress in semiflexible biopolymer gels*, Nature Materials, 6 (2007), pp. 4–7.

[35] P. A. Janmey, J. P. Winer, and J. W. Weisel, *Fibrin gels and their clinical and bioengineering applications*, J R Soc Interface, 6 (2009), pp. 1–10.

[36] K. A. Jansen, A. J. Licup, A. Sharma, R. Rens, F. C. MacKintosh, and G. H. Koenderink, *The role of network architecture in collagen mechanics*, Biophys J, 114 (2018), pp. 2665–2678.

[37] J.Nocedal and S.Wright, *Numerical Optimization*, Springer.

[38] E. Jones, T. Oliphant, P. Peterson, et al., *SciPy: Open source scientific tools for Python*, 2001.
`http://www.scipy.org/`.

[39] K. E. Kasza, A. C. Rowat, J. Liu, T. E. Angelini, C. P. Brangwynne, G. H. Koenderink, and D. A. Weitz, *The cell as a material*.

[40] O. V. Kim, R. I. Litvinov, J. W. Weisel, and M. S. Alber, *Biomaterials Structural basis for the nonlinear mechanics of fi brin networks under compression*, Biomaterials, 35 (2014), pp. 6739–6749.

[41] R. Kolasangiani, T. C. Bidone, and M. A. Schwartz, *Integrin conformational dynamics and mechanotransduction*, Cells, 11 (2022).

[42] T. Korff and H. G. Augustin, *Tensional forces in fibrillar extracellular matrices control directional capillary sprouting*, J Cell Sci, 112 (Pt 19) (1999), pp. 3249–3258.

[43] R. Lakes, P. Rosakis, and A. Ruina, *Microbuckling instability in elastomeric cellular solids*, Journal of Materials Science, 28 (1993), pp. 4667–4672.

[44] L. Liang, C. Jones, S. Chen, B. Sun, and Y. Jiao, *Heterogeneous force network in 3d cellularized collagen networks*, Physical Biology, 13 (2016), p. 066001.

[45] C. M. Lo, H. B. Wang, M. Dembo, and Y. L. Wang, *Cell movement is guided by the rigidity of the substrate*, Biophysical Journal, 79 (2000), pp. 144–152.

[46] Y. Ma, T. Han, Q. Yang, J. Wang, B. Feng, Y. Jia, Z. Wei, and F. Xu, *Viscoelastic cell microenvironment: Hydrogel-based strategy for recapitulating dynamic ecm mechanics*, Advanced Functional Materials, 31 (2021), p. 2100848.

[47] A. Malandrino, M. Mak, R. D. Kamm, and E. Moeendarbary, *Complex mechanics of the heterogeneous extracellular matrix in cancer*, Extreme Mech Lett, 21 (2018), pp. 25–34.

[48] A. Mann, R. S. Sopher, S. Goren, O. Shelah, O. Tchaicheeyan, and A. Lesman, *Force chains in cell–cell mechanical communication*, J. R. Soc. Interface, (2019).

[49] S. Münster, L. M. Jawerth, B. A. Leslie, J. I. Weitz, B. Fabry, and D. A. Weitz, *Strain history dependence of the nonlinear stress response of fibrin and collagen networks*, Proceedings of the National Academy of Sciences, 110 (2013), pp. 12197–12202.

[50] I. Nitsan, S. Drori, Y. E. Lewis, S. Cohen, and S. Tzlil, *Mechanical communication in cardiac cell synchronized beating*, Nature Physics, 12 (2016), pp. 472–477.

[51] J. Nocedal and S. J. Wright, *Numerical optimization*, Springer Series in Operations Research and Financial Engineering.

[52] J. Notbohm, A. Lesman, P. Rosakis, D. A. Tirrell, and G. Ravichandran, *Microbuckling of fibrin provides a mechanism for cell mechanosensing*, J. R. Soc. Interface, (2015).

[53] R. Oria, T. Wiegand, J. Escribano, A. Elosegui-Artola, J. J. Uriarte, C. Moreno-Pulido, I. Platzman, P. Delcanale, L. Albertazzi, D. Navajas, X. Trepat, J. M. García-Aznar, E. A. Cavalcanti-Adam, and P. Roca-Cusachs, *Force loading explains spatial sensing of ligands by cells*, Nature, 552 (2017), pp. 219–224.

[54] D. Park, E. Wershof, S. Boeing, A. Labernadie, R. P. Jenkins, S. George, X. Trepat, P. A. Bates, and E. Sahai, *Extracellular matrix anisotropy is determined by tfap2c-dependent regulation of cell collisions*, Nature Materials, 19 (2020), pp. 227–238.

[55] D. A. Pecknold, J. Ghaboussi, and T. J. Healey, *Snap-through and bifurcation in a simple structure*, Journal of Engineering Mechanics, 111 (1985), pp. 909–922.

[56] S. R. Peyton, Æ. C. M. Ghajar, C. B. Khatiwala, and Æ. A. J. Putnam, *The emergence of ECM mechanics and cytoskeletal tension as important regulators of cell function*, Cell Biochemistry and Biophysics, (2007), pp. 300–320.

[57] I. K. Piechocka, R. G. Bacabac, M. Potters, F. C. Mackintosh, and G. H. Koenderink, *Structural Hierarchy Governs Fibrin Gel Mechanics*, Biophysj, 98 (2010), pp. 2281–2289.

[58] S. V. Plotnikov, A. M. Pasapera, B. Sabass, and C. M. Waterman, *Force fluctuations within focal adhesions mediate ECM-rigidity sensing to guide directed cell migration*, Cell, 151 (2012), pp. 1513–1527.

[59] P. P. Provenzano, K. W. Eliceiri, J. M. Campbell, D. R. Inman, J. G. White, and P. J. Keely, *Collagen reorganization at the tumor-stromal interface facilitates local invasion*, BMC MED, (2006), pp. 1–15.

[60] P. P. Provenzano, D. R. Inman, K. W. Eliceiri, J. G. Knittel, L. Yan, C. T. Rueden, J. G. White, and P. J. Keely, *Collagen density promotes mammary tumor initiation and progression*, BMC Medicine, 6 (2008), p. 11.

[61] P. P. Provenzano, D. R. Inman, K. W. Eliceiri, S. M. Trier, and P. J. Keely, *Contact guidance mediated three-dimensional cell migration is regulated by Rho/ROCK-dependent matrix reorganization*, Biophysical Journal, 95 (2008), pp. 5374–5384.

[62] Python Core Team, *Python: A dynamic, open source programming language.*, Python Software Foundation, 2015.
`https://www.python.org/`.

[63] R Core Team, *R: A Language and Environment for Statistical Computing*, R Foundation for Statistical Computing, Vienna, Austria, 2014.
`http://www.R-project.org/`.

[64] K. Riching, B. L. Cox, M. Salick, C. Pehlke, A. Riching, S. M. Ponik, B. Bass, W. Crone, Y. Jiang, A. M. Weaver, K. Eliceiri, and P. Keely, *3D Collagen Alignment Limits Protrusions to Enhance Breast Cancer Cell Persistence*, Biophysical Journal, 107 (2014), pp. 2546–2558.

[65] P. Ronceray, C. P. Broedersz, and M. Lenz, *Fiber networks amplify active stress*, Proceedings of the National Academy of Sciences, 113 (2016), pp. 2827–2832.

[66] P. Rosakis, J. Notbohm, and G. Ravichandran, *Journal of the Mechanics and Physics of Solids A model for compression-weakening materials and the elastic fields due to contractile cells*, Journal of the Mechanics and Physics of Solids, 85 (2015), pp. 16–32.

[67] T. Rozario and D. W. DeSimone, *The extracellular matrix in development and morphogenesis: a dynamic view*, Dev Biol, 341 (2009), pp. 126–140.

[68] J. W. Ruberti and N. J. Hallab, *Strain-controlled enzymatic cleavage of collagen in loaded matrix*, Biochem Biophys Res Commun, 336 (2005), pp. 483–489.

[69] M. S. Rudnicki, H. A. Cirka, M. Aghvami, E. A. Sander, Q. Wen, and K. L. Billiar, *Nonlinear strain stiffening is not sufficient to explain how far cells can feel on fibrous protein gels*, Biophysical Journal, 105 (2013), pp. 11–20.

[70] R. K. Sawhney and J. Howard, *Slow local movements of collagen fibers by fibroblasts drive the rapid global self-organization of collagen gels*, J Cell Biol, 157 (2002), pp. 1083–1091.

[71] Q. Shi, R. P. Ghosh, H. Engelke, C. H. Rycroft, L. Cassereau, J. A. Sethian, V. M. Weaver, and J. T. Liphardt, *Rapid disorganization of mechanically interacting systems of mammary acini*, Proceedings of the National Academy of Sciences, 111 (2014), pp. 658–663.

[72] M. L. Smith, D. Gourdon, W. C. Little, K. E. Kubow, R. A. Eguiluz, S. Luna-Morris, and V. Vogel, *Force-induced unfolding of fibronectin in the extracellular matrix of living cells*, PLoS Biol, 5 (2007), p. e268.

[73] R. S. Sopher, H. Tokash, S. Natan, M. Sharabi, O. Shelah, O. Tchaicheeyan, and A. Lesman, *Nonlinear Elasticity of the ECM Fibers Facilitates Efficient Intercellular Communication*, Biophysj, 115 (2018), pp. 1357–1370.

[74] D. Stopak and A. K. Harris, *Connective tissue morphogenesis by fibroblast traction: I. tissue culture observations*, Developmental Biology, 90 (1982), pp. 383–398.

[75] C. Storm, J. J. Pastore, F. C. MacKintosh, T. C. Lubensky, and P. A. Janmey, *Nonlinear elasticity in biological gels*, Nature, 435 (2005), pp. 191–194.

[76] M. Tarantino and K. Danas, *Programmable higher-order euler buckling modes in hierarchical beams*, International Journal of Solids and Structures, 167 (2019), pp. 170–183.

[77] D. Vader, A. Kabla, D. Weitz, and L. Mahadevan, *Strain-Induced Alignment in Collagen Gels*, PLoS ONE, 4 (2009).

[78] J. A. J. van der Rijt, K. O. van der Werf, M. L. Bennink, P. J. Dijkstra, and J. Feijen, *Micromechanical testing of individual collagen fibrils*, Macromolecular Bioscience, 6 (2006), pp. 697–702.

[79] R. G. Wells, *The Role of Matrix Stiffness in Hepatic Stellate Cell Activation and Liver Fibrosis*, Journal of Clinical Gastroenterology, 39 (2005).

[80] Q. Wen and P. A. Janmey, *Effects of non-linearity on cell – ECM interactions*, Experimental Cell Research, 319 (2013), pp. 2481–2489.

[81] J. P. Winer, S. Oake, and P. A. Janmey, *Non-linear elasticity of extracellular matrices enables contractile cells to communicate local position and orientation*, PLoS ONE, 4 (2009).

[82] X. Xu and S. A. Safran, *Nonlinearities of biopolymer gels increase the range of force transmission*, Phys. Rev. E, 032728 (2015), pp. 1–10.

[83] T. Yeung, P. C. Georges, L. A. Flanagan, B. Marg, M. Ortiz, M. Funaki, N. Zahir, W. Ming, V. Weaver, and P. A. Janmey, *Effects of Substrate Stiffness on Cell Morphology , Cytoskeletal Structure , and Adhesion*, Cell Motility and the Cytoskeleton, 34 (2005), pp. 24–34.

[84] H. Yu, J. K. Mouw, and V. M. Weaver, *Forcing form and function: Biomechanical regulation of tumor evolution*, jan 2011.